THE FRICTION SAWING OF WOOD

by

KWEI CHO YU

B. Sc., National University of Chekiang, Hanchow, China, 1946.

A THESIS SUBMITTED IN PARTIAL FULFILMENT OF

THE REQUIREMENTS FOR THE DEGREE OF

MASTER OF APPLIED SCIENCE

in the Department

of

Mechanical Engineering

We accept this thesis as conforming to the

required standard

THE UNIVERSITY OF BRITISH COLUMBIA

September, 1966.

In presenting this thesis in partial fulfilment of the requirements for an advanced degree at the University of British Columbia, I agree that the Library shall make it freely available for reference and study. I further agree that permission for extensive copying of this thesis for scholarly purposes may be granted by the Head of my Department or by his representatives. It is understood that copying or publication of this thesis for financial gain shall not be allowed without my written permission.

Department of Mechanical Engineering

The University of British Columbia
Vancouver 8, Canada

Date Feb. 15, 1967.

ABSTRACT

The friction sawing of wood by a high speed rotating disk has been studied. The present experiments were carried out by sawing two commonly used timbers; namely, Douglas fir and Western red cedar of different moisture contents. A 14 inch diameter, 14 gauge steel disk with a smooth edge, driven at a rotating speed of 4,620 rpm was used for the research. A theoretical analysis of heat transmission characteristics and temperature distribution in the sawing disk is presented.

Experimental results showed that the frictional forces, power consumed and cutting temperatures increased as feed speeds increased. The results also showed that the moisture content of the wood had no noticeable influence on the sawing action. A narrow kerf, straight, smooth and polished cut surfaces are some of the advantageous features of the process.

At low feed speeds the calculated cutting edge temperatures were well below the ignition temperature of the wood specimen. However at high feed speeds the experimental horse power values increased and high calculated cutting edge temperatures consequently obtained. Excessive power consumption and high cutting edge temperatures were believed to be related to the difficulty of disposition of cut material with a smooth edge disk.

Reasonably high feed speeds were evident in cutting plywood and veneer. For these materials clean, smooth and polished cut surfaces were evident. The method may be advantageous in the cutting of plastic sheets.

When cutting thicker lumber with this method the feed speed was confined to an impractical low level and power consumed was far higher than that required for ordinary sawing. Thus, whether this method of sawing can be put into practical use or not is determined by the possibility of having

an effective means to dispose of cut material. In this connection several methods of modifying the disk for more efficient cutting and waste disposal are presented.

NOMENCLATURE

Symbol	Quantity	Preferred Units
	LETTER SYMBOLS	
A_1	Cross section area of outer periphery of annulus	sq. ft.
A_2	Cross section area of inner periphery of annulus	sq. ft.
b	Thickness of sawing disk	ft. , in.
D	Disk diameter	ft. , in.
F_f	Friction force on the cutting edge	lb.
F_N	Normal force exerted on the wood	lb.
F_T	Feed thrust	lb.
h_a	Coefficient of heat transfer at the side surface of the disk	$Btu/ft^2-hr.-^oF$
J	Mechanical equivalent of heat 778	ft.-lb/Btu
K_a	Thermal conductivity of surrounding air	$Btu/ft-hr-^oF$
K_s	Thermal conductivity of steel	$Btu/ft-hr-^oF$
L_w	Length of wood specimen	Ft.
ℓ	Distance between reaction R and axis Y-Y'	Ft.
ℓ_1	Distance between tail edge of wood and axis Y-Y'	Ft.
ℓ_2	Distance between reaction R_2 and axis Y-Y'	Ft.
ℓ_G	Distance between tail edge and centre of gravity of wood specimen	Ft.
ℓ_w	Distance between cutting edge and tail edge of the wood specimen	Ft.
N	Rotating speed of disk	rpm
$\dot{Q}_1$	Rate of heat inflow through the outer circumference of annulus	Btu/hr.
$\dot{Q}_2$	Rate of heat outflow through inner circumference of annulus	Btu/hr.

Symbol	Quantity	Preferred Units
$\dot{Q}_R$	Rate of heat transfer by radiation	Btu/hr.
$\dot{Q}_v$	Rate of heat convected through side surfaces	Btu/hr.
R	Table support strain ring reaction	lb.
R_1	Reaction exerted by tail edge of wood specimen on the table	lb.
R_2	Reaction exerted on the wood specimen by the roller on the upper guide block	lb.
r	Inner radius of an annulus of the disk	ft.
r_o	Radius of sawing disk	ft., in.
δ_r	Increment of radius	ft.
S	Area of two side surface of annulus	sq. ft.
T	$= \tau - \tau_{am}$	^oF
T(r)	Disk temperature, function of radius	^oF
T_{ab}	Absolute disk temperature	(^oR)
V_f	Feed speed	in./min.
W	Weight of specimen	lb.
W_c	Weight of specimen after being cut and before being dried.	lb.
W_D	Oven-dried weight of wood specimen	lb.

GREEK LETTERS

α	Angle between the axis Y-Y' and the radius of the disk passing through top of cutting edge	Degree
β	Angle between the axis Y-Y' and the radius of the disk passing through bottom of cutting edge.	Degree
θ	Angle between normal force F_N and axis Y-Y'	Degree
κ	Diffusivity of steel	$ft^2/hr.$
λ	$=\sqrt{\frac{2h_a}{K_s b}}$	$ft.^{-1}$

Symbol	Quantity	Preferred Units
ν	Kinematic viscosity of surrounding air	$ft^2/sec.$, $ft^2/hr.$
σ	Stefan - Boltzman constant	$Btu/hr.-ft^2-(^oR)$
τ	Local temperature	^oF
τ_{am}	Ambient temperature	^oF
$\Delta\tau_{max}$	Maximum temperature difference between disk temperature and ambient temperature	^oF
ω	Angular velocity of sawing disk	rad/sec , rad/hr.

DIMENSIONLESS GROUP

C_1 & C_2	Constants in the solution of Bessel Equation
ϵ	Emissivity of sawing disk
I_o	Modified Bessel function, order 0, 1st kind
I_1	Modified Bessel function, order 1, 1st kind
$K = \frac{(\ell_G-\ell_1)\ W+13.95R}{5.53}$	
K_o	Modified Bessel function, order 0, 2nd kind.
N_u	Nusselt number
P_r	Prantdl number
R_e	Rotational Reynolds number
μ	Coefficient of friction between disk and wood

ACKNOWLEDGEMENT

This experimental work was carried out in the Lubrication Laboratory, Department of Mechanical Engineering, University of British Columbia. Financial assistance was received from the National Research Council of Canada under Grant Number A-1065.

The author is grateful to the MacMillan, Bloedel and Powell River (B.C.) Ltd., for the supply of woods for this experimental work; to the Vancouver Laboratory, Forest Products Laboratories of Canada for the seasoning of wood specimens. The author wishes to thank the Staff of Mechanical Engineering Department and Mr. J.E. Jones of the Lubrication Laboratory for their valuable assistance.

The author also thanks Dr. Z. Rotem for his constructive suggestions on heat transmission in the development of the theory of this thesis.

Particular thanks are due to Dr. C.A. Brockley, the author's research Superviser, for his sound direction and constant encouragement in the course of developing this thesis.

TABLE OF CONTENTS

TABLE OF CONTENTS Contd.

LIST OF FIGURES

LIST OF FIGURES Contd.

LIST OF FIGURES Contd.

CHAPTER I.

I.1 INTRODUCTION

Friction appears as a resistance to the relative motion of two solid bodies in contact. Frictional energy may be converted into heat thus raising the temperature of the contacting surfaces. In most engineering applications temperature effects associated with friction are considered to be undesirable but for friction sawing the heat may be usefully employed for cutting materials.

Friction sawing of metals has been successfully applied by utilizing the frictional heat to soften the metal and then sweep it away by the saw blade [1]. Friction sawing of wood is based on similar principles. A theoretical analysis of temperature distribution in the sawing disk and the relation between the cutting edge temperature and power consumed can be made by considering heat transmission in a rotating disk with heat generated at the periphery. To raise the cutting edge temperature and then maintain it,

a sufficient amount of heat must be generated in order to balance the losses. Heat loss through the wood specimen is negligible. This method of sawing wood by the use of frictional heat, insofar as can be determined, has not been previously studied.

The frictional heat utilized for sawing is related to the coefficient of friction at the cutting edge. Furthermore, the feed speed may influence the values of the forces involved. Therefore the first purpose of the experimental investigation was to establish the force values and their interrelationships during actual cutting. The measurement of the temperature near the cutting edge was also included in the investigation. Power consumed, wood saving and the condition of the cut surface are important economic factors and received attention in the present investigation. Moisture content affects the strength of the wood and influences ordinary toothed sawing processes [2], hence it was treated as a variable in the present research.

CHAPTER II.

II.1. THEORY

During friction sawing heat is generated at the interface between the edge of the sawing disk and the wood specimen. The amount of heat generated at the interface and the heat transmission characteristics determine the temperature distribution in the system. The majority of the heat generated is transmitted to the disk since the ratio of the thermal conductivity of wood to that of steel is as small as 1:13 to 1:26 (average thermal conductivity of Douglas fir - 1.0 to 2.0 Btu./hr. ft. ^{o}F [3] and the thermal conductivity of steel - 26 Btu./hr. ft. ^{o}F [4]).

The system under consideration is actually a rotating disk with heat generated at the periphery. As the amount of heat generated is a function of the frictional force the relation between the cutting temperature and the frictional force may be obtained as follows.

Assumptions:

1. The disk is thin compared with its diameter; hence the temperature variation normal to the plane of symmetry may be neglected.

2. Heat is only generated at the portion of the disk where it is instantaneously rubbing on the wood. However, with the disk rotating at high speed (4,620 rpm) the period $2\pi/\omega$ is only a small fraction of a second (0.013 sec. or 3.6×10^{-6} hr.), the radius of the disk $r_o = 7/12$ ft. and diffusivity of steel $\kappa = 0.48$ ft.^{2}/hr. [5] hence the product

$$\frac{2\pi}{\omega} * \frac{\kappa}{r_o^2} << 1$$

Therefore we may consider the periphery of the disk to be isothermal at a quasi-steady state condition. [8]

3. The amount of heat transfer by radiation is small in comparison with convective and conductive processes and may be neglected. A theoretical justification is given in Appendix G.

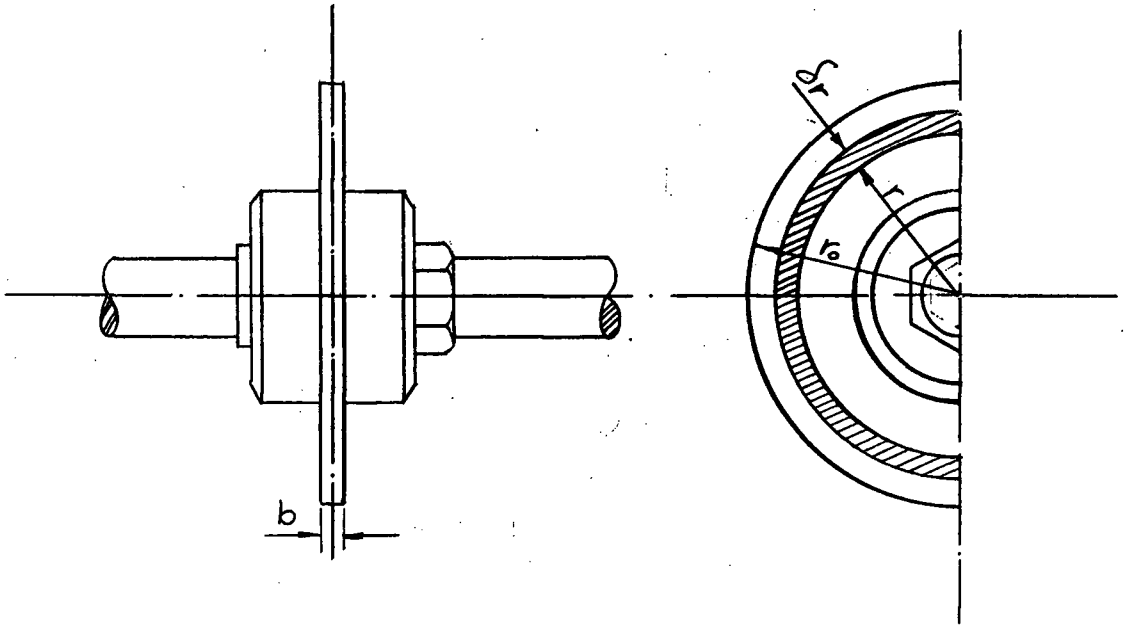

Fig. 1 Sawing Disk and Collars.

Consider the heat balance in an annulus having inner radius r and outer radius r + δr (Fig. 1).

Heat inflow through the outer circumference of the annulus per unit time is given by:

$$\dot{Q}_1 = + K_s A_1 \frac{\partial}{\partial r} (\tau + \frac{\partial \tau}{\partial r} dr) \quad \ldots\ldots\ldots\ldots (2\text{-}1)$$

where K_s = thermal conductivity of steel

A_1 = cross-section area of outer periphery of annulus

$= 2\pi (r + \delta r)b$

τ = local temperature

b = thickness of disk

Heat outflow through inner circumference per unit time:

$$\dot{Q}_2 = + K_s A_2 \frac{\partial \tau}{\partial r} \quad \ldots\ldots\ldots\ldots\ldots\ldots\ldots (2\text{-}2)$$

where A_2 = cross section area of inner periphery of annulus

$= 2\pi rb$

Heat convected through side surfaces per unit time:

$$\dot{Q}_v = + Sh_a (\tau - \tau_{am}) \quad \ldots\ldots\ldots\ldots\ldots\ldots (2\text{-}3)$$

where S = area of two side surfaces of annulus

$= 2\pi \left[(r + \delta r)^2 - r^2\right]$

h_a = coefficient of heat transfer at the side surfaces of the disk.

τ_{am} = ambient temperature

Under steady conditions the rate of heat inflow to the annulus must be equal to the heat outflow, and as defined in the assumptions (1), (2) and (3) we may neglect temperature variation normal to the plane of symmetry; the periodicity of heat input and transfer of heat by radiation, we may have

$$\dot{Q}_1 = \dot{Q}_2 + \dot{Q}_v \quad \ldots\ldots\ldots\ldots\ldots\ldots\ldots\ldots\ldots \quad (2\text{-}4)$$

From equations (2-1), (2-2), (2-3) and (2-4) the diffusion equation for the system is obtained (neglecting $(dr)^2$ terms).

$$\frac{d^2T}{dr^2} + \frac{1}{r}\frac{dT}{dr} - \lambda^2 T = 0 \quad \ldots\ldots\ldots\ldots\ldots\ldots\ldots \quad (2\text{-}5)$$

where $T = \tau - \tau_{am}$

$$\lambda = \sqrt{\frac{2h_a}{K_s b}}$$

This is the form of a modified Bessel equation of order 0 with parameter λ. The complete solution of (2-5) is

$$T(r) = C_1 I_o(\lambda r) + C_2 K_o(\lambda r) \ldots\ldots\ldots\ldots\ldots\ldots \quad (2\text{-}6)$$

Where C_1 and C_2 are constants to be determined by boundary conditions.

I_o = modified Bessel function, order 0, 1st kind

K_o = modified Bessel function, order 0, 2nd kind

Boundary Conditions

(a) Since r = 0 is included in the range, but $\lim_{x \to 0} K_o(x) \to \infty$, we must have

$$C_2 = 0$$

giving

$$T(r) = C_1 I_o(\lambda r)$$

(b) At the outer periphery where the heat is generated, the temperature is a maximum

$$T(r_o) = \Delta \tau_{max}$$

$$C_1 = \frac{\Delta \tau_{max}}{I_o(\lambda r_o)}$$

Hence

$$T(r) = \frac{I_o(\lambda r)}{I_o(\lambda r_o)} \Delta \tau_{max} \quad \ldots\ldots\ldots\ldots\ldots\ldots\ldots\ldots \quad (2\text{-}7)$$

Thus, for instance, $I_0(\lambda r_o) = 2{,}200$ (Appendix F) at $r = 0$

$$T(0) = \frac{\Delta \tau_{max}}{2{,}200} \text{ i.e. less than } 0.5\% \Delta \tau_{max}$$

At $r = 3$ inches, the part of the disk in contact with the collar

$$I_0(4.17) = 13.09 \text{ (Appendix F)}$$

$$T\ (3/12) = \frac{13.09}{2{,}200} \text{ i.e. slightly more than } 0.5\% \ \Delta \tau_{max}$$

Differentiate (2-7) with respect to r

$$\frac{dT(r)}{dr} = \frac{d\tau}{dr} = \frac{I_1(\lambda r)}{I_o(\lambda r_o)} \lambda \Delta \tau_{max} \quad \ldots\ldots\ldots\ldots\ldots\ldots \quad (2\text{-}8)$$

where I_1 = modified Bessel function, order 1, 1st kind

Hence the temperature gradient at the disk periphery

$$\left.\frac{d\tau}{dr}\right|_{r_o} = \frac{I_1(\lambda r_o)}{I_o(\lambda r_o)} \lambda \Delta \tau_{max} \quad \ldots\ldots\ldots\ldots\ldots\ldots \quad (2\text{-}9)$$

Substituting (2-9) in (2-1) gives the expression for heat flux at the disk periphery

$$\left.\dot{Q}_1\right|_{r_o} = -\, 2\pi K_s b r_o \left.\frac{d\tau}{dr}\right|_{r_o}$$

or

$$\left.\dot{Q}_1\right|_{r_o} = -\, 2\pi K_s b r_o \frac{I_1(\lambda r_o)}{I_o(\lambda r_o)} \lambda \Delta \tau_{max} \quad \ldots\ldots\ldots \quad (2\text{-}10)$$

Heat generated at the disk periphery is

$$\dot{Q}_F = \frac{\mu F_N \omega r_o}{J} \quad [7]$$

where μ = coefficient of friction between the disk and the wood

ω = angular velocity of disk

J = mechanical equivalent of heat

F_N = normal force exerted on the wood

$\therefore$ + (Heat input to disk) = (Heat flux at periphery)

$$\therefore \quad + \frac{\mu F_N \omega r_o}{J} = + 2\pi K_s b r_o \frac{I_o(\lambda r_o)}{I_1(\lambda r_o)} \lambda \Delta T_{max}$$

Rearranging terms,

$$\mu F_N = \frac{2\pi J K_s b}{\omega} \frac{I_1(\lambda r_o)}{I_o(\lambda r_o)} \lambda \Delta T_{max} \qquad (2\text{-}11)$$

Evaluation of the Parameter λ :

The experiments were carried out with a 14 inch diameter sawing disk rotating at 4,620 rpm. (ω = 483.9 rad./sec.). The rotational Reynolds number is given by

$$R_e = \frac{\omega r_o^2}{\nu_a}$$

where r_o = radius of disk

ω = angular velocity of disk

ν_a = kinematic viscosity of surrounding air

In the present case

r_o = 0.5835 ft.

ω = 483.9 rad./sec.

ν_a = 0.00018 ft^2/sec. [8]

Hence

R_e = 915,200

Results for the coefficient of heat transfer, at the side surface of the disk, h_a may be obtained from data by Cobb and Saunders [9]. By the value of the Reynolds number we see that the present condition is at the turbulent end of the transition region. Thus using Cobb and Saunders' Fig.4 [9], we found that the mean Nusselt number ($\bar{N}_u = 0.15R^{0.8}$)

$$\bar{N}_u = 875$$

Since $$N_u = \frac{h_a r_o}{K_a}$$

Hence $$h_a = 875 \frac{K_a}{r_o}$$

and since $$\lambda = \sqrt{\frac{2h_a}{K_s b}}$$

$$\therefore \lambda = 41.83 \sqrt{\frac{K_a}{K_s b r_o}} \quad \ldots\ldots\ldots \quad (2\text{-}12)$$

Power Consumed:

$$\text{Power} = J\dot{Q}_1 \Big|_{r_o}$$

$$\therefore \text{Power} = 2\pi J K_s b r_o \frac{I_1(\lambda r_o)}{I_o(\lambda r_o)} \lambda \Delta\tau_{max} \quad (2\text{-}13)$$

and

$$\Delta\tau_{max} = \frac{I_o(\lambda r_o)}{I_1(\lambda r_o)} \frac{\text{Power}}{2\pi J K_s b r_o \lambda} \quad \ldots\ldots\ldots\ldots\ldots \quad (2\text{-}14)$$

CHAPTER III.

III.1. APPARATUS

The apparatus consisted of three sub-assemblies:

i. The sawing disk and drive;

ii. The table and guide;

iii. The feed mechanism.

Figs 2 and 3 show the general arrangement of these three sub-assemblies. The sawing disk and its shaft was driven by an induction motor through a V-belt drive. The table carrying the wood specimen pivoted about the axis of the disk shaft. The specimen feed mechanism was driven by another induction motor through an hydraulic transmission unit. The wood specimen on the table was fed into the saw by the push rod of the feed mechanism. The feed speed of the specimen could be set to desired values by adjusting the hydraulic speed control unit.

i. THE SAWING DISK AND DRIVE (Fig. 2)

(ia) The Sawing Disk and Shaft

The 14 gauge sawing disk was made of SP plate steel of hardness Rockwell C48. The outer periphery of the disk had a smooth surface without teeth. The disk had an outside diameter of 14 inches and an inner bore of $1\frac{1}{4}$ inches. The disk was mounted on an one inch diameter, SPS Atlas steel shaft between two supporting collars 6 inches O.D. and $1\frac{1}{4}$ inches I.D. which were retained by a lock nut (Fig. 4). The shaft was mounted on three bearings.

(ib) The Motor and the V-Belt Drive

A 15 H.P., 3,540 R.P.M. induction motor was used to drive the disk shaft. The power was transmitted by four size B, V-belts. A 9-3/8 inches O.D. pulley was attached to the disk shaft. With this pulley arrangement the speed of the disk was stepped up to 4,620 R.P.M. giving a peripheral disk speed of 282 ft./sec. (16,920 ft./min).

ii. THE TABLE AND GUIDE (Figs 4, 5, 6 & 7)

(iia) The Table

The 30 inches x 16 inches x $\frac{1}{4}$ inch aluminum table was mounted 4 inches above the centre line of the disk. Along the longitudinal centre line a 14 inches by 3/8 inch slot was cut to permit the disk to emerge 3 inches above the table. The table was supported by two aluminum arms at each side of the disk (Fig. 4). A short spindle was attached to each supporting arm. The spindle between the two left hand bearings shown in Fig. 4 was made hollow in order to permit access for the disk shaft. The spindle bearings were flanged mounting ball bearings and were fixed on the two upper guard stands. The concentricity of the disk shaft and the table

supporting arm spindles simplified the calculation of the table forces by elimination of the moments of supporting reaction forces when taking moments about the axis of the disk shaft.

(iib) Guide

On the front part of the table a guide consisting of three aluminum blocks were attached (Fig. 5). The two side blocks with slots cut for the positioning bolts could be moved laterally in order to compensate for the variation of specimen width. The upper block could be adjusted vertically to suit a variation of wood thickness.

(iic) Arrangements to Reduce Frictional Forces Between Wood Specimen and Table/Guide

The frictional forces between the wood specimen and the table and guide were reduced to negligible values. The inner walls of the two side blocks of the guide were lined with Arborite sheets. Fig. 6 shows that at the far end of the upper block of the guide a steel roller was installed in order to prevent the wood specimen from tilting up too far and to reduce the frictional force between the specimen and the upper guide block. A $9\frac{1}{2}$ inches x 2 inches x 1/16 inch Teflon strip was attached from the front edge along the centre line of the table. A tail piece with two Teflon rollers fixed at the rear corner was fastened to each specimen. Fig. 6 shows that during cutting the contact points between the specimen and the upper guide and between the specimen and the table were A and B respectively.

(iid) Arrangement for Measuring Table Forces

A strain ring was mounted on a stand under the table and was 13.95 inches in front of the vertical centre line of the sawing disk. The ring was made of mild steel with 3-3/16 inches O.D and 3 inches I.D. (i.e. 3/32 inches thick). (Fig. 7).

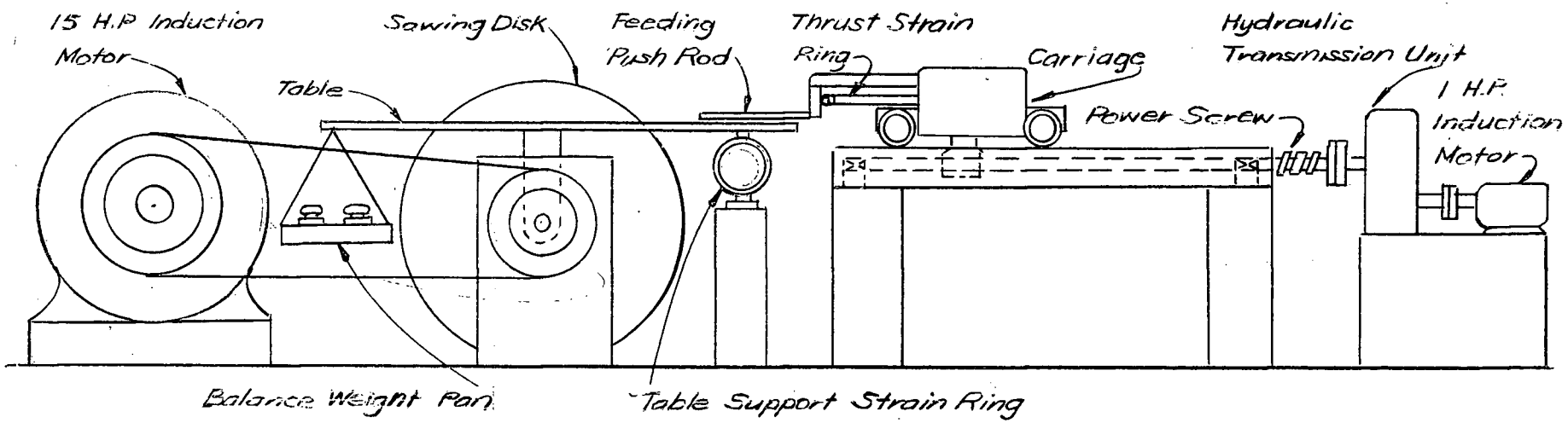

Fig. 2 Schematic Drawing of the General Arrangement of the Friction Saw.

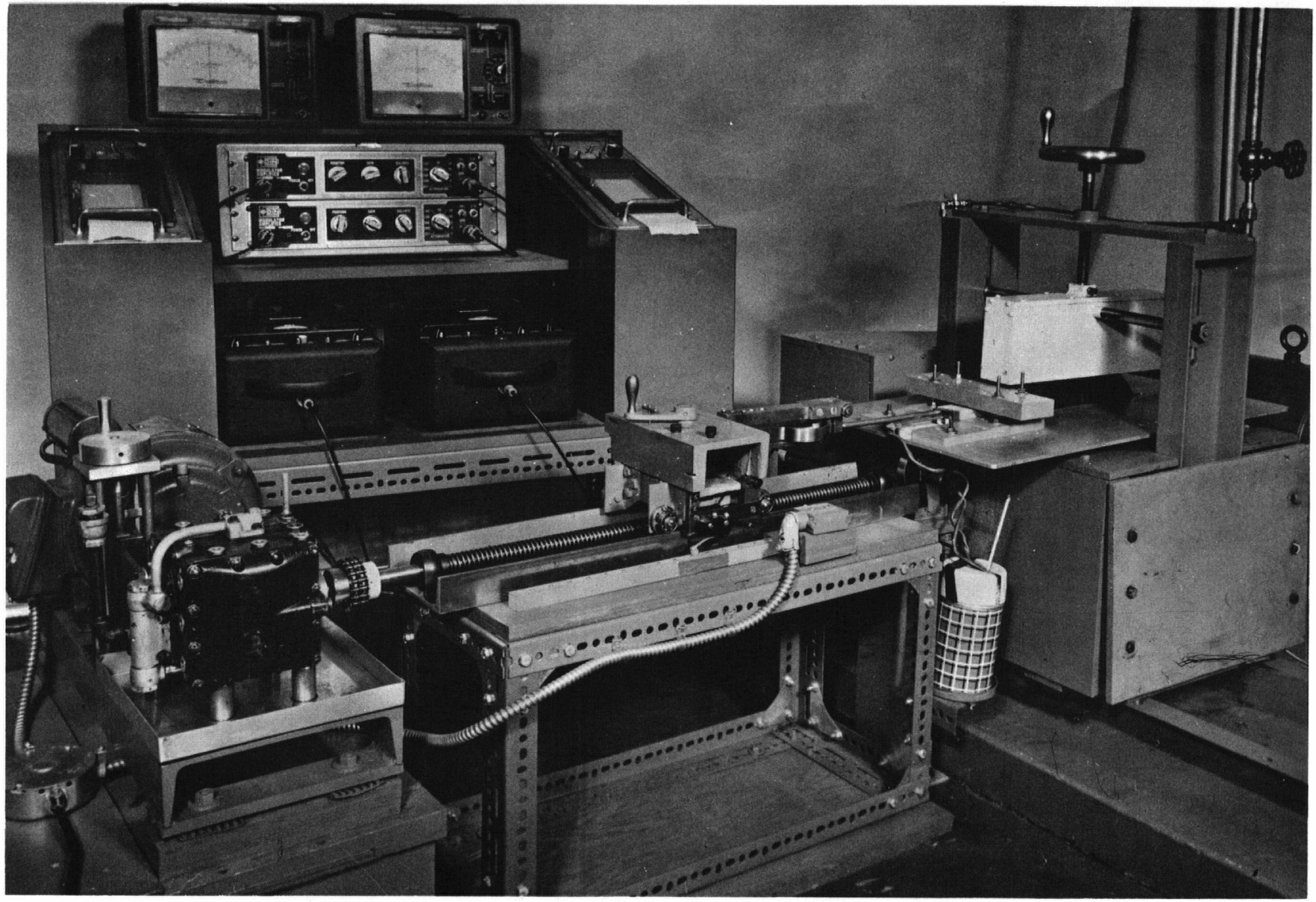

Fig. 3 General Arrangement of Instrument and the Friction Saw.

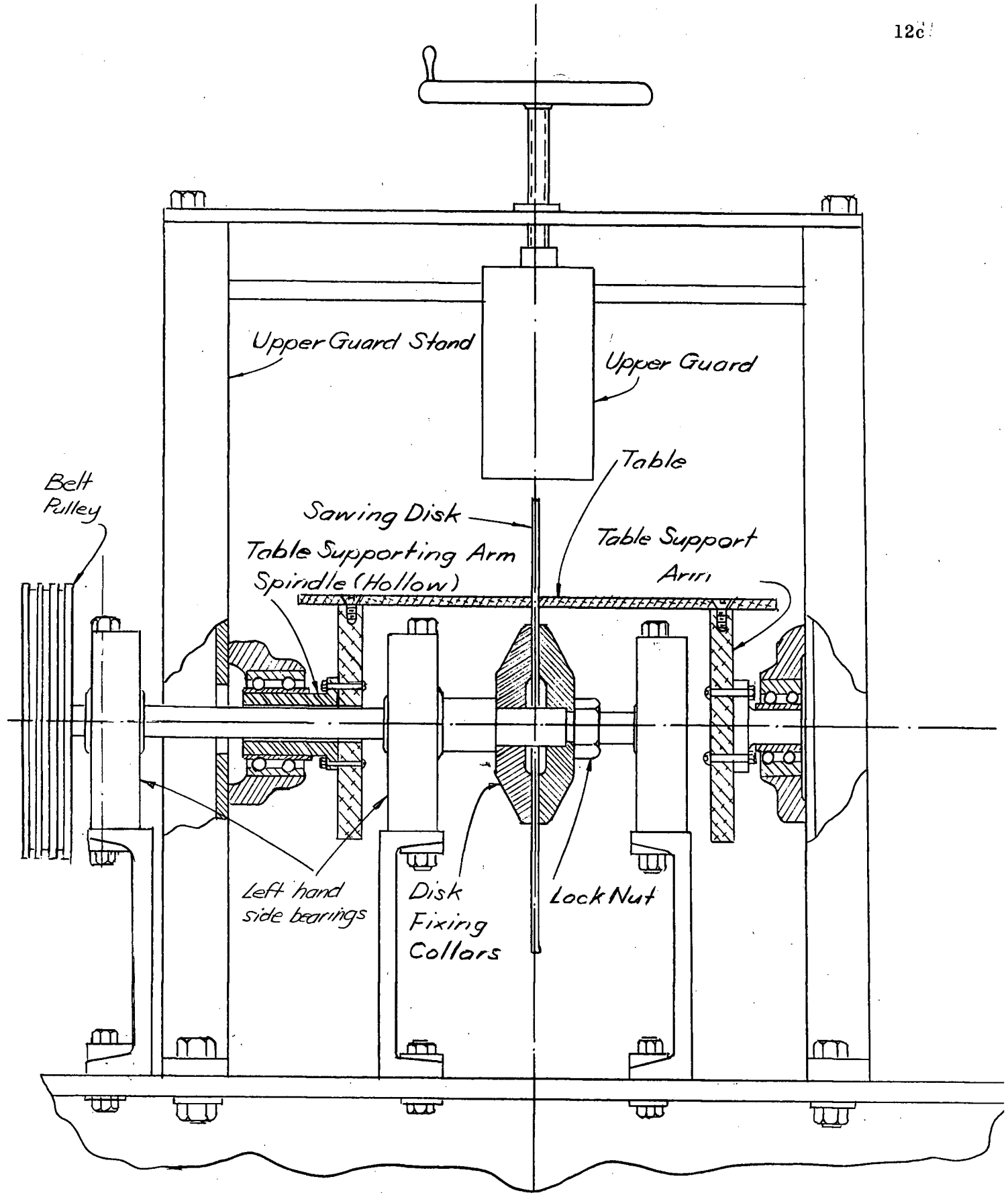

Fig. 4 Sawing Disk and Table.

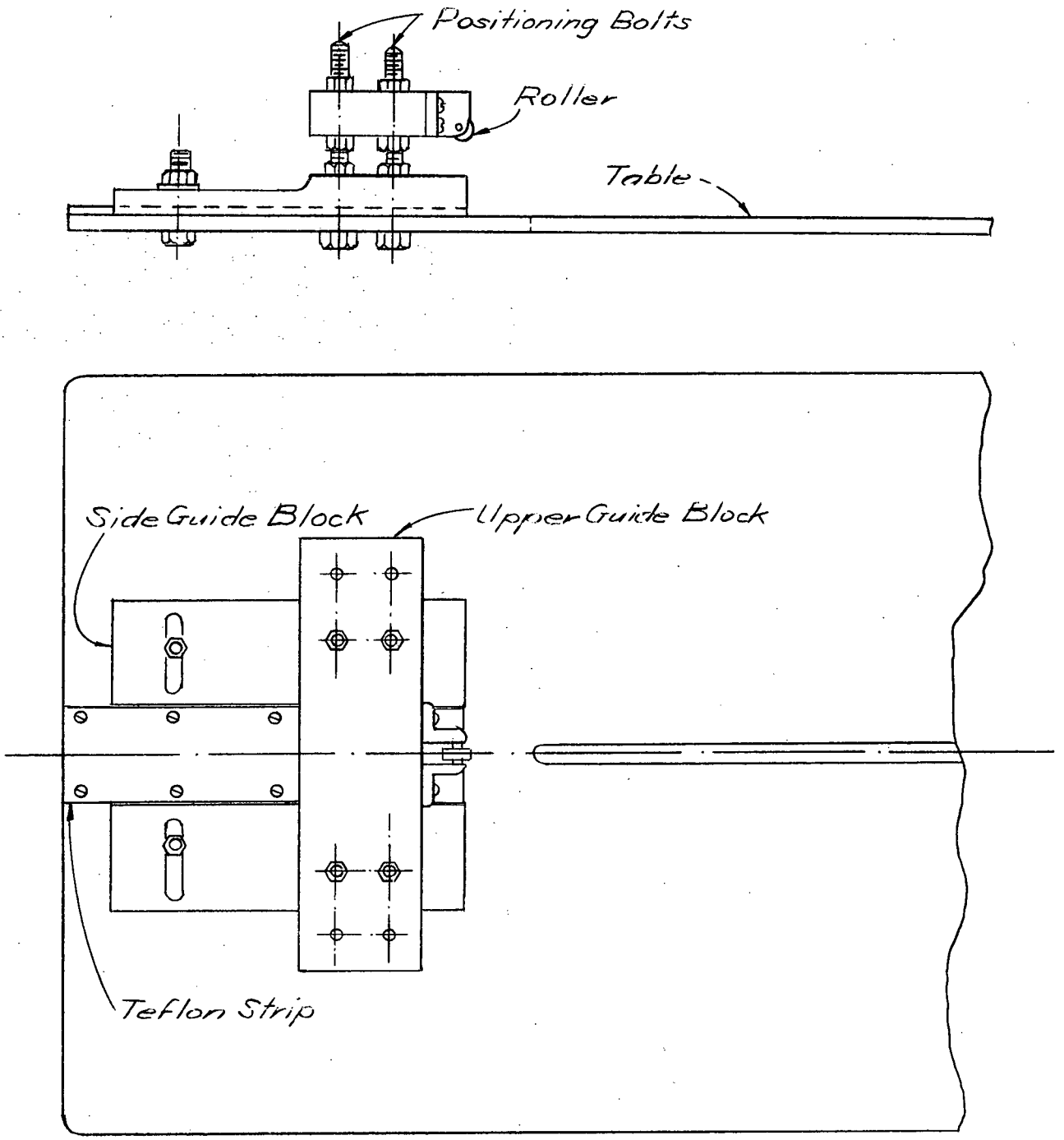

Fig. 5 Guide Blocks

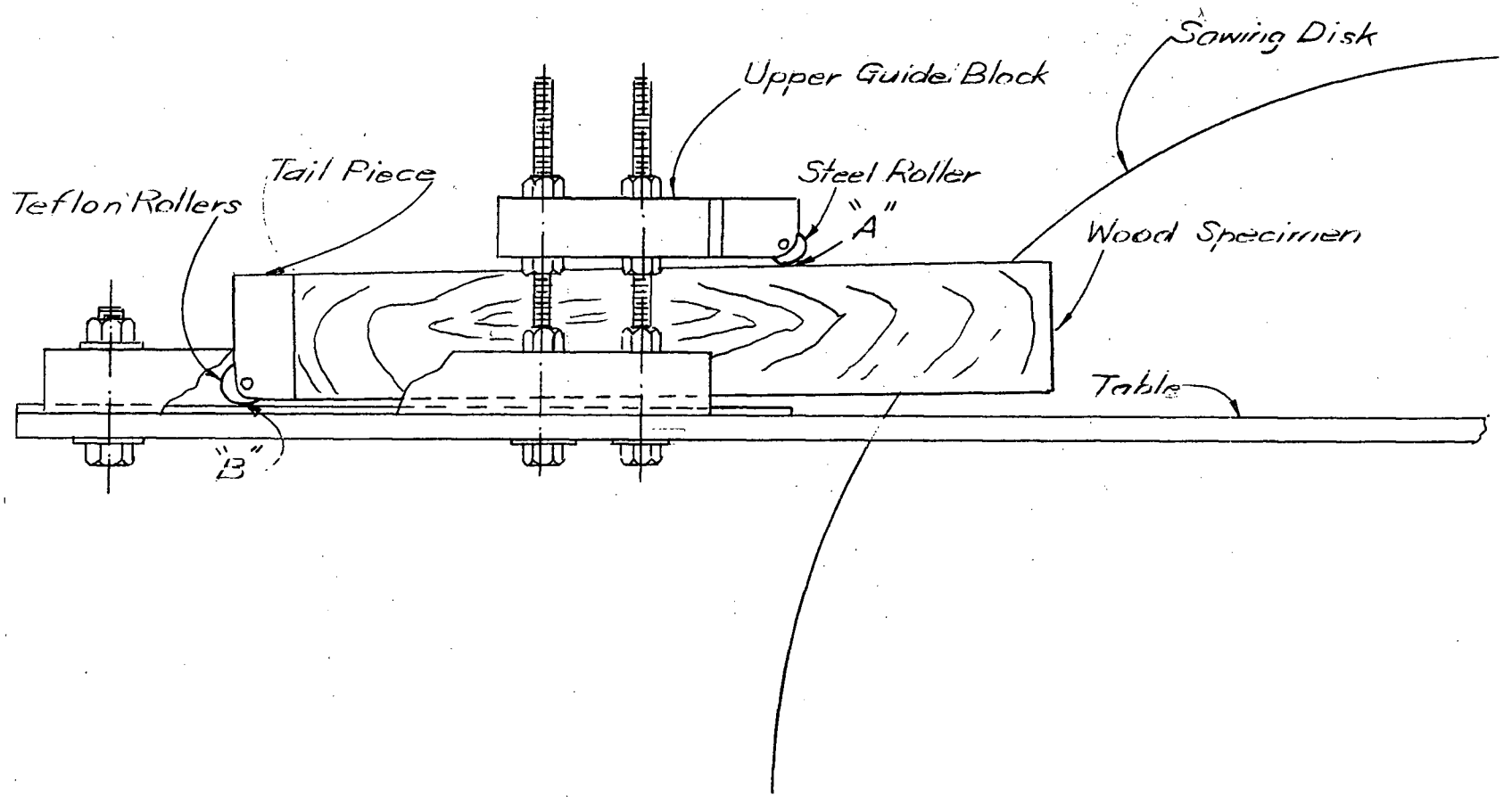

Fig. 6 Position of Specimen when Sawing is Proceeding.

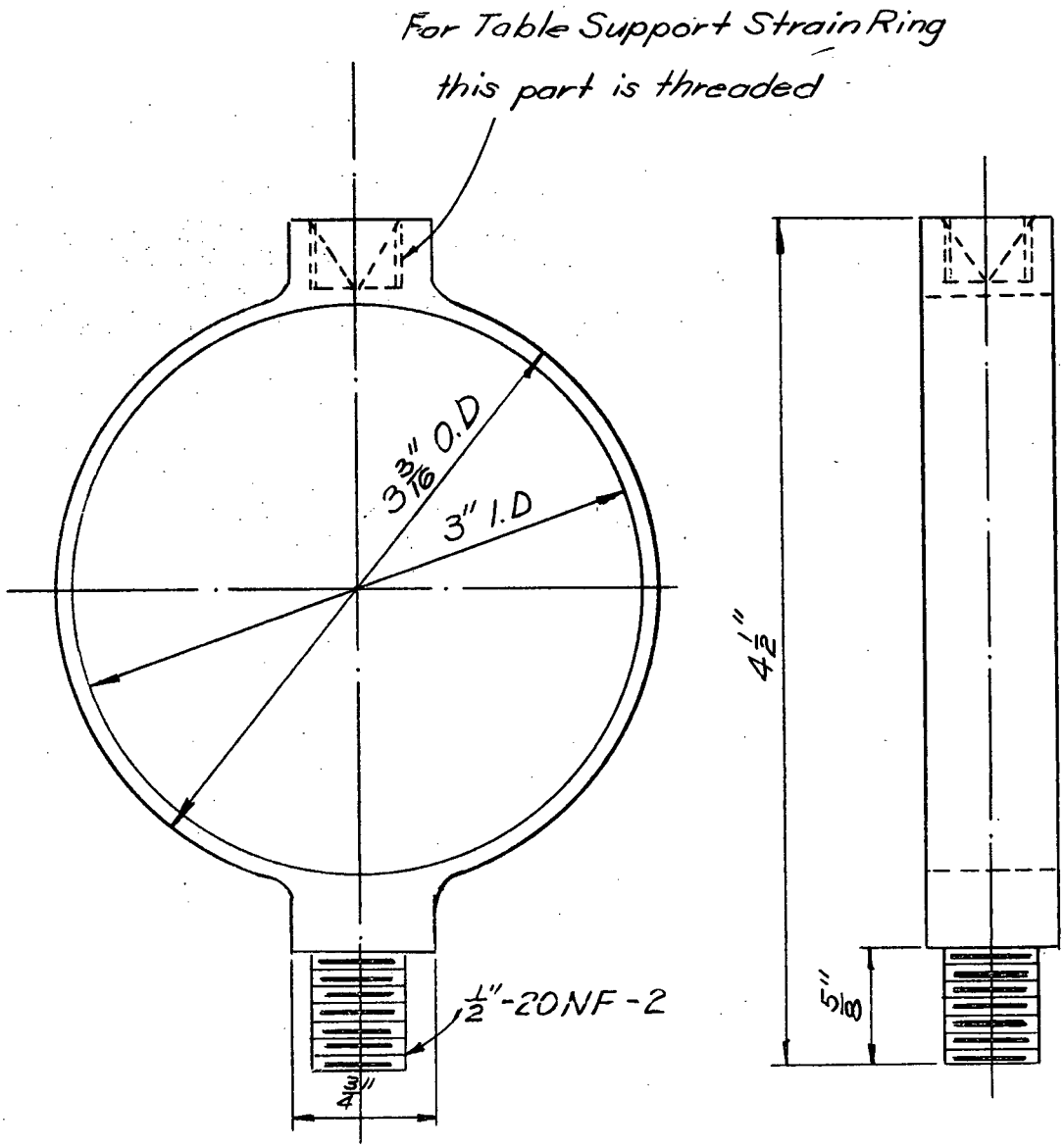

Material: Mild Steel

Fig. 7 Strain Ring

A weight pan at the rear end of the table was used for balancing. Sufficient weights were applied to the pan in order to give zero load on the table strain ring (Fig. 2)

iii. THE FEED MECHANISM

(iiia) The Driving Motor and the Transmission

The feed mechanism was driven by an one horse power, 1,750 r.p.m., single phase induction motor through a hydraulic transmission unit. (Vickers Double Power Unit, Model AA-16801). The speed of the output shaft of the transmission could be varied continously from 0-550 r.p.m..

(iiib) The Carriage and its Power Screw

The output shaft of the hydraulic transmission was coupled to a single start 4 threads per inch power screw which in turn drove the carriage. A split nut on the carriage enabled it to be engaged and disengaged from the power screw. The speed of the power screw and consequently the feed speed of the carriage could be changed by adjusting the output shaft speed of the hydraulic transmission. The speed of the output shaft of the hydraulic transmission had a continuous variation in the range from 0-550 r.p.m., hence the feed speed had a continuous variation from 0 to 137.5 inches per minute.

(iiic) Push Rod and Thrust Measuring Strain Ring

The push rod was mounted on the front face of the carriage (Fig. 9). The push rod M was rigidly fixed to the lever arm K which was pivoted at O. The reaction of the feed thrust, F_T, applied to the push rod, was transmitted through the lever arm K and the steel ball J to the strain ring N, which measured the feed thrust F_T. The mild steel strain ring had the same dimensions as the table strain ring. (Fig. 7)

III.2 MEASUREMENTS

The following quantities were measured or calculated from measured data:

i. Disk speed;

ii. Table force;

iii. Feed Thrust;

iv. Feed speed;

v. Cutting temperature;

vi. Specimen weight;

vii. Specimen centre of gravity;

viii. Coefficient of Friction between the Wood Specimen and the Sawing Disk.

i. Disk Speed

The disk speed was measured by a "Smith" tachometer. The ranges of the tachometer were 0-5,000 and 0-50,000 r.p.m.

ii. Table Force

A mild steel strain ring was attached underneath the table 13.95 inches from the axis of the disk shaft. (Fig. 2) The table was pivoted about the axis of the disk shaft, hence multiplication of the load at the strain ring by the distance between the ring and the disk centre line gave the resultant moment on the table about the axis.

The deflection of the strain ring was detected by a "Daytronic" 103A-80 linear displacement transducer. The transducer was calibrated to read directly the load applied to the ring in pounds. The method of calibration is described in Appendix A.

Excitation of the transducer was supplied by a "Daytronic" differential transformer indicator (Model 300BF). A visual display of strain ring deflection in milli-inches was shown by the indicator. (Fig. 8)

The centre of gravity of the wood specimen was moving during sawing; hence continuous variation of forces resulted and thus a chart record of

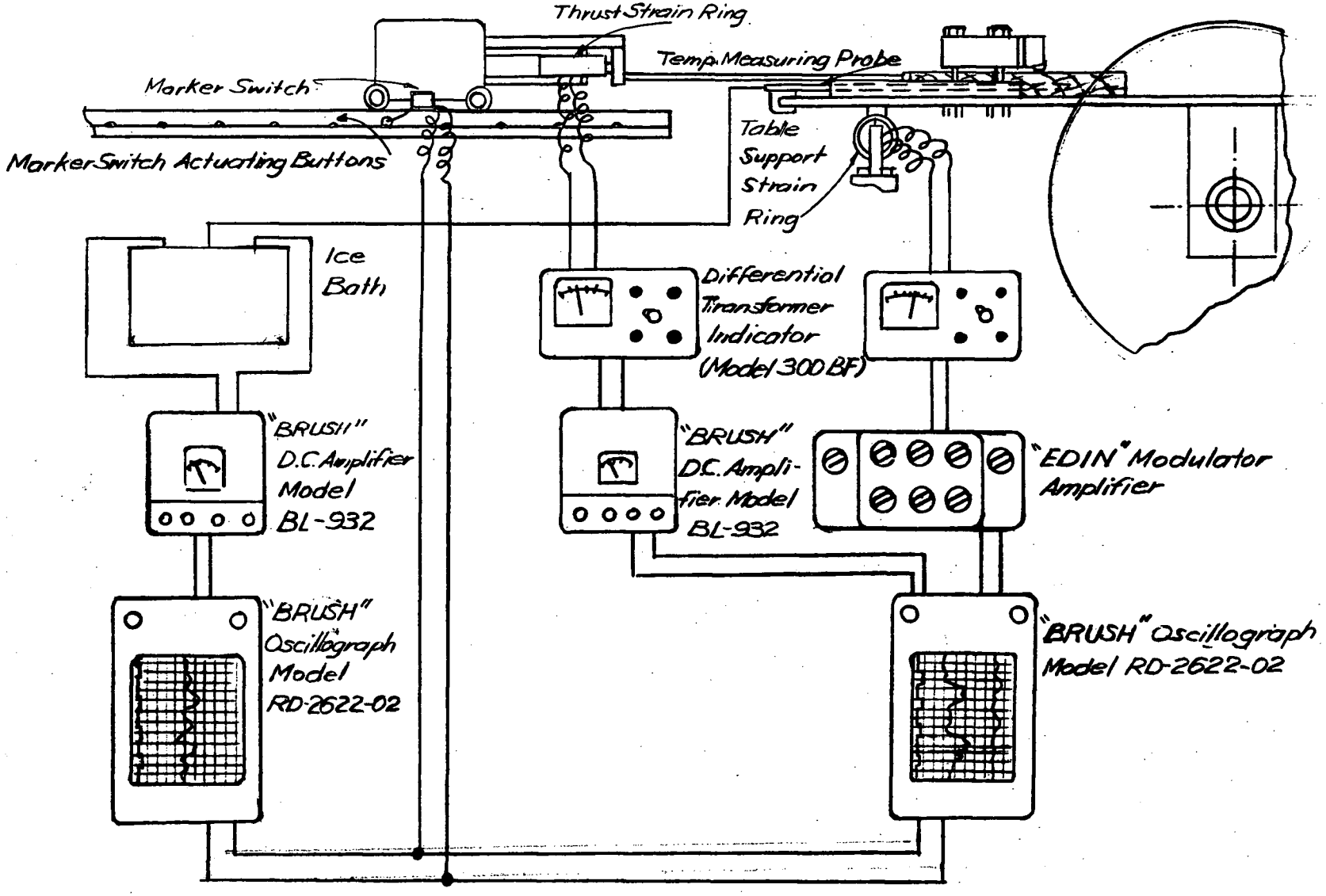

Fig. 8 Instrument Connections Block Diagram.

force versus position or displacement of the specimen was required.

The output from the differential transformer indicator was amplified by an "Edin" modulator amplifier. The amplified voltage was used to drive a "Brush" oscillograph (Model RD-2622-02). A marker switch was fitted to one side of the carriage. Along the surface of a strip attached to the rail stand, buttons were fitted at one inch intervals. The buttons actuated the marker switch which was connected to the marker recorder pen in the oscillograph. Hence a chart record of table force versus displacement of wood specimen could be obtained.

iii. Feed Thrust

Thrust was transmitted from the push rod to a mild steel strain ring by a lever arm and a steel ball (Fig. 9). The strain ring was mounted on the leading edge of the carriage. The deflection of the ring was detected by a "Daytronic" 103A-80 linear displacement transducer. The transducer was calibrated to read directly the force applied on the push rod in pounds. The method of calibration is described in Appendix B.

In the same way as described in the previous section, excitation of the transducer was supplied by a "Daytronic" differential indicator (Model 300BF) which also gave a visual indication of the deflection of the strain ring.

The output of the "Daytronic" differential transformer indicator was amplified by a "Brush" D.C. amplifier (Model BL-932) and was used to drive the other channel of the "Brush" oscillograph described in the previous section. From the two channels of the oscillograph, chart records of feed thrust and table force versus displacement of wood specimen could be obtained (Fig. 8).

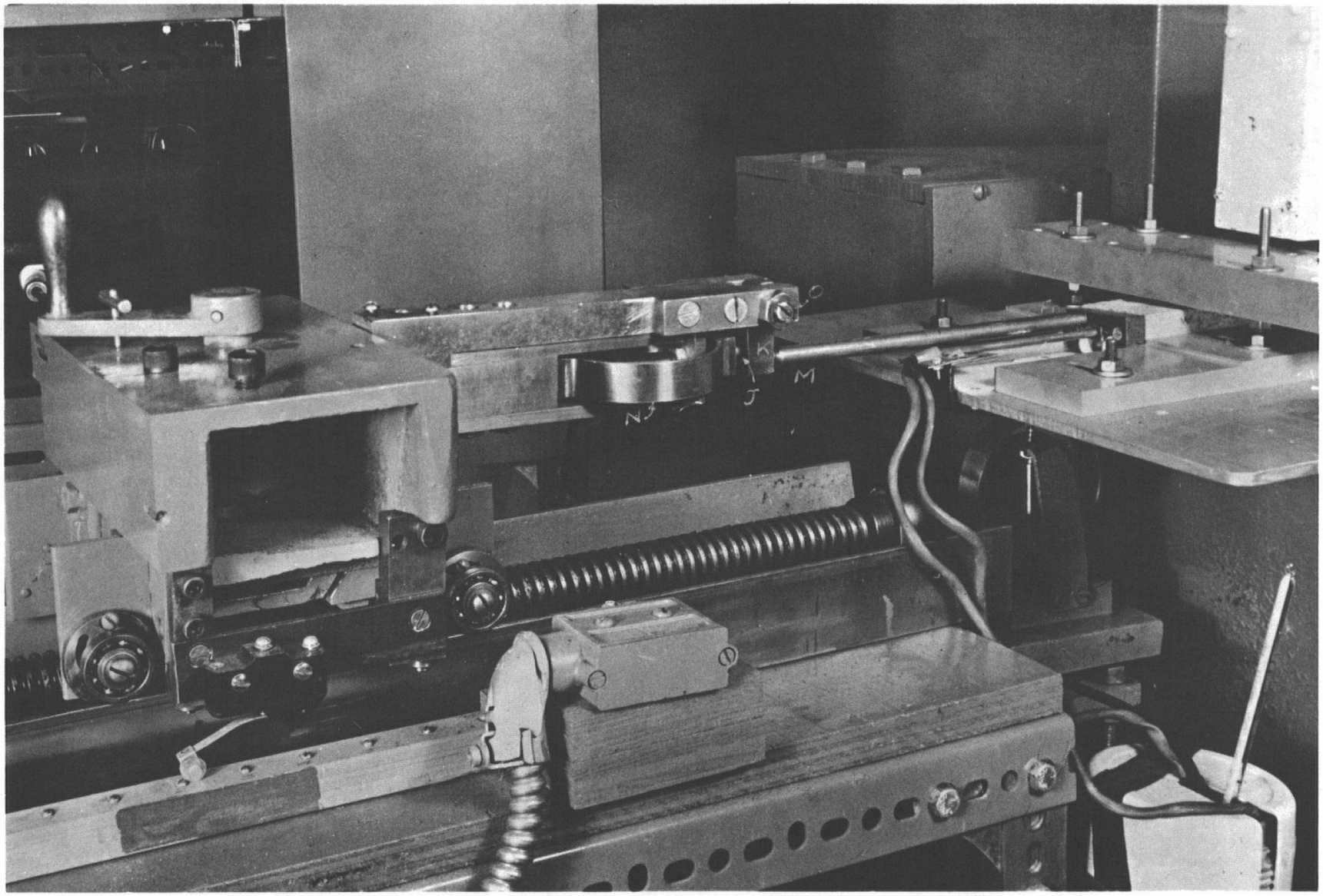

Fig. 9 Carriage, Power Screw and Push Rod for Feeding.

iv. Feed Speed

The feed speed was obtained by timing the carriage over a known travel distance.

v. Cutting Temperature

Temperature was measured by means of a measuring probe which consisted of a 3/16 inch O.d., 11 inches long brass tube holding two chromel-constantan thermacouples. The thermacouples were connected in series with the cold junctions being placed in an ice bath. The tip of the brass tube was insulated by a Teflon ring (Fig. 10).

A 9/32 inch diameter hole was drilled through each wood specimen along its longitudinal axis. The probe was inserted through this hole and was fixed in position by a copper clamp fastened to the front edge of the table. The tip of the probe was adjusted so that it was 1/8 inch from the cutting edge of the disk. Since the probe was fixed on the tabel, the hot junctions of the thermocouples remained in the same position during cutting. Fig. 10a shows that outer edge of the Teflon ring was tapered in order to equalize the distance between the sawing edge and the two thermocouples.

The signal from the thermocouples was amplified by a "Brush" D.C. amplifier (Model BL-932) and the resulting voltage was used to drive a "Brush" oscillograph (Model RD-2622-02). The marker switch on the push rod carriage was also connected to this oscillograph in order to operate its marker recorder pen (Fig. 8). By this connection a chart record of cutting temperature versus displacement of the wood specimen could be obtained. The thermocouple chart was calibrated to give a direct reading of the cutting temperature in degrees F. The method of calibration is described in Appendix C.

However, it should be stated that the temperatures measured were not entirely representative of true interface values.

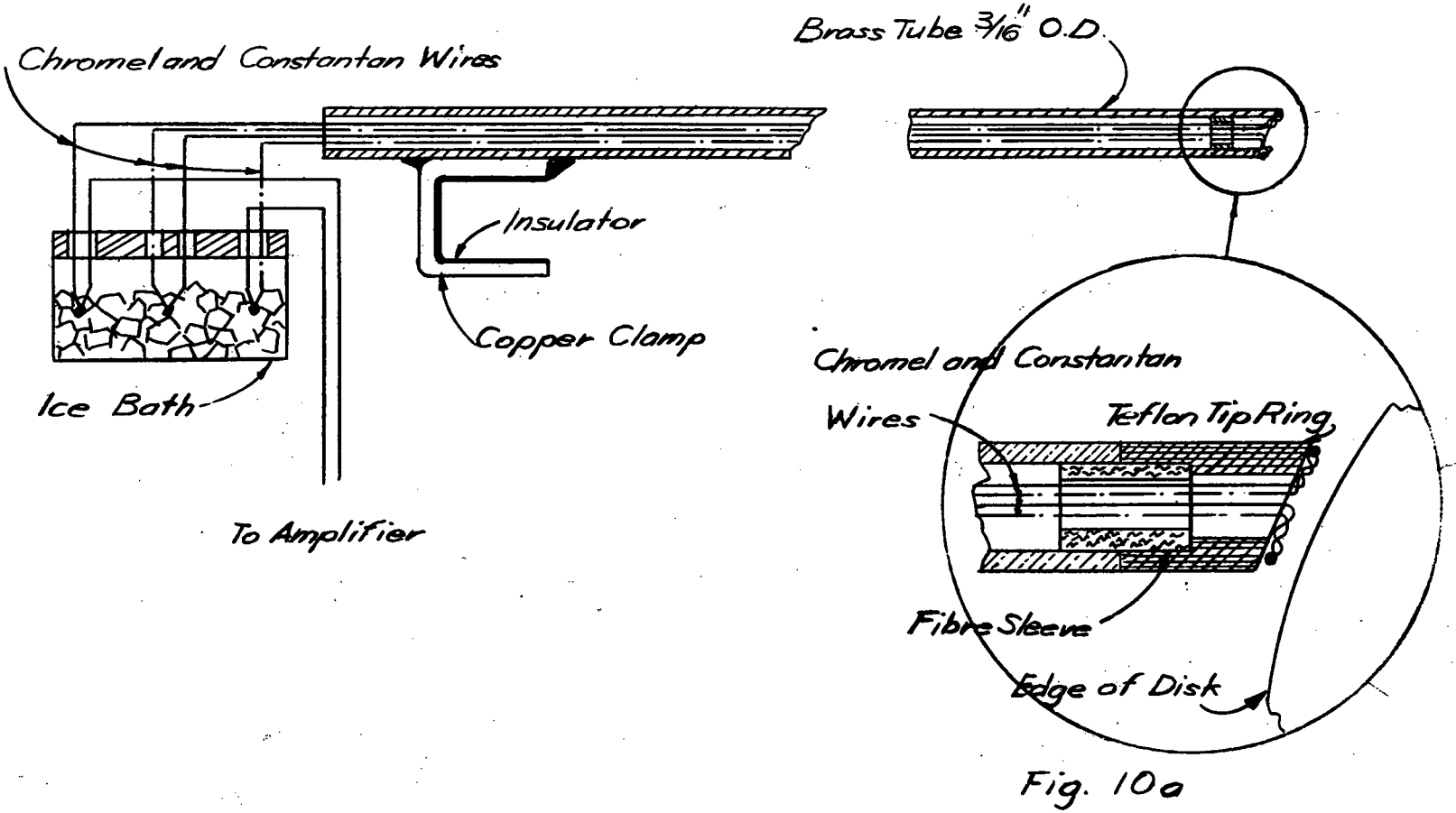

Fig. 10 Detail of Temperature Measuring Probe

vi. Specimen Weight

The weight was determined by a Howe scale having a range from 0 to 1 pound.

vii. Specimen Centre of Gravity

The distance of the centre of gravity of a specimen from its rear edge was determined by the use of a knife edge.

viii. Coefficient of Friction (μ) between the Wood Specimen and the Sawing Disk (Fig. 11).

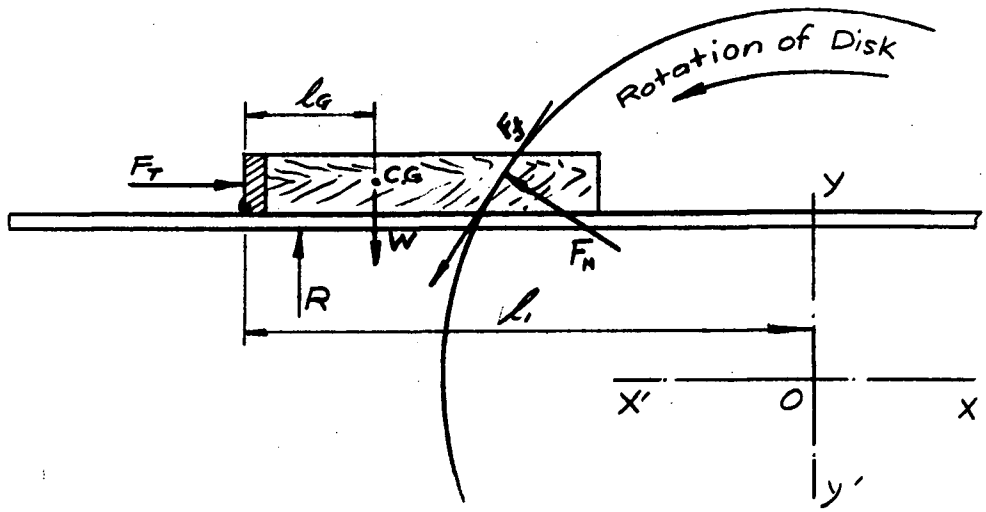

Fig. 11 Forces on Wood Specimen.

F_N = Normal force on the cutting edge;

F_f = Friction force on the cutting edge;

F_T = Feeding thrust;

R = Table support strain ring reaction;

W = Weight of specimen;

l_1 = Distance between tail edge of wood and y-y'.

l_G = Distance between tail edge and centre of gravity of wood.

The coefficient of friction between the wood specimen and the sawing disk was calculated by the following equations. The force analysis and derivation of these equations are described in Appendix E.

(a) Normal force exerted on the cutting face of the wood specimen by the sawing disk:

$$F_N = 0.789\ F_T + 0.614\ K$$

$$\text{Where } K = \frac{(\ell_G - \ell_1)W + 13.95\ R}{5.53}$$

(b) Frictional force between the wood specimen and the sawing disk:

$$F_f = 0.614\ F_T - 0.789\ K$$

(c) The coefficient of friction:

$$\mu = \frac{F_f}{F_N} = \frac{0.614\ F_T - 0.789\ K}{0.789\ F_T - 0.614\ K}$$

III.3 SPECIMENS

Edge grain green fir and red cedar were selected for the specimens. The dimensions of each specimen were 8 inches x 2 inches x 1 inch. Half of the specimens of each type of wood were cut with the wood grain along the 8 inch side of the specimen. The remaining specimens were cut with the grain along the 2 inch side of the specimen. The former specimens were used for along-the-grain cutting and the latter were used for across-the-grain cutting.

In order to investigate the influence of moisture content on sawing, the specimens were seasoned to six different moisture contents. The average moisture contents were 11%, 19%, 25%, 32%, 34% and 72%. The method of seasoning is described in Appendix D.

After seasoning a 9/32 inch dia. hole was drilled through each specimen along the longitudinal axis (Fig. 12). A tail piece was fastened to one end of the specimen. The tail piece was made of Formica fibre board with Teflon rollers affixed at the lower corner in order to minimize the friction between the table and the specimen.

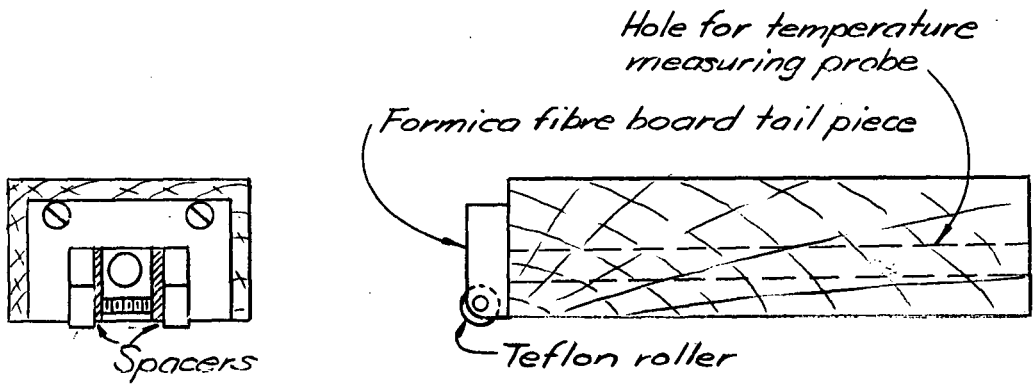

Fig. 12 Wood Specimen and Tail Piece

III.4 EXPERIMENTAL PROCEDURE

At the beginning of each set of experiments the electronic instruments were warmed up until they were stable. When there was no load on the table and the feeding push rod the correct reading of the force measuring instruments was zero; the reading of temperature measuring instruments was $32^{o}F$ with the probe tip being immersed in ice. The adjusting procedure was repeated every three hours in order to correct for instrument drift.

Before each experiment the rim of the sawing disk was cleaned with a strip of copper in order to remove the residue composed of resin, carbon and sawdust which had adhered on the rim from previous cutting.

The experiments were carried out under five different feeding speeds in order to study the influence of feeding speed on cutting. The speeds used were 4, 8, 12, 16 and 18 inches per minute.

The specimen weight and centre of gravity was determined immediately before each test. The carriage was then engaged to the power screw and was stopped automatically after 5 inches of cutting by a stop switch. The cut specimen was detached from its tail piece and weighed, thus giving the weight W_c before kiln drying. The specimen was then placed in an oven maintained at a temperature of 250^{o}F and was dried until constant weight was obtained - this weight was the oven dried weight, W_D, of the specimen. The actual moisture content was determined as follows:

$$\text{Moisture Content} = \frac{W_C - W_D}{W_D} \times 100\%$$

Where

W_C = weight of specimen after being cut and before being dried;

W_D = oven-dried weight of specimen.

CHAPTER IV

IV.1 RESULTS

(1a) Friction Force (F_f) versus Feed Speed (V_f) and Normal Force (F_N) versus Feed Speed (V_f) (Fig. 13 to 24 inclusive)

The forces increase as the feed speed increases independently of the moisture content. In general, cutting forces for fir are greater than those for cedar. The slopes of the curves for the normal forces (F_N) increase at a greater rate than the curves for frictional forces (F_f).

(1b) Coefficient of Friction versus Feed Speed (Fig. 25 to 30 inclusive)

There are two different shapes of curves. One group of the curves are concave upward, high values of μ occur at very low and very high feed speeds. Another group of curves are just the reverse - they are concave downward with low values of μ at very low and very high feed speeds.

(1c) Frictional Force (F_f) versus Moisture Content (Fig. 31 to 34 inclusive)

No significant variations of frictional force (F_f) with moisture content are evident. However, it may be stated that the forces are slightly

smaller at the high moisture contents.

(1d) Power Consumed versus Feed Speed (Fig. 35 to 40 inclusive)

The values of power consumed was obtained from the following equation:

$$H.P. = \frac{F_f \pi D N}{33,000}$$

Where F_f = frictional force in lbs.

D = disk diameter in ft.

N = rotating speed of disk in rpm.

All the horsepower curves rise as feed speed increases.

(1e) Cutting Temperature versus Feed Speed (Fig. 41)

The cutting temperature rises as feed speed or thrust increases.

(1f) Power Consumed versus Moisture Content (Fig. 42 and 43)

There is no significant change in power consumed for variation in moisture content.

(1g) Appearance of Cut Surfaces

Examination of the wood specimens after being cut revealed that the width of the kerf was almost the same as the thickness of the disk. The cut surfaces were smooth and polished and were of a dark brown colour. Examination of the cut surfaces at a magnification of 10x showed that the whole surface was covered with a layer of resin which appeared to have melted and then set. In comparison with the ordinary sawn surfaces the friction cut surface was far more smooth. (Fig. 44 and 45).

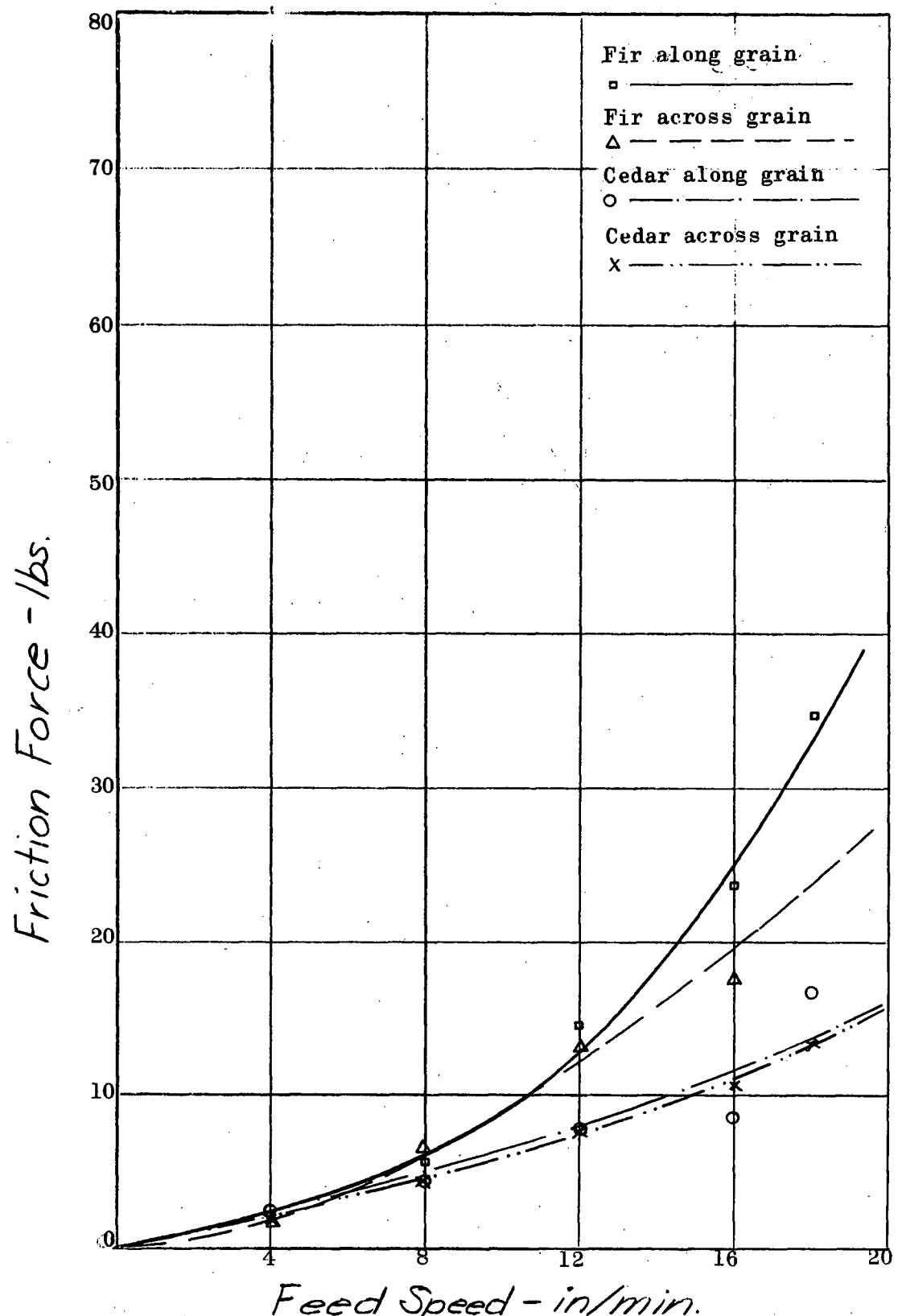

Fig. 13 Graph of Frictional Force versus Feed Speed with Moisture content 11%.

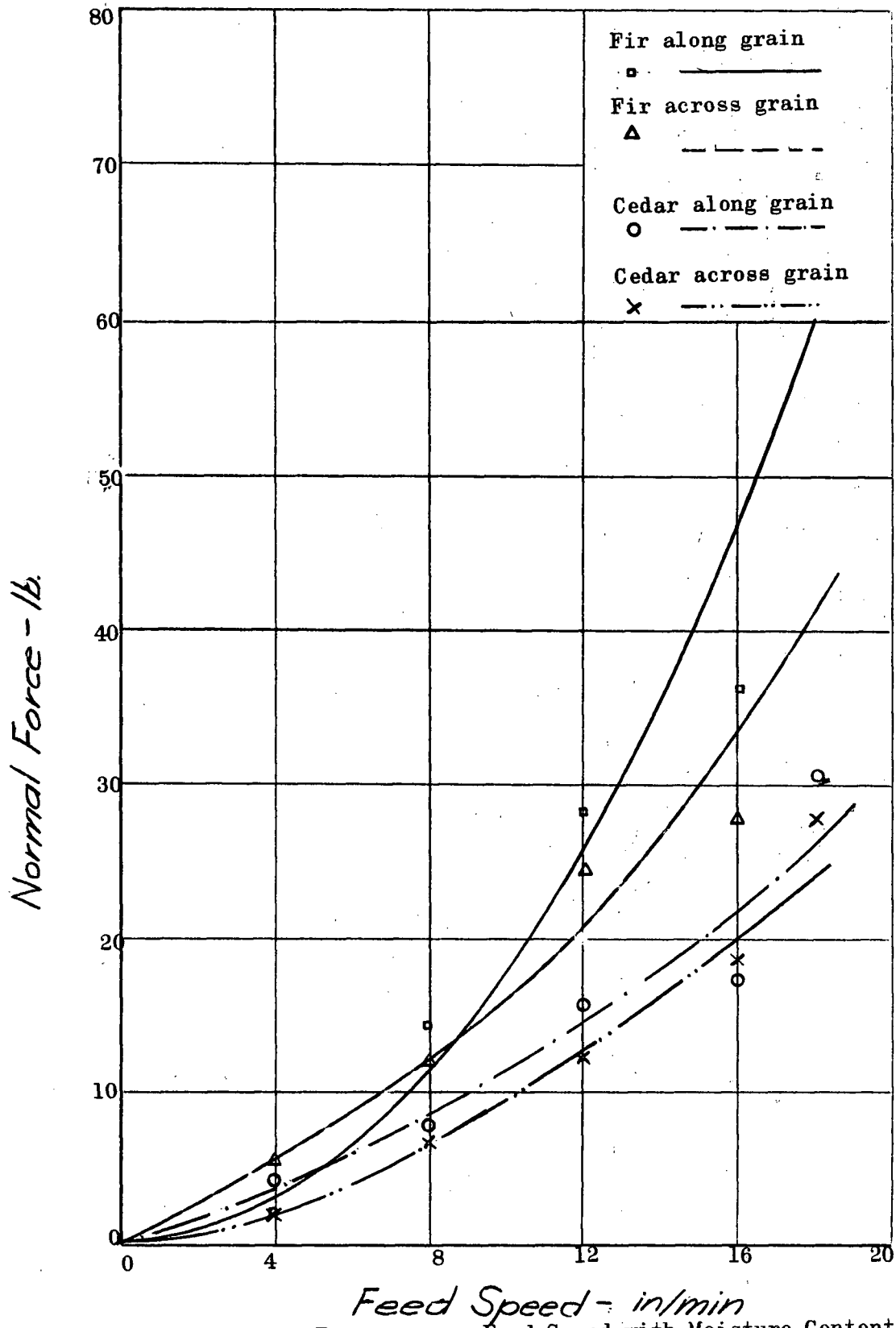

Fig. 14 Graph of Normal Force versus Feed Speed with Moisture Content - 11%.

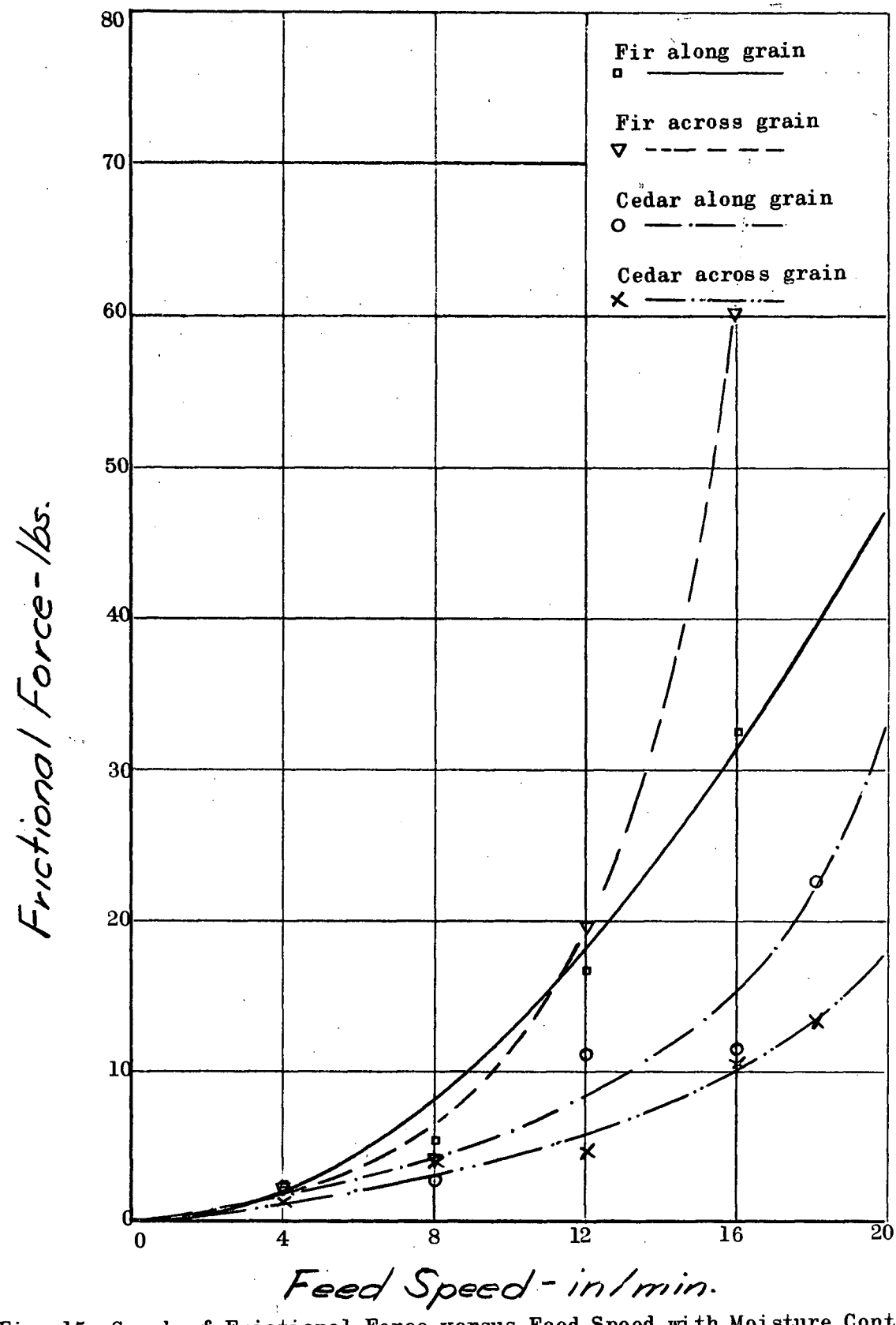

Fig. 15 Graph of Frictional Force versus Feed Speed with Moisture Content=19%.

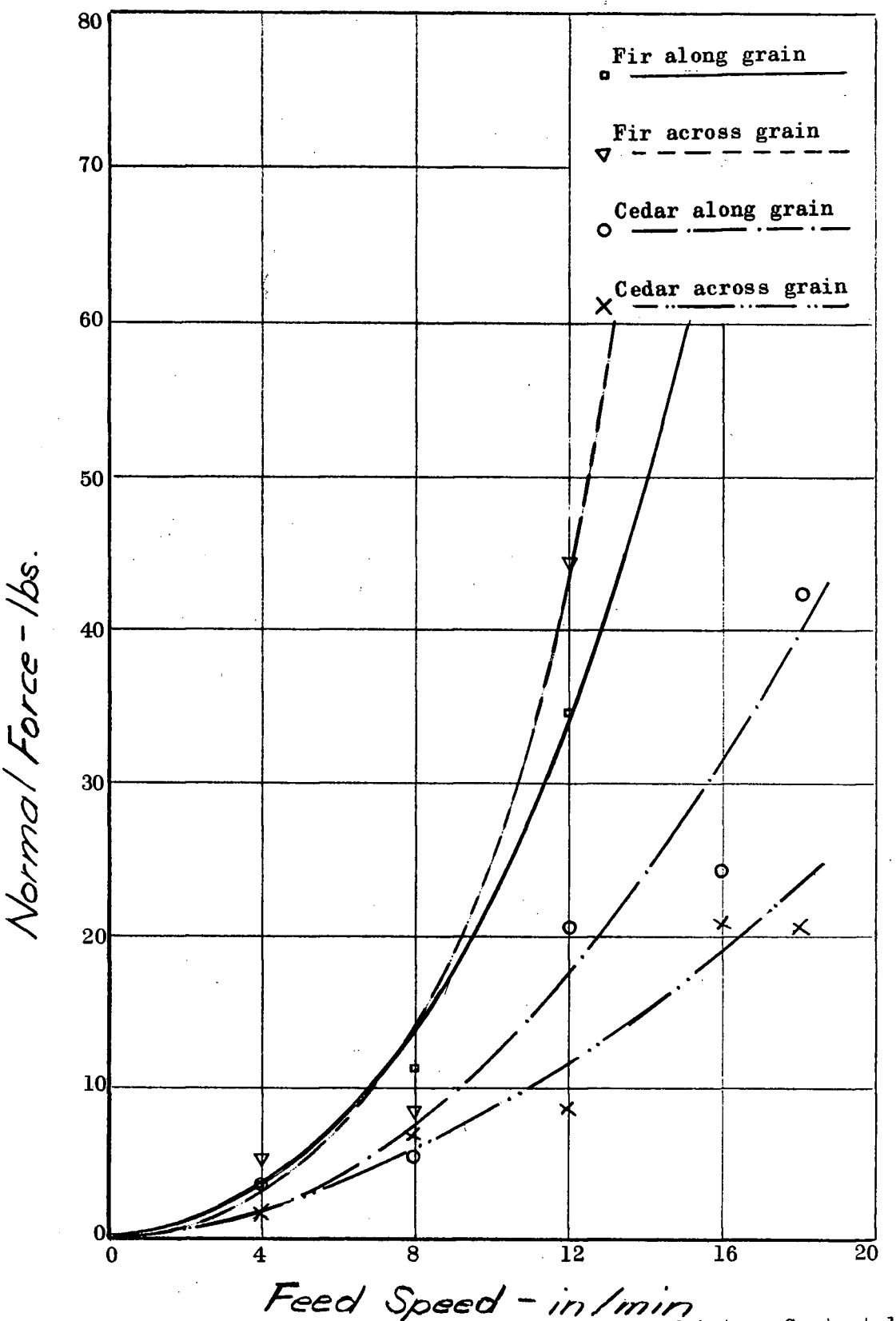

Fig. 16 Graph of Normal Force versus Feed Speed with Moisture Content=19%.

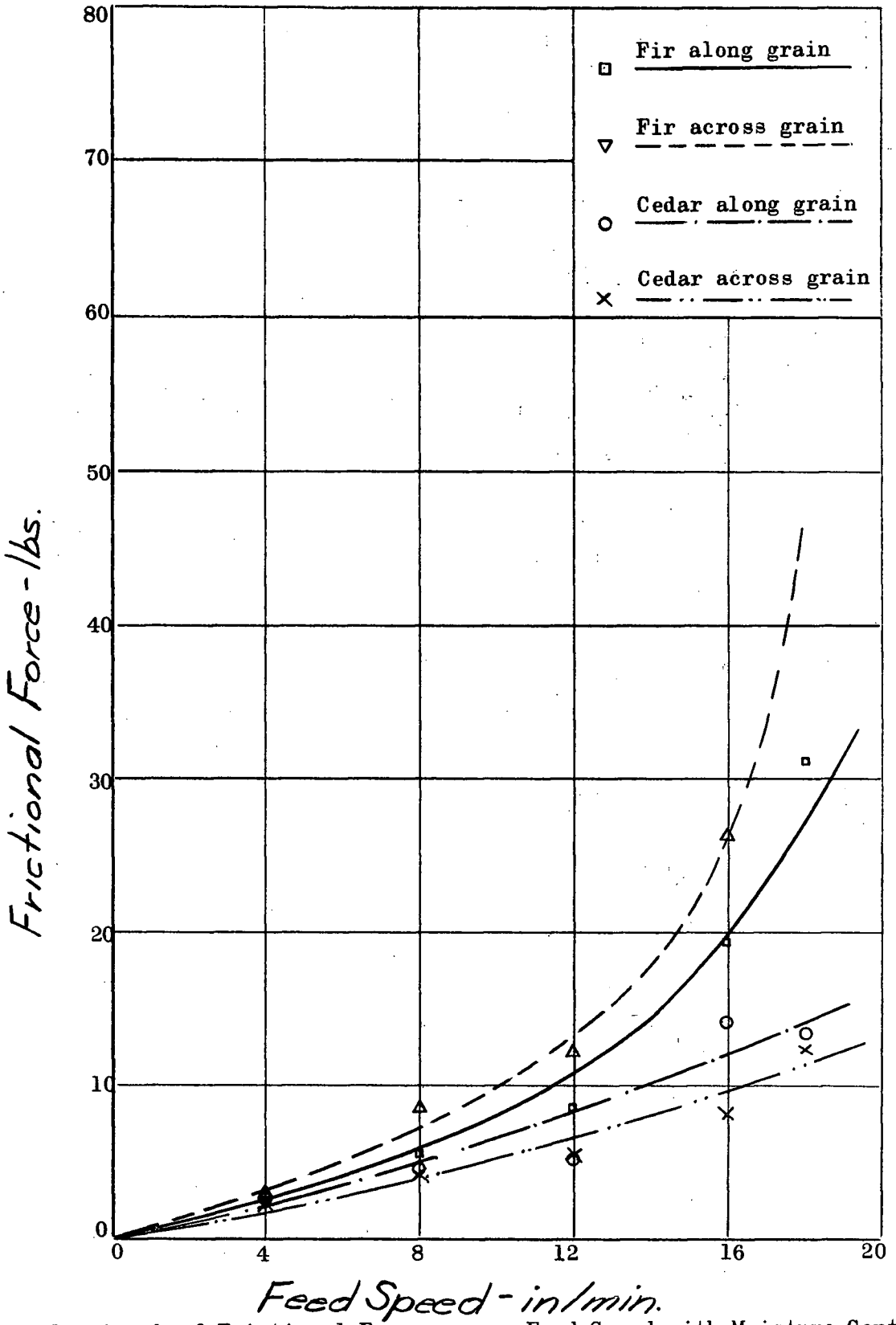

Fig. 17 Graph of Frictional Force versus Feed Speed with Moisture Content=25%.

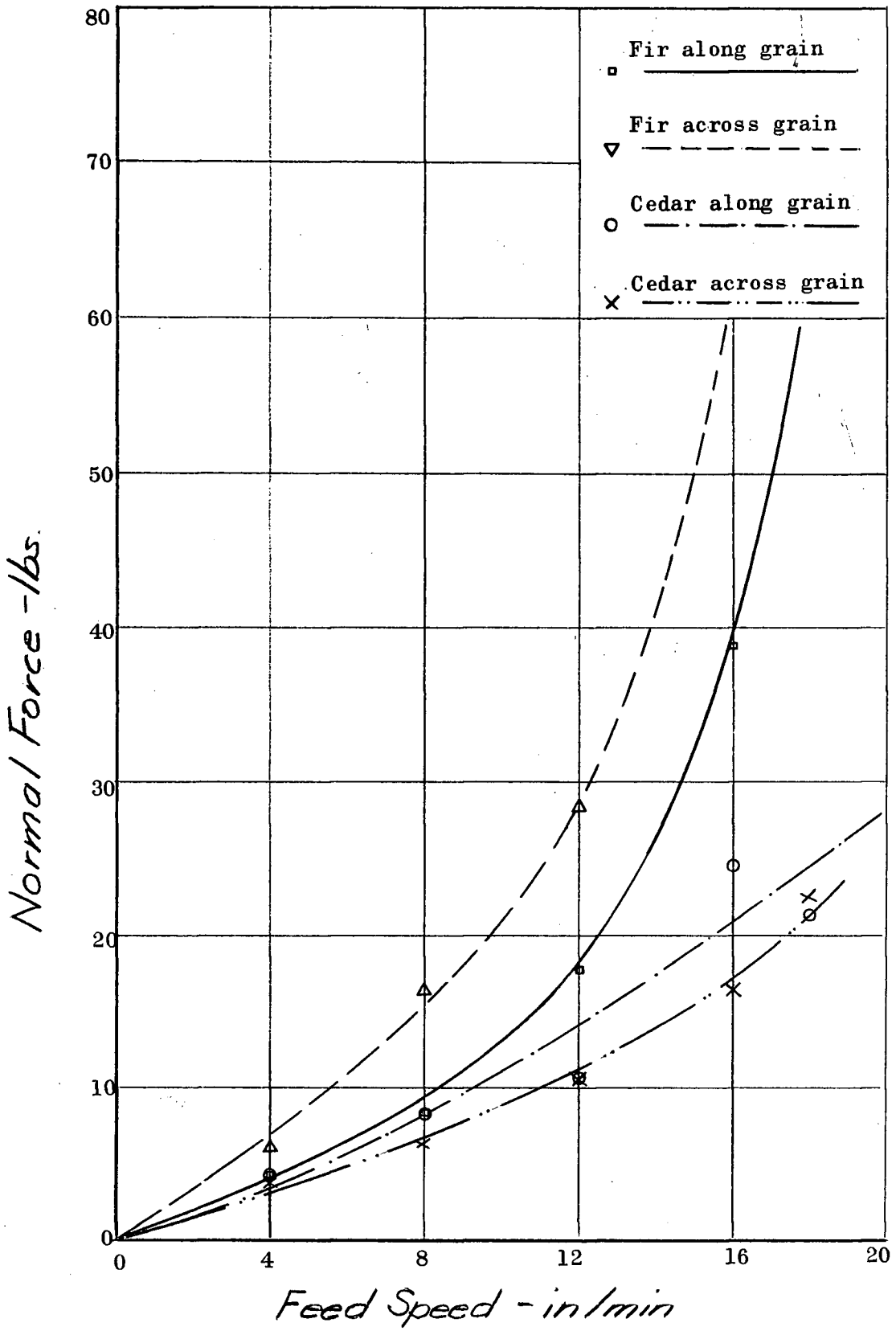

Fig. 18 Graph of Normal Force versus Feed Speed with Moisture Content = 25%.

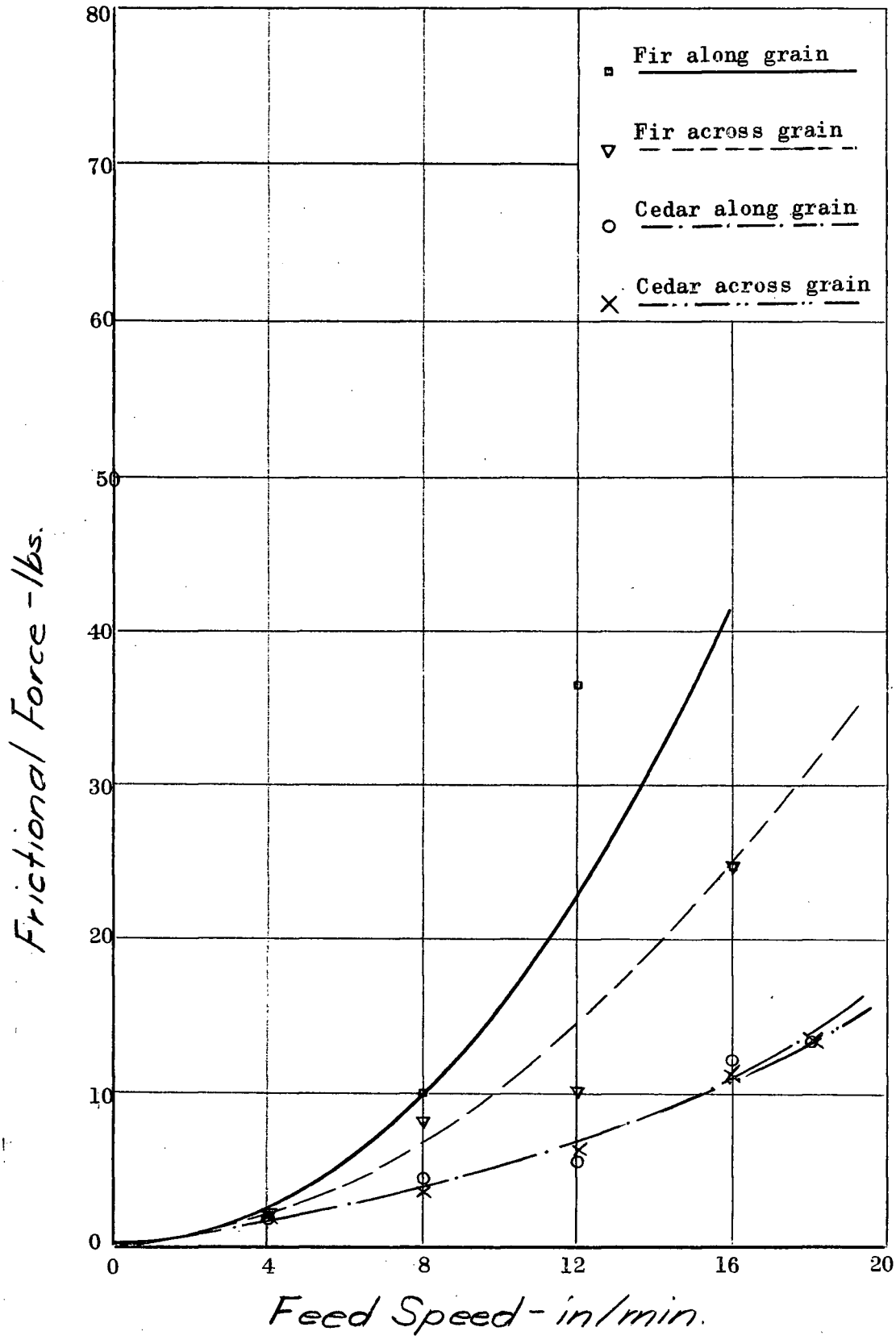

Fig. 19 Graph of Frictional Force versus Feed Speed with Moisture Content=32%.

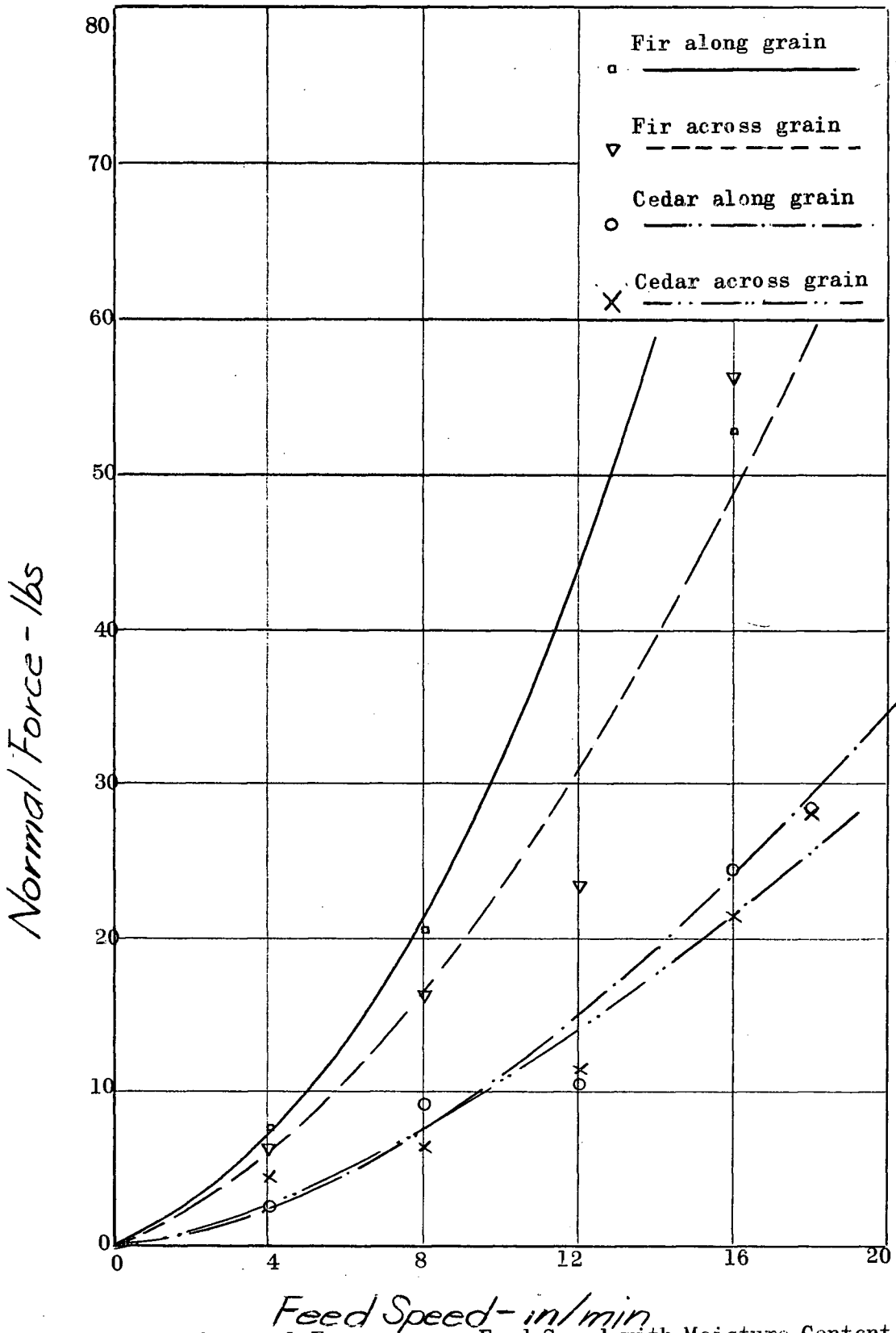

Fig. 20 Graph of Normal Force versus Feed Speed with Moisture Content = 32%.

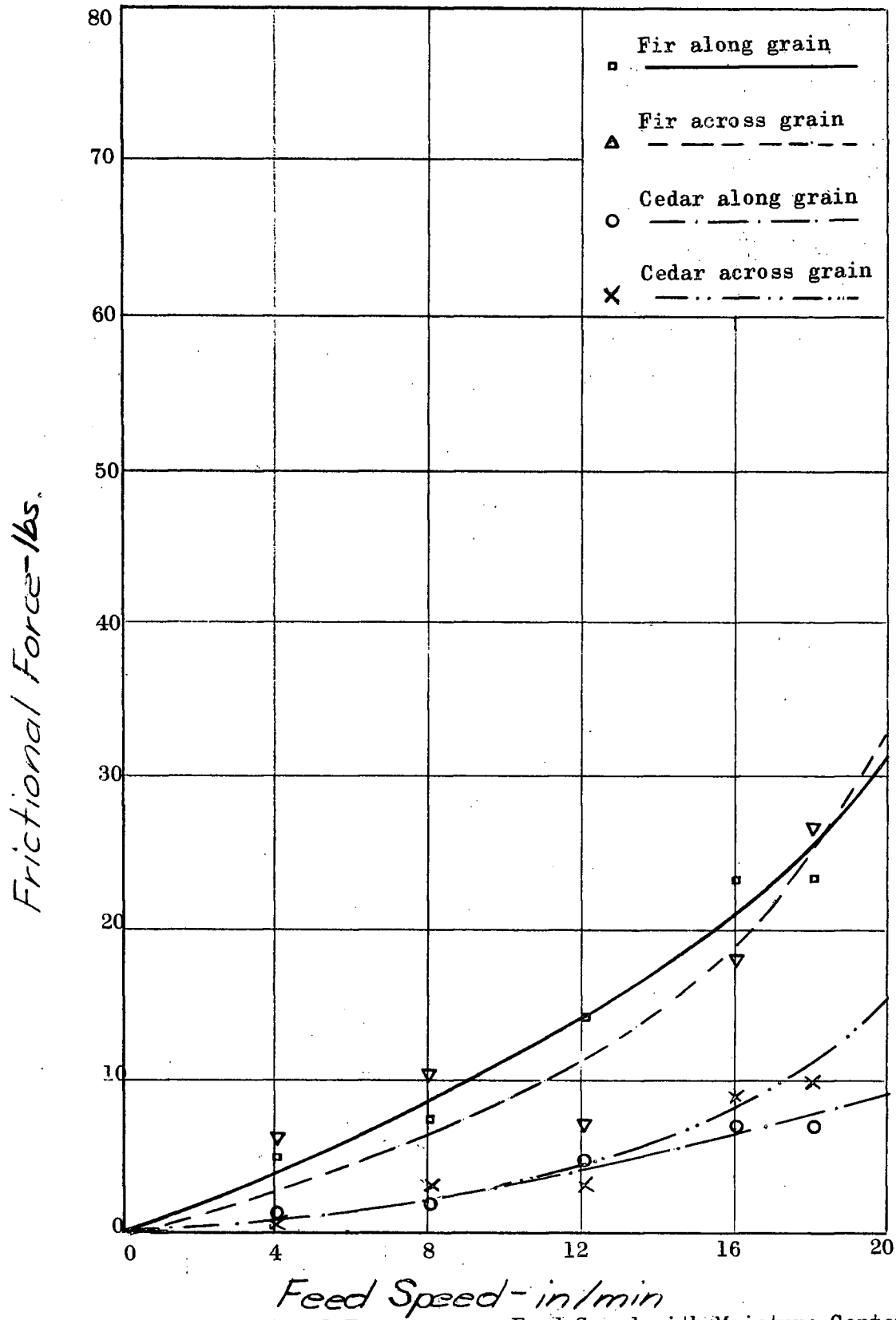

Fig. 21 Graph of Frictional Force versus Feed Speed with Moisture Content=34%.

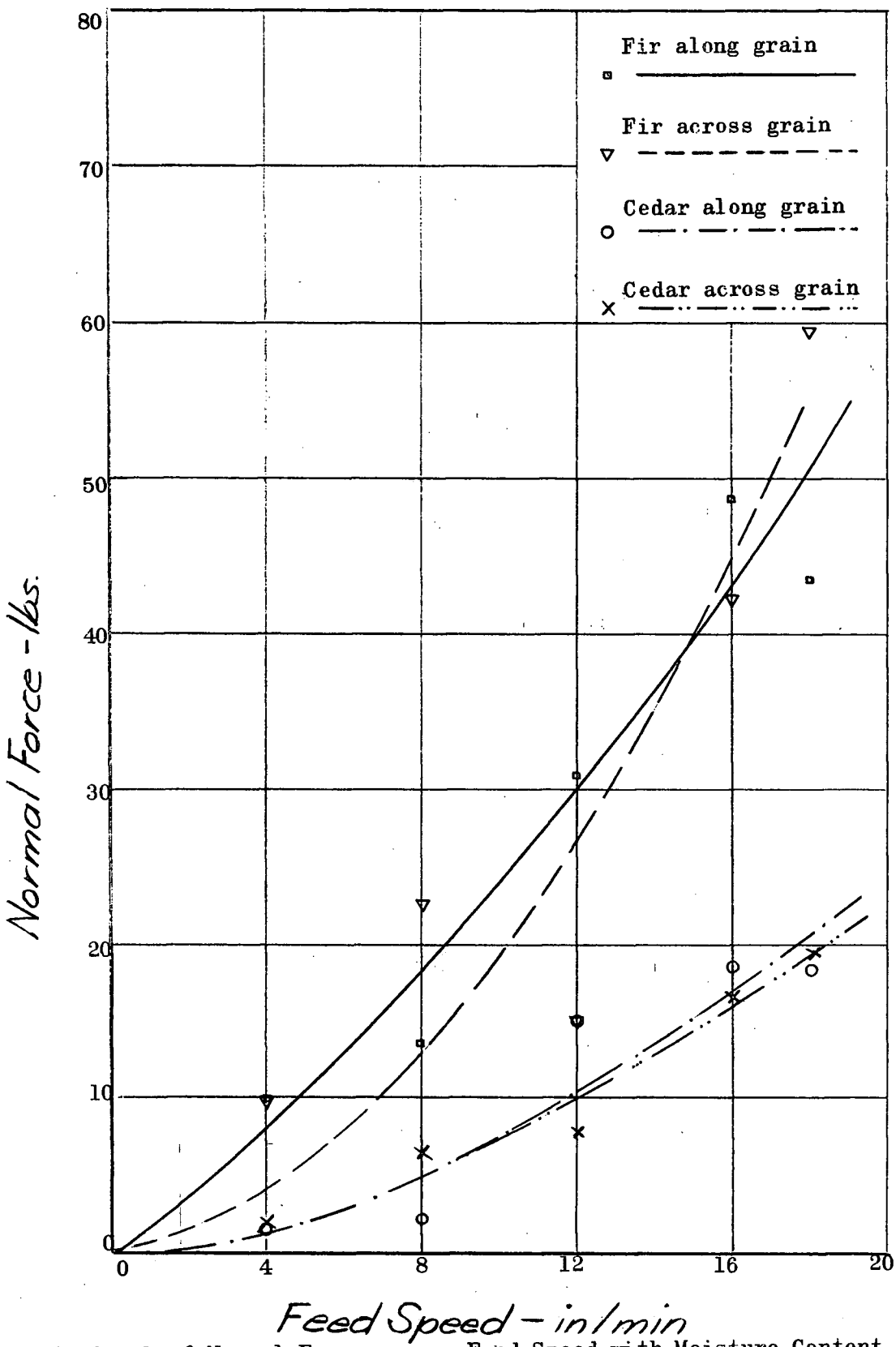

Fig. 22 Graph of Normal Force versus Feed Speed with Moisture Content = 34%.

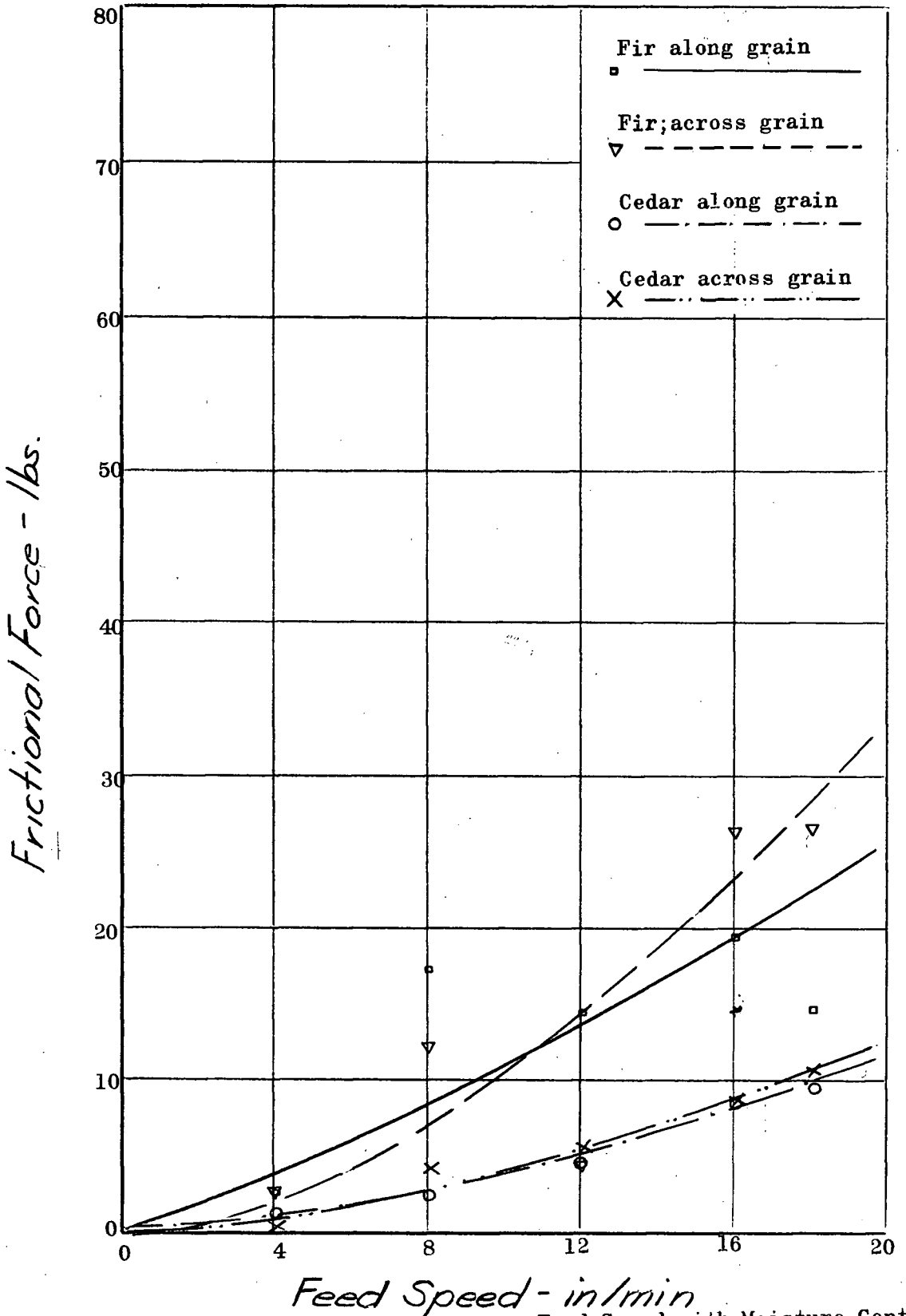

Fig. 23 Graph of Frictional Force versus Feed Speed with Moisture Content=72%.

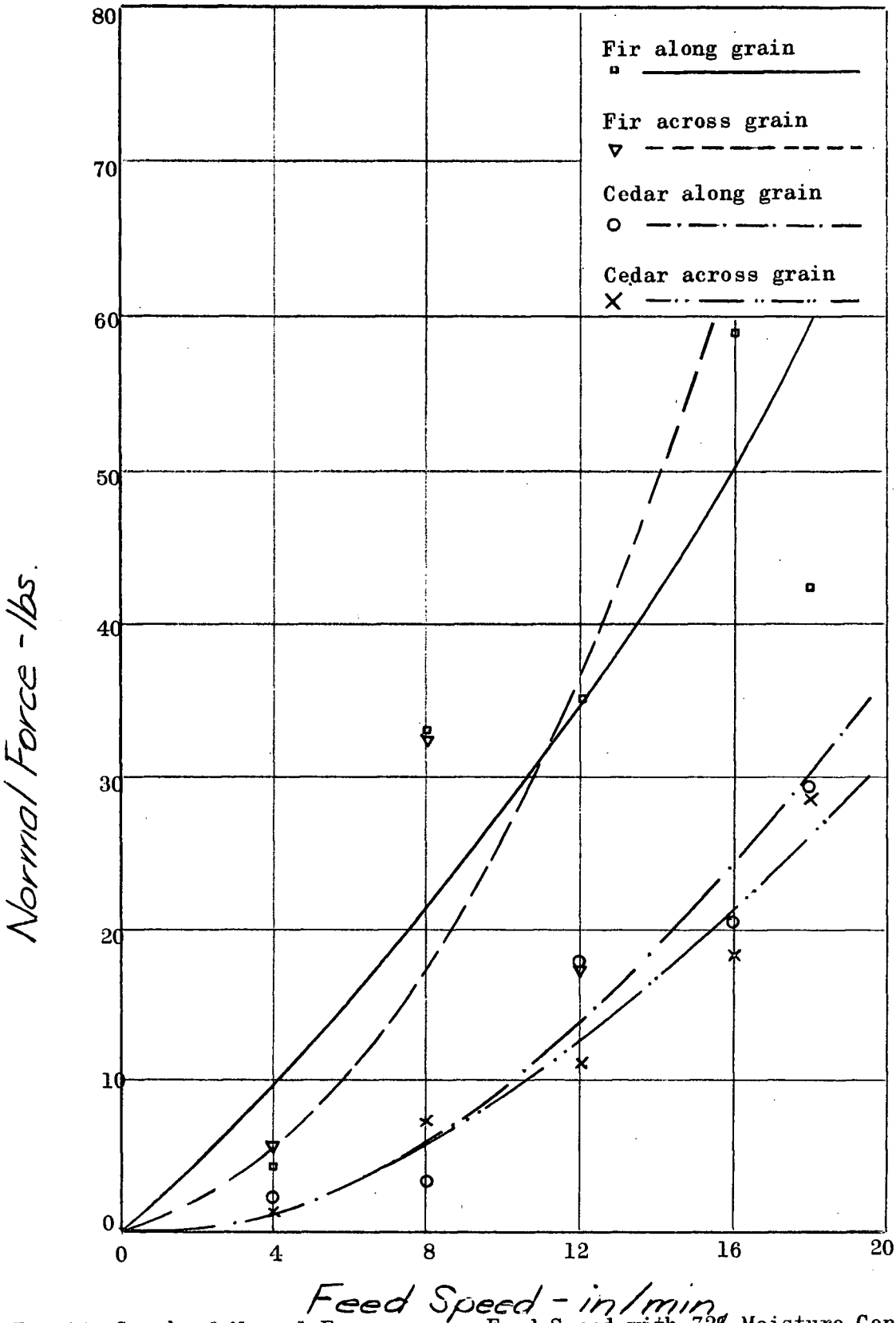

Fig.24 Graph of Normal Force versus Feed Speed with 72% Moisture Content.

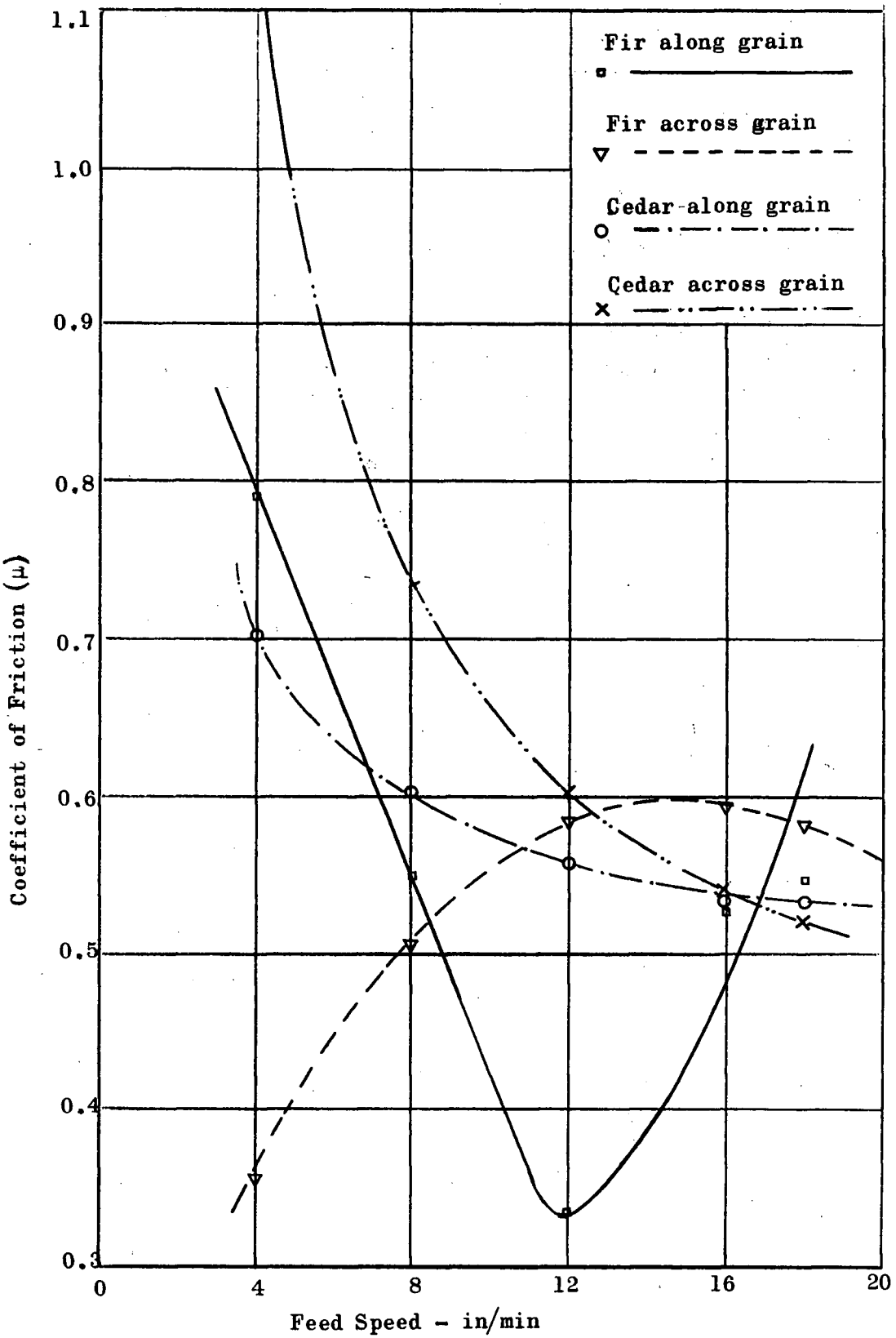

Fig. 25 Graph of Coefficient of Friction versus Feed Speed with 11% moisture content.

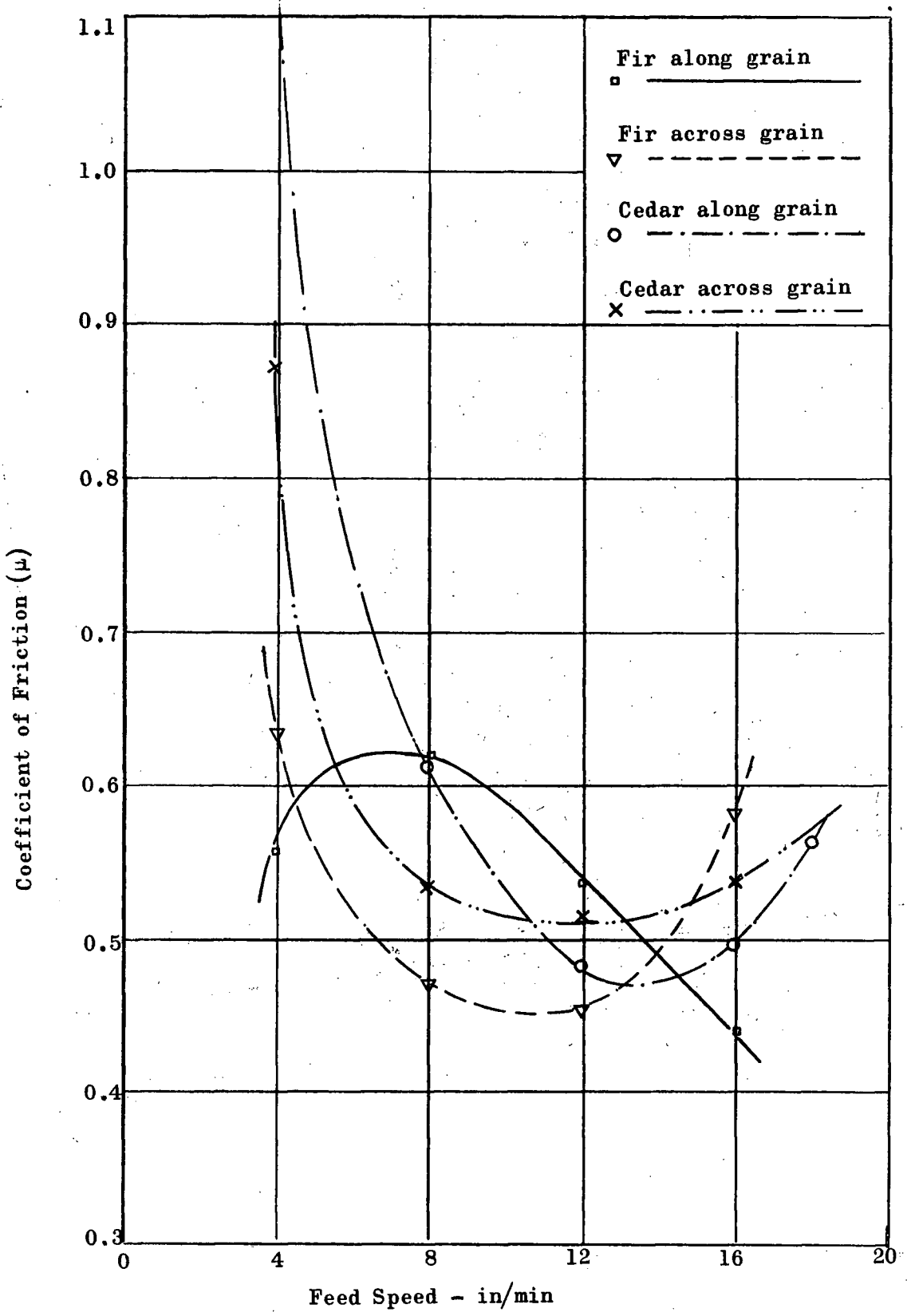

Fig. 26 Graph of Coefficient of Friction versus Feed Speed with 19% Moisture Content.

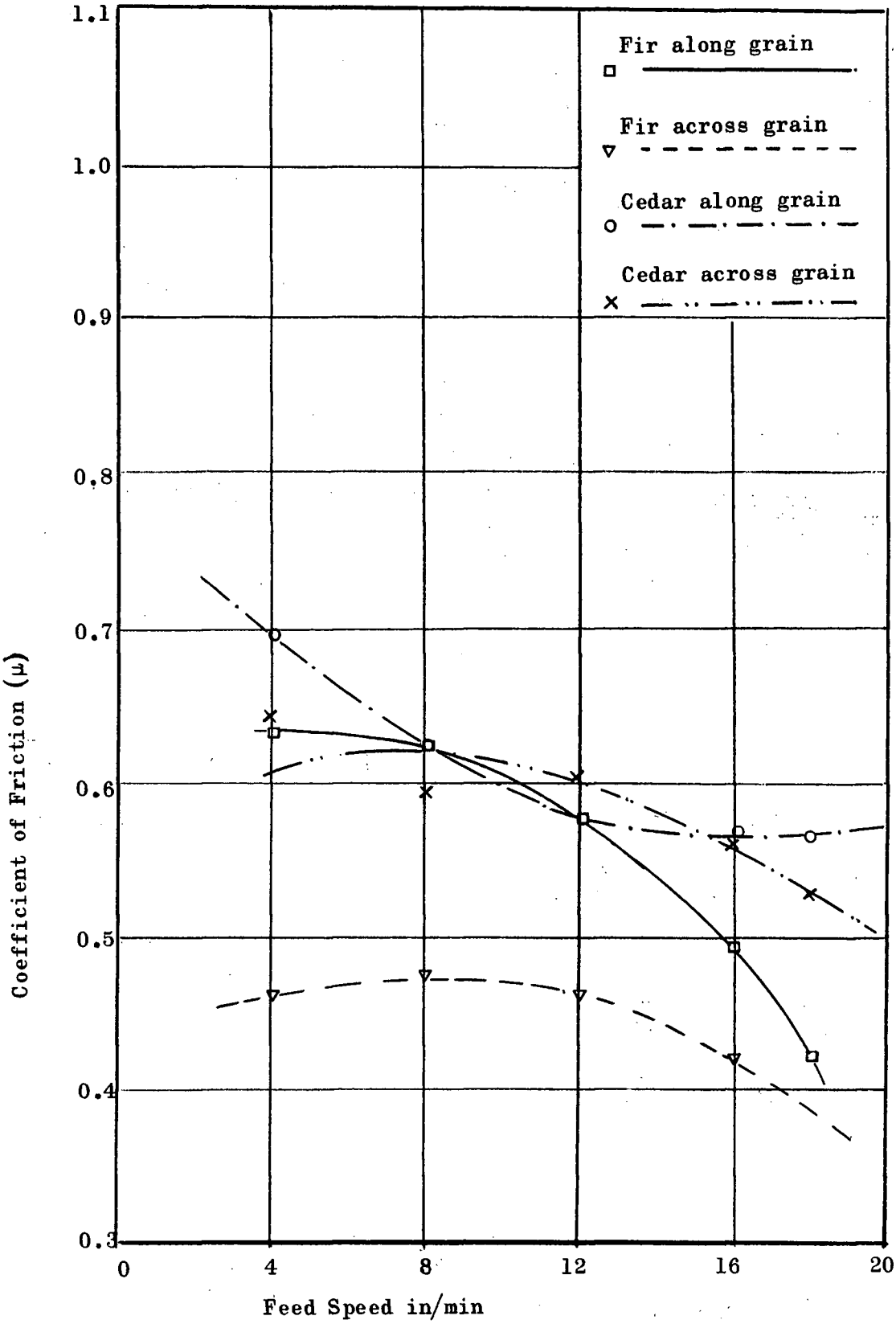

Fig. 27 Graph of Coefficient of Friction versus Feed Speed with 25% Moisture Content.

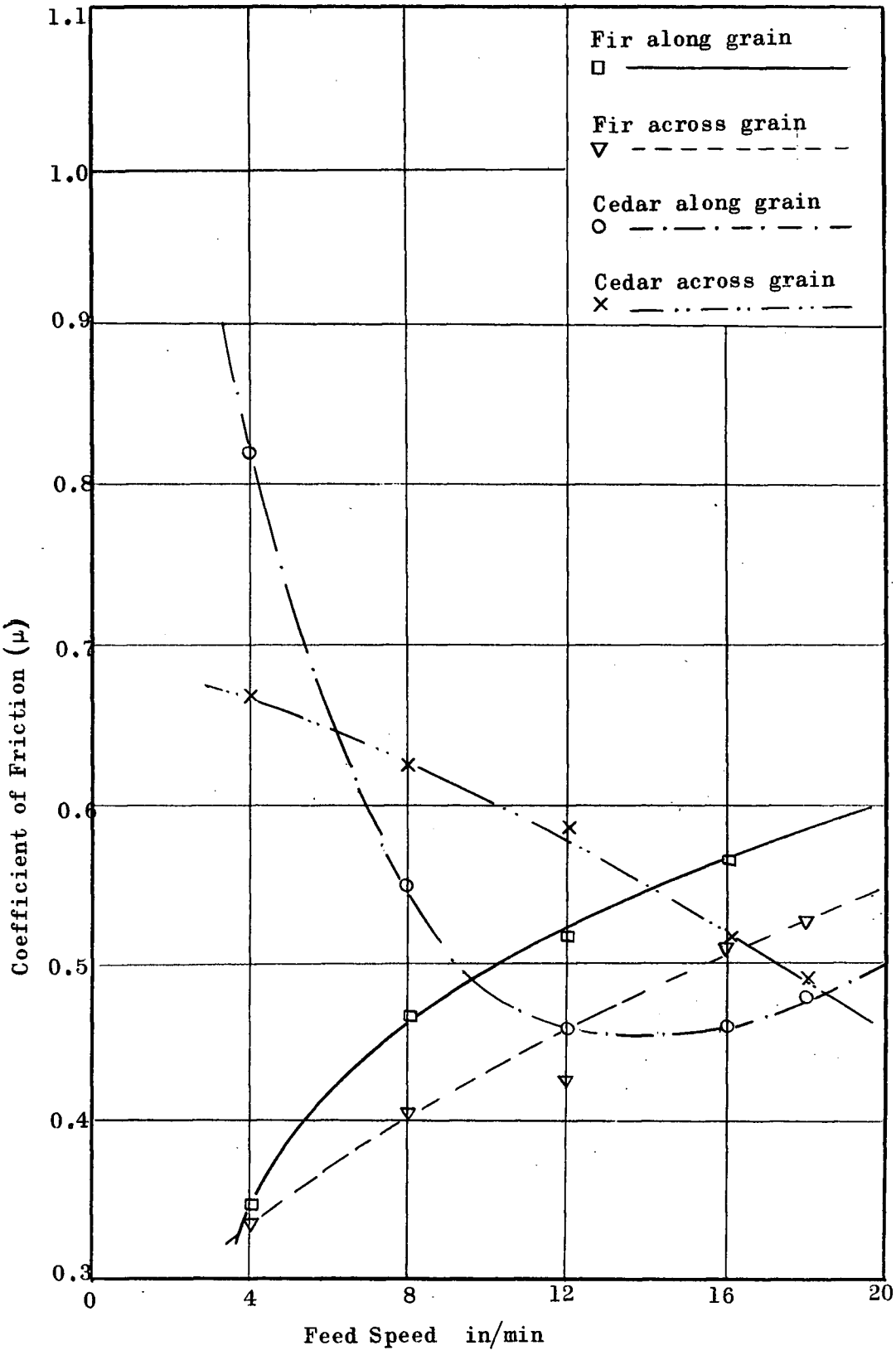

Fig. 28 Graph of Coefficient of Friction versus Feed Speed with 32% Moisture Content.

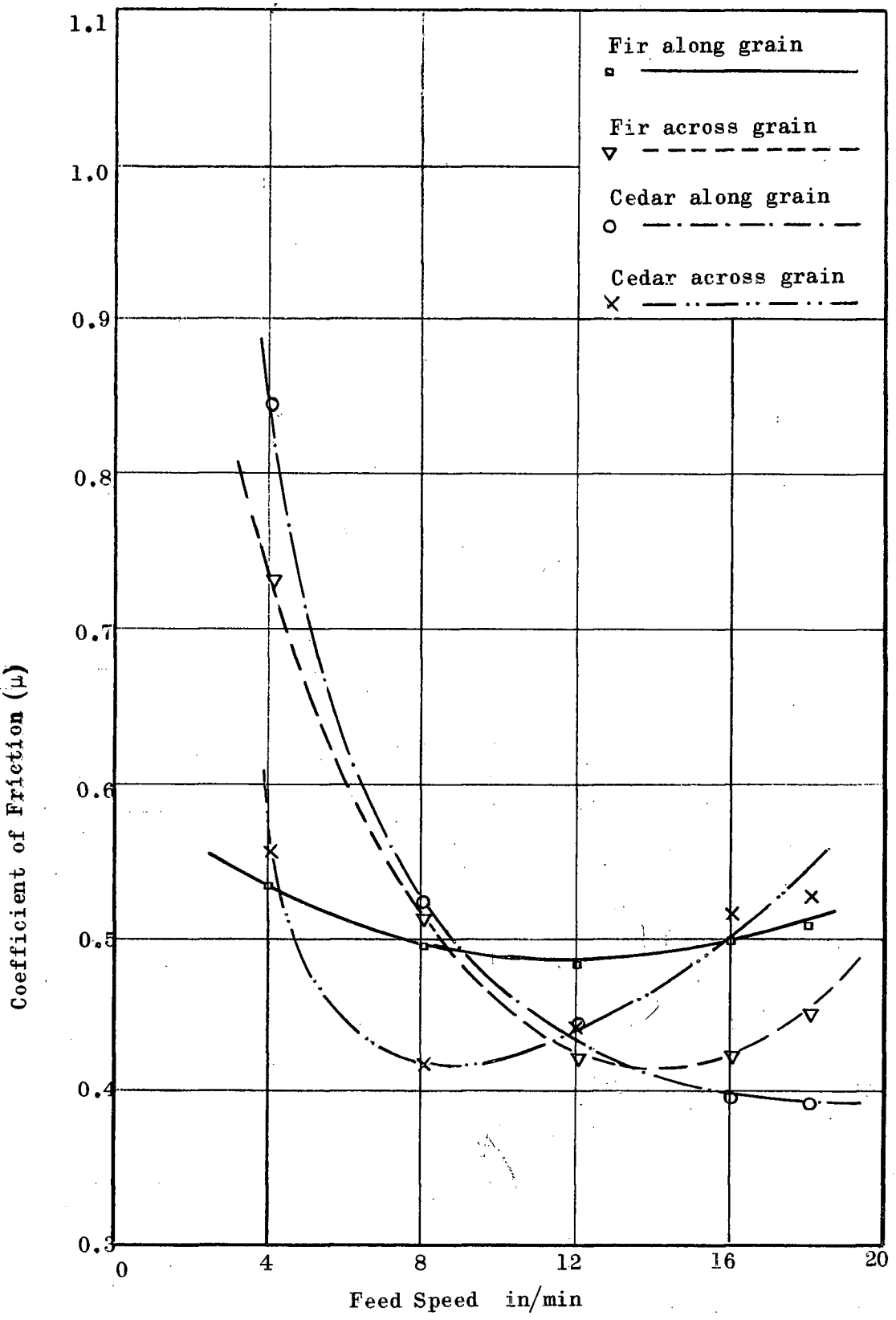

Fig. 29 Graph of Coefficient of Friction versus Feed Speed with 34% Moisture Content.

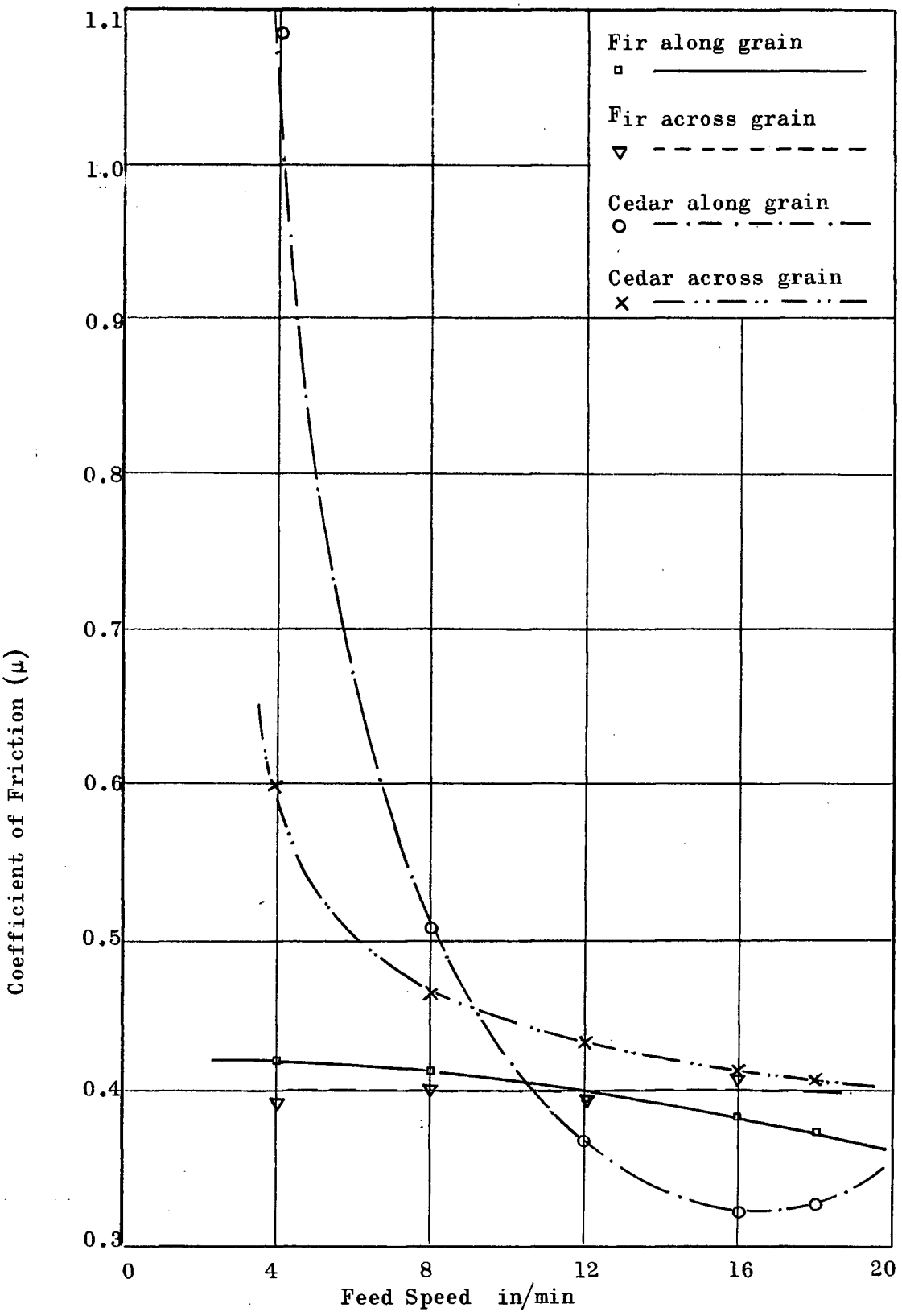

Fig. 30 Graph of Coefficient of Friction versus Feed Speed with 72% Moisture Content.

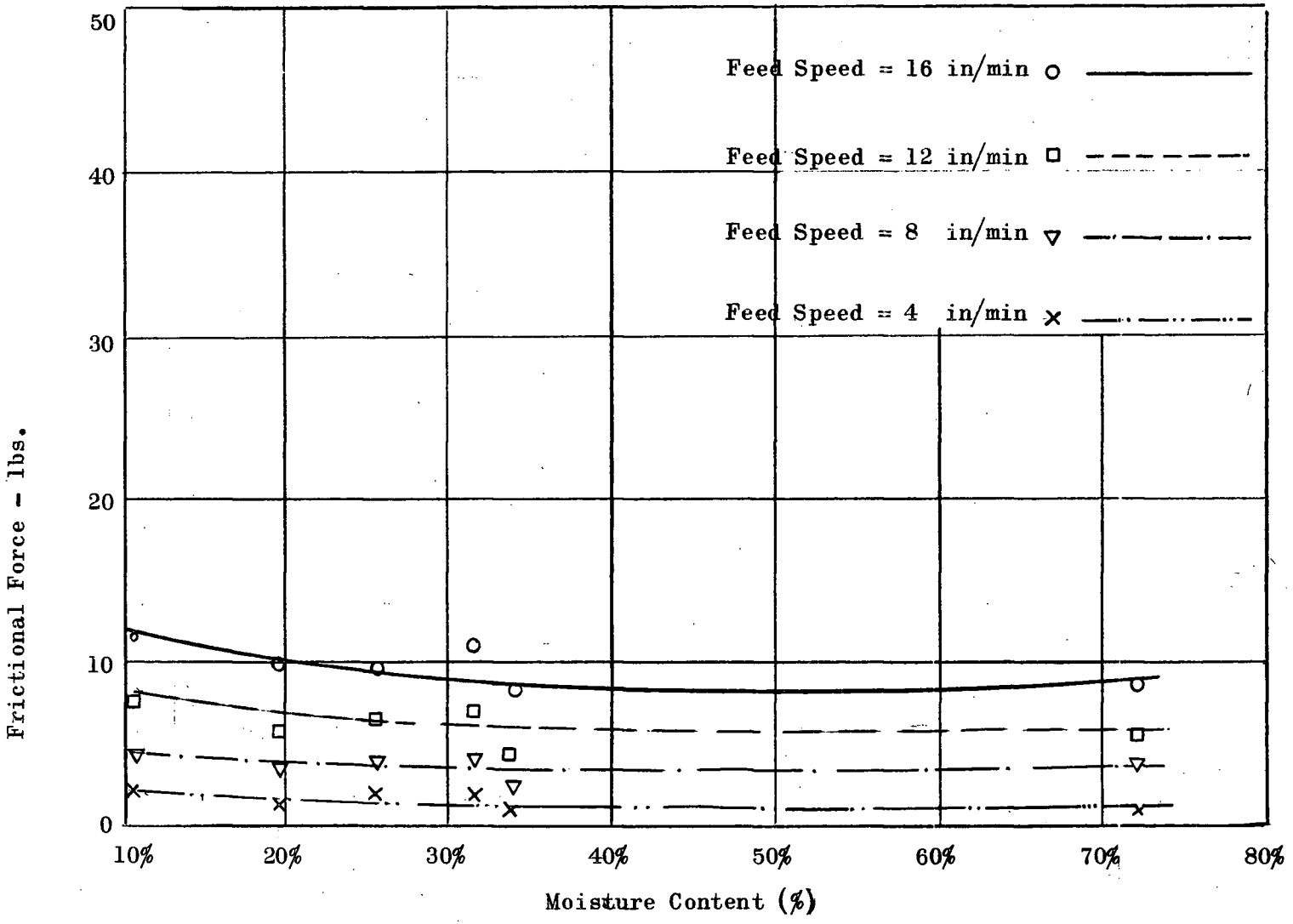

Fig. 31 Graph of Frictional Force Versus Moisture Content. Cedar Across Grain.

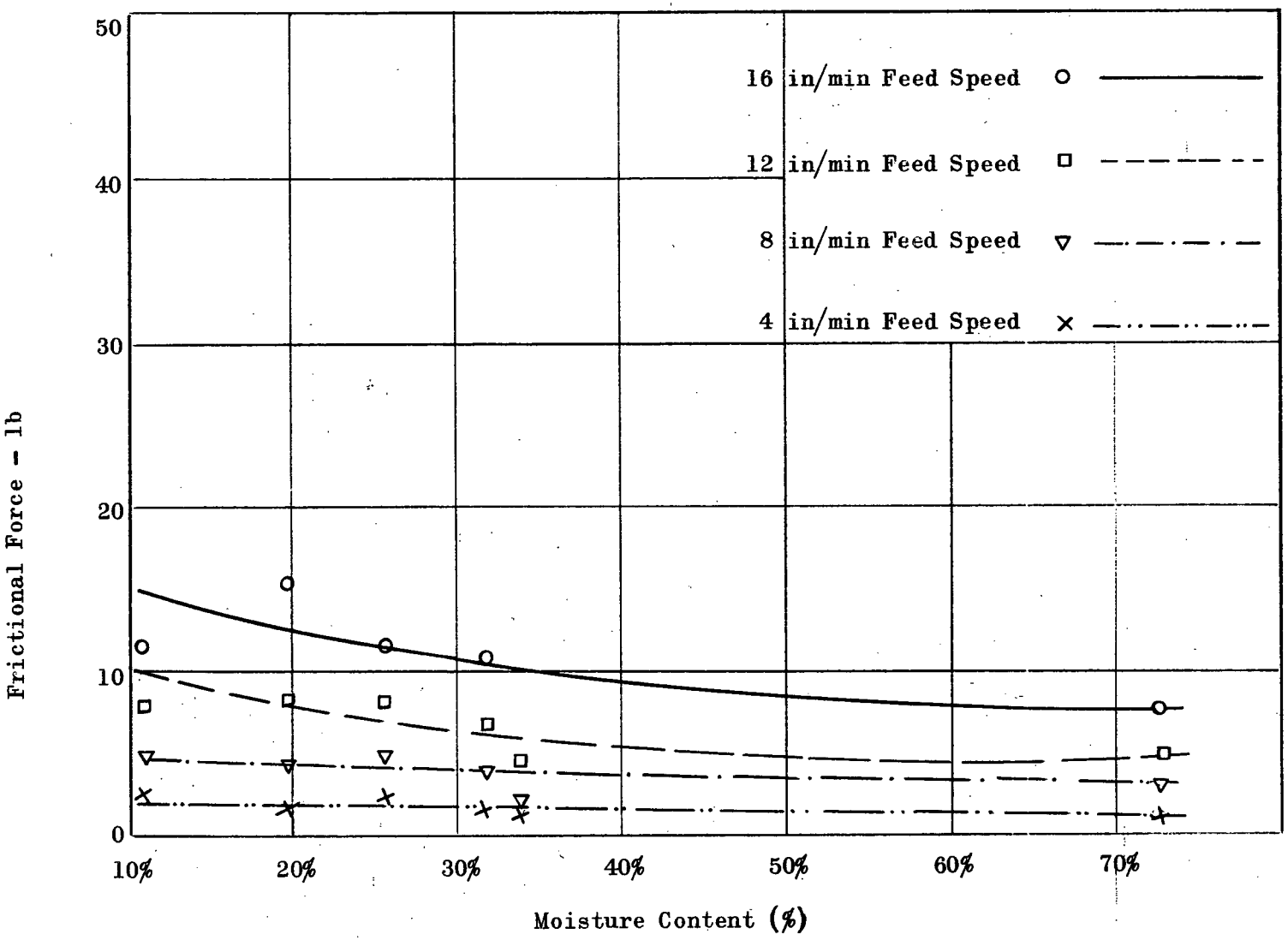

Fig. 32 Graph of Frictional Force versus Moisture Content - Cedar Along Grain

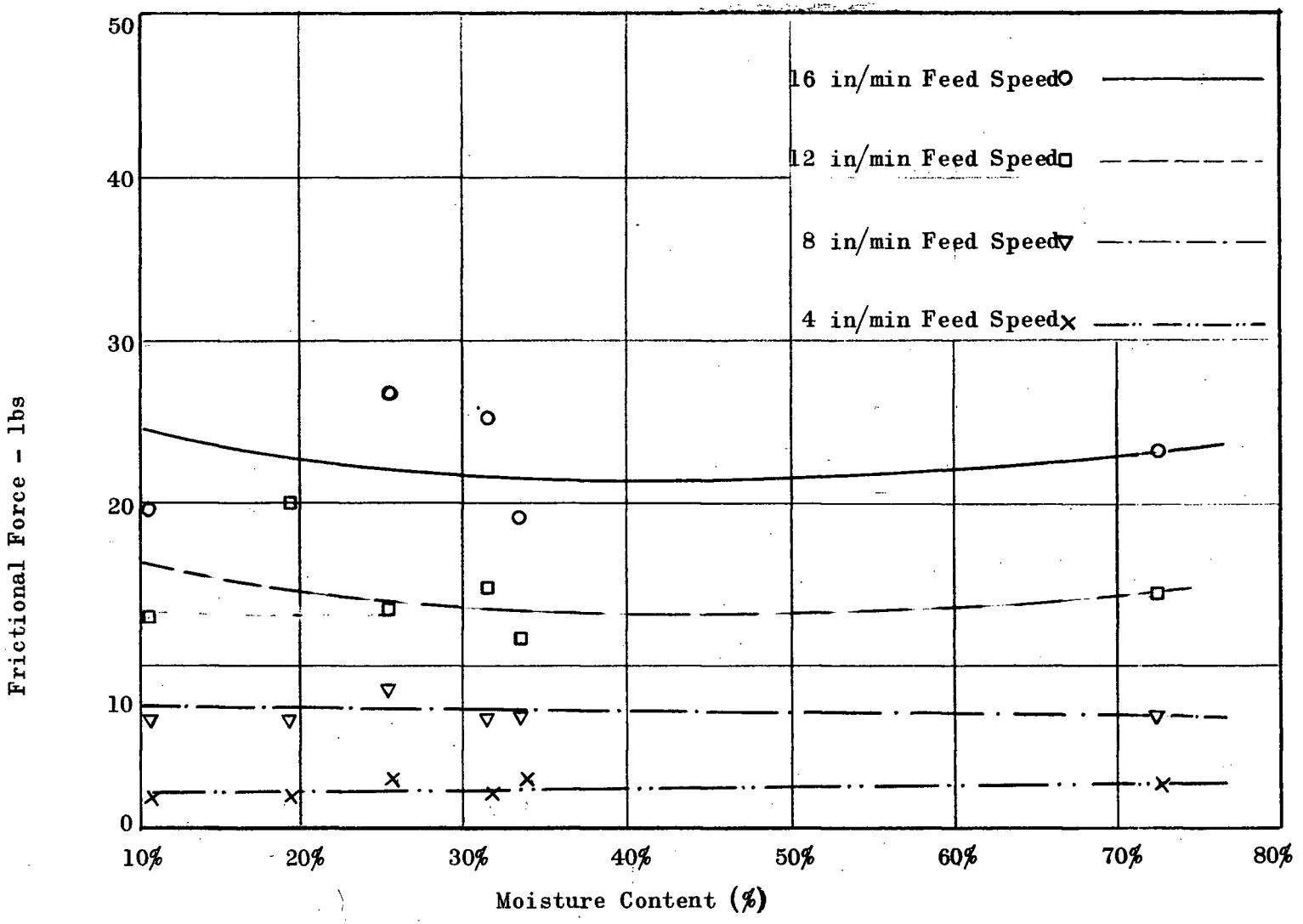

Fig. 33 Graph of Frictional Force versus Moisture Content - Fir Across Grain.

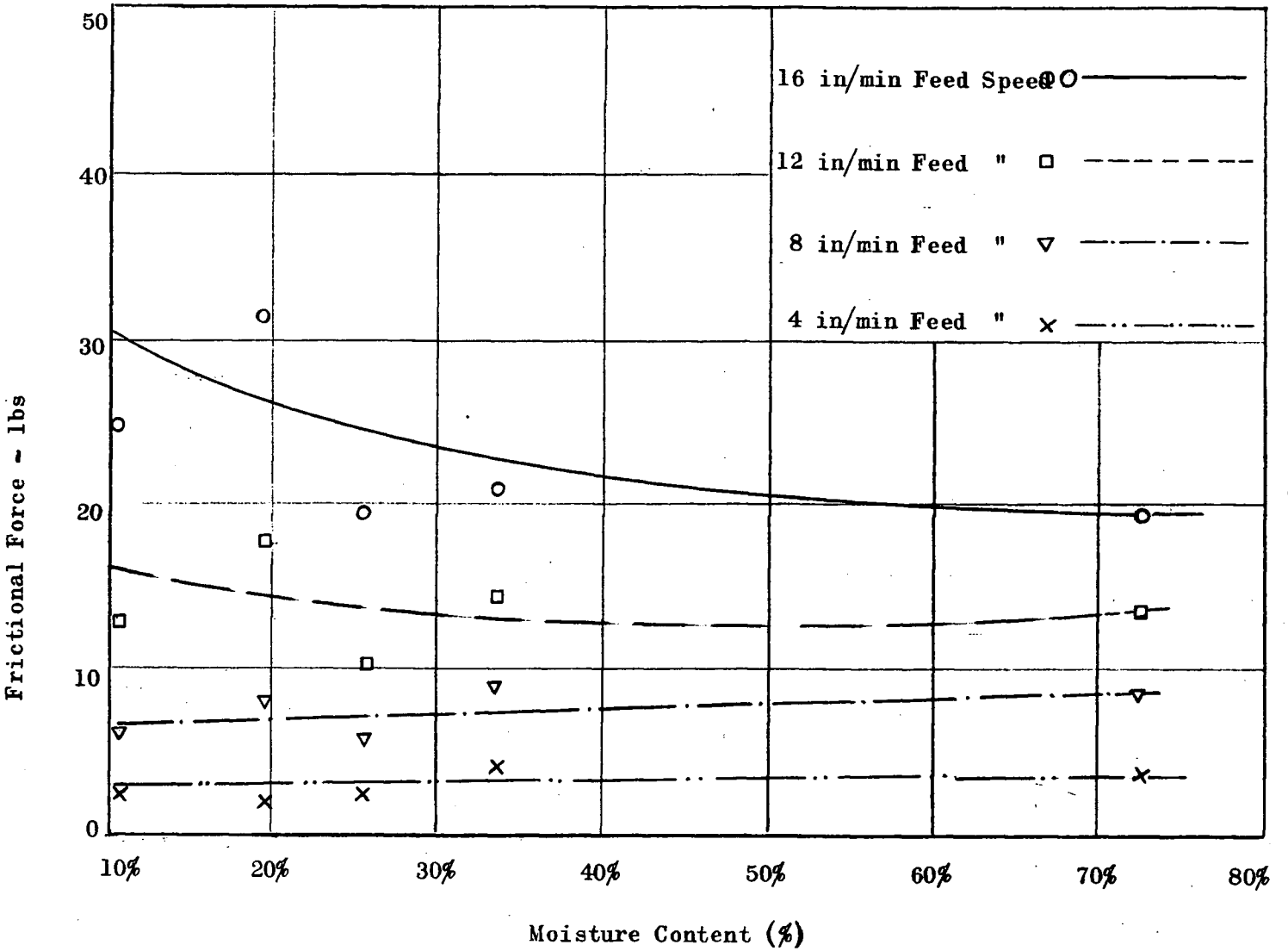

Fig. 34 Graph of Frictional Force versus Moisture Content - Fir Along Grain.

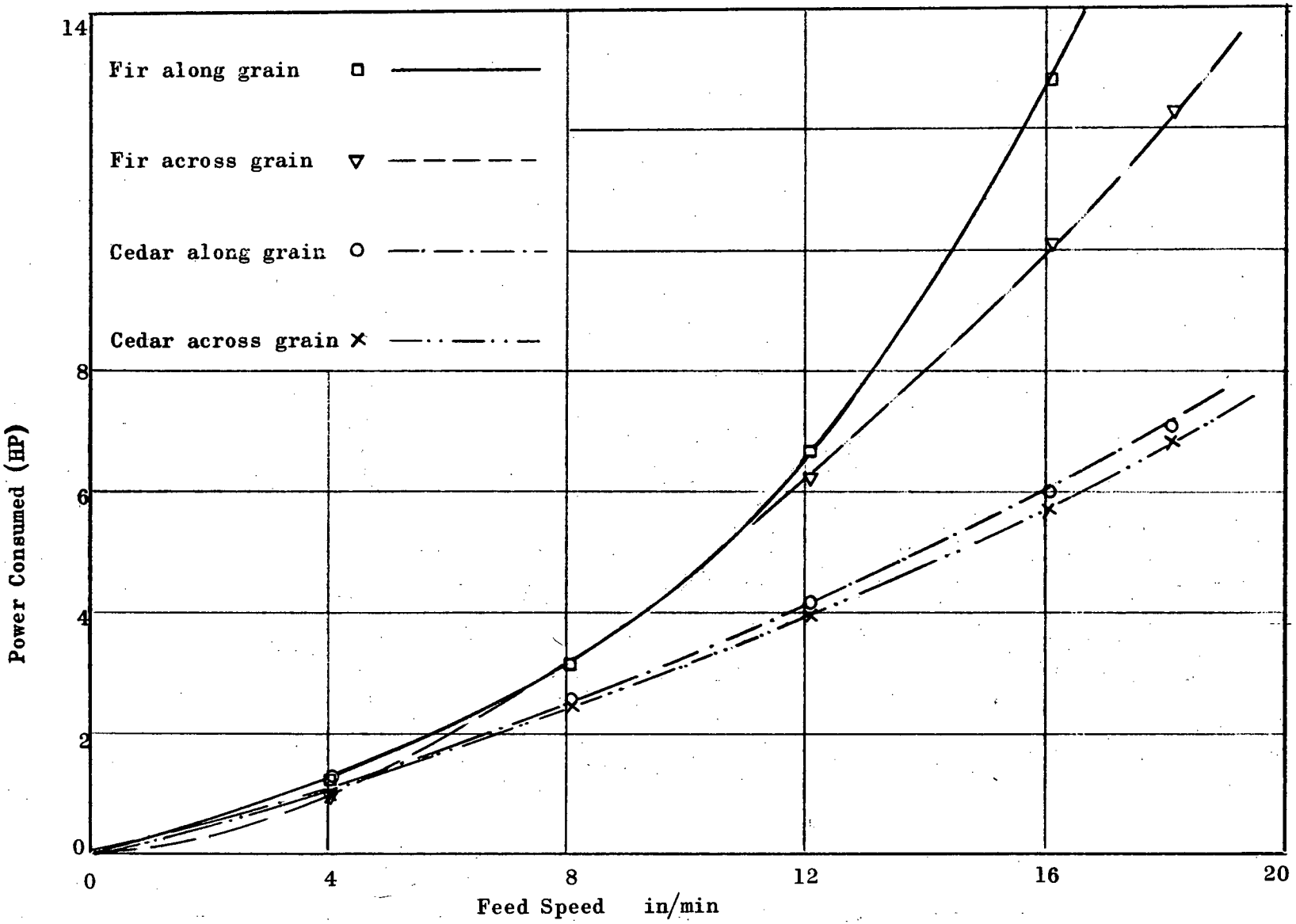

Fig. 35 Graph of Power Consumed versus Feed Speed with 11% Moisture Content.

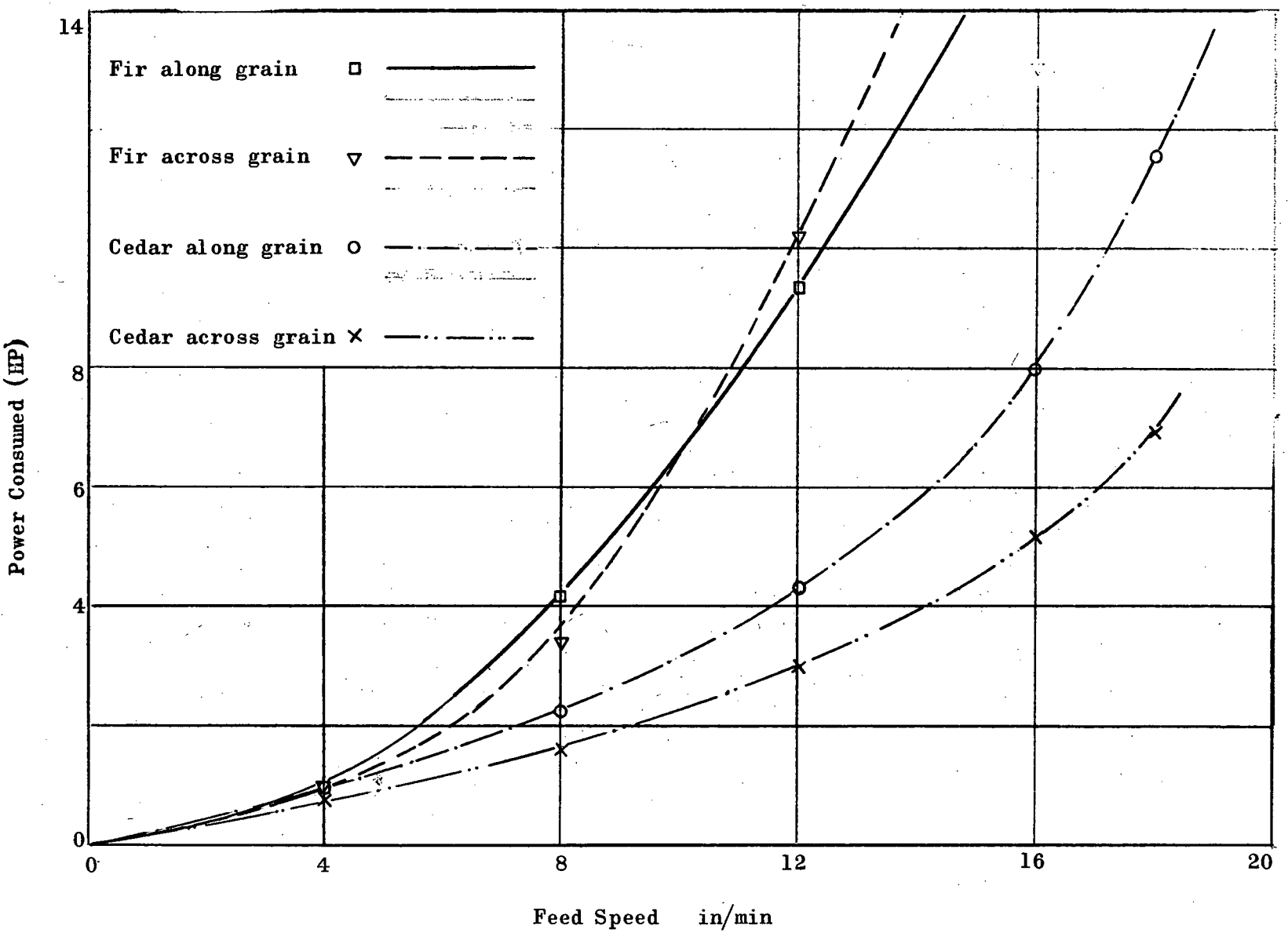

Fig. 36 Graph of Power Consumed versus Feed Speed with 19% Moisture Content.

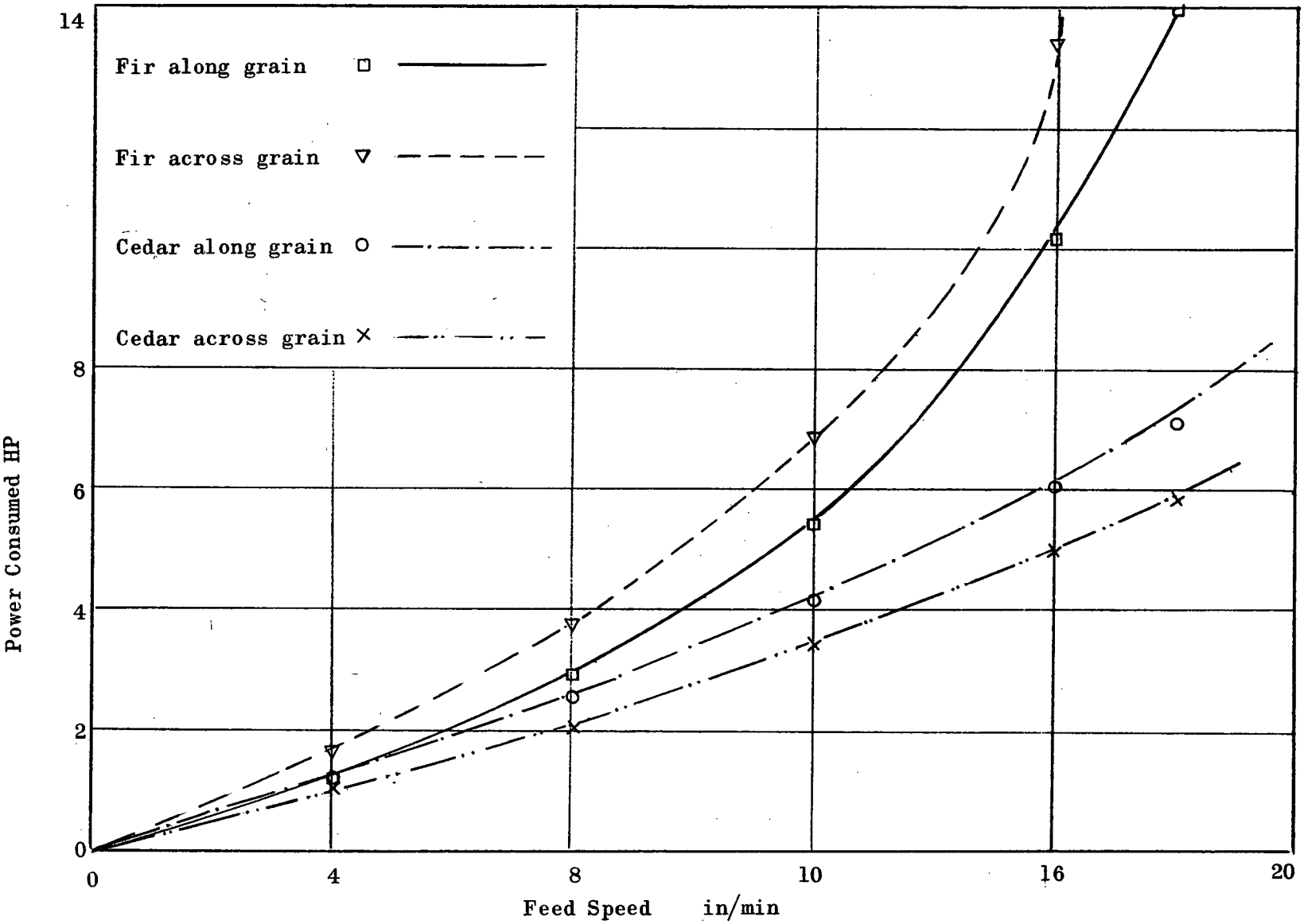

Fig. 37 Graph of Power Consumed versus Feed Speed with 25% Moisture Content.

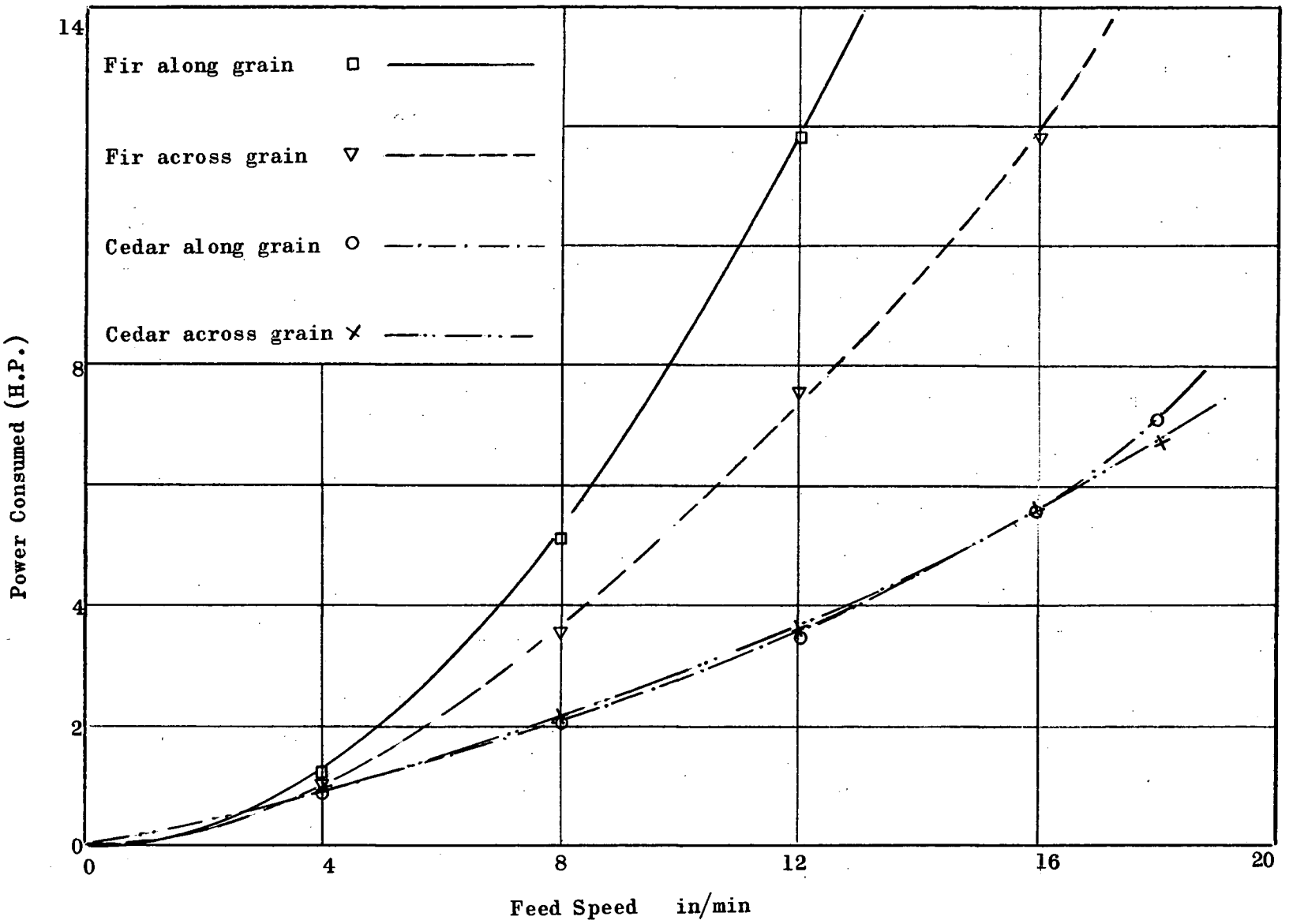

Fig. 38 Graph of Power Consumed versus Feed Speed with 32% Moisture Content.

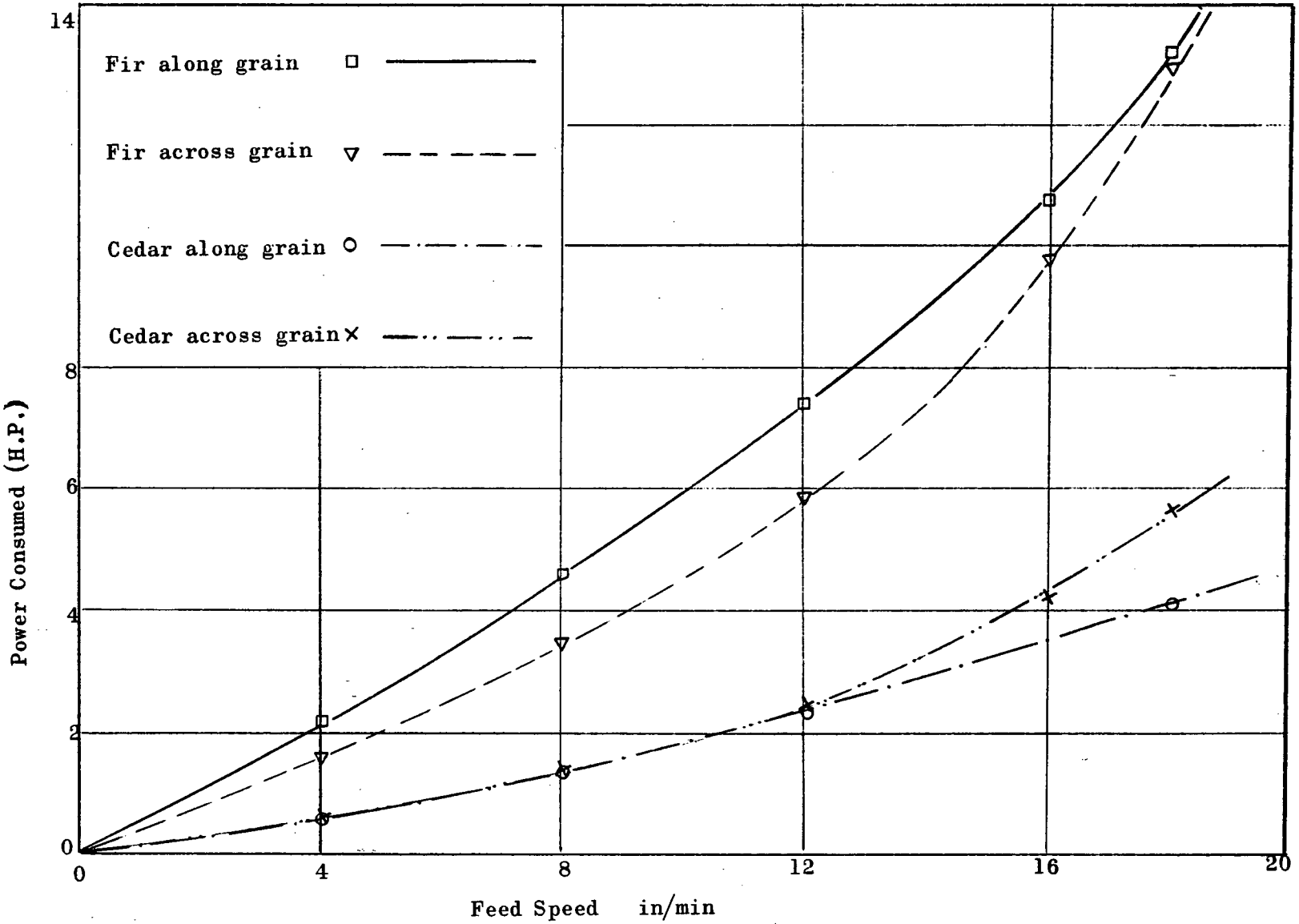

Fig. 39 Graph of Power Consumed versus Feed Speed with 34% Moisture Content.

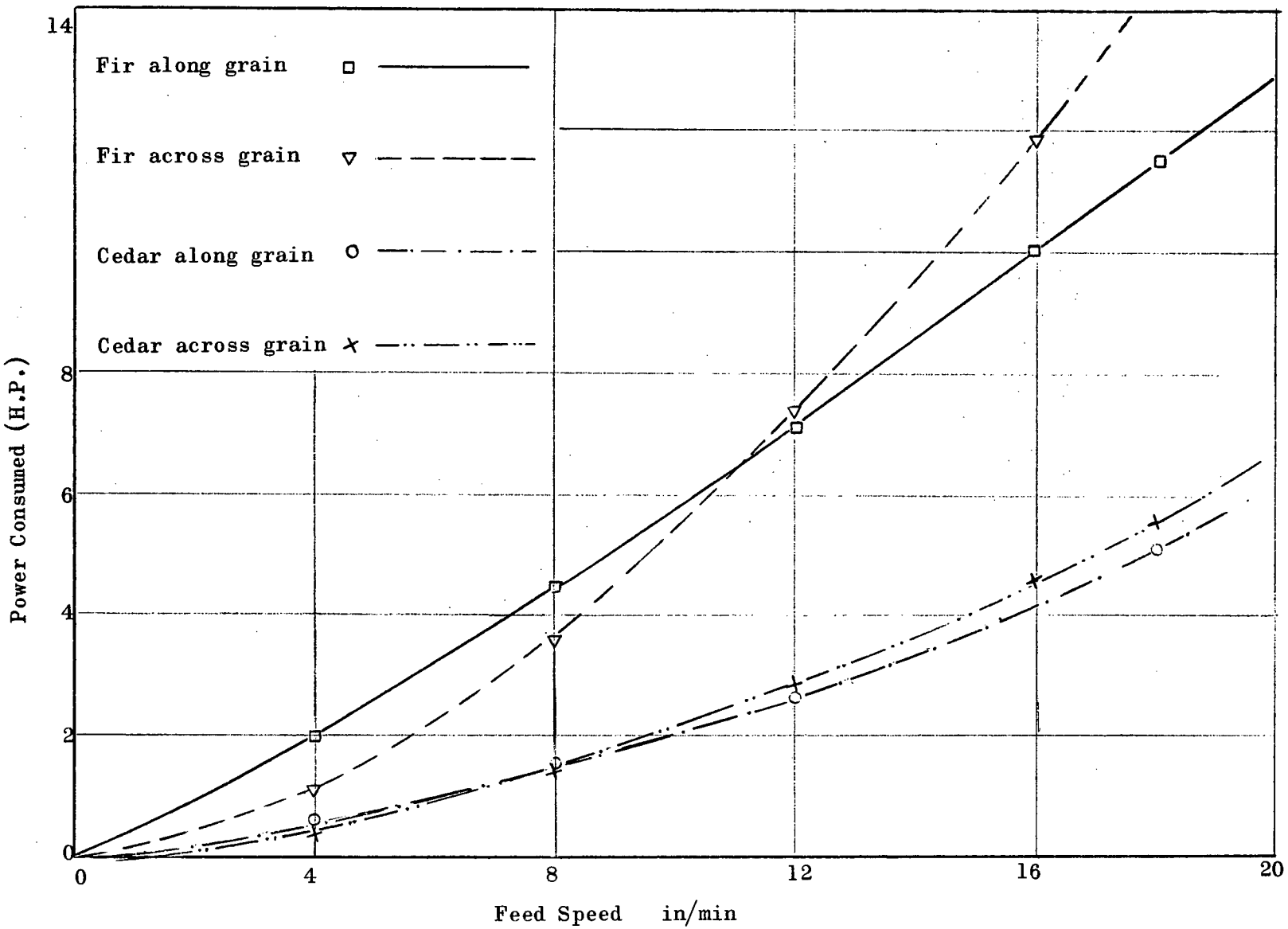

Fig. 40 Graph of Power Consumed versus Feed Speed with 72% Moisture Content.

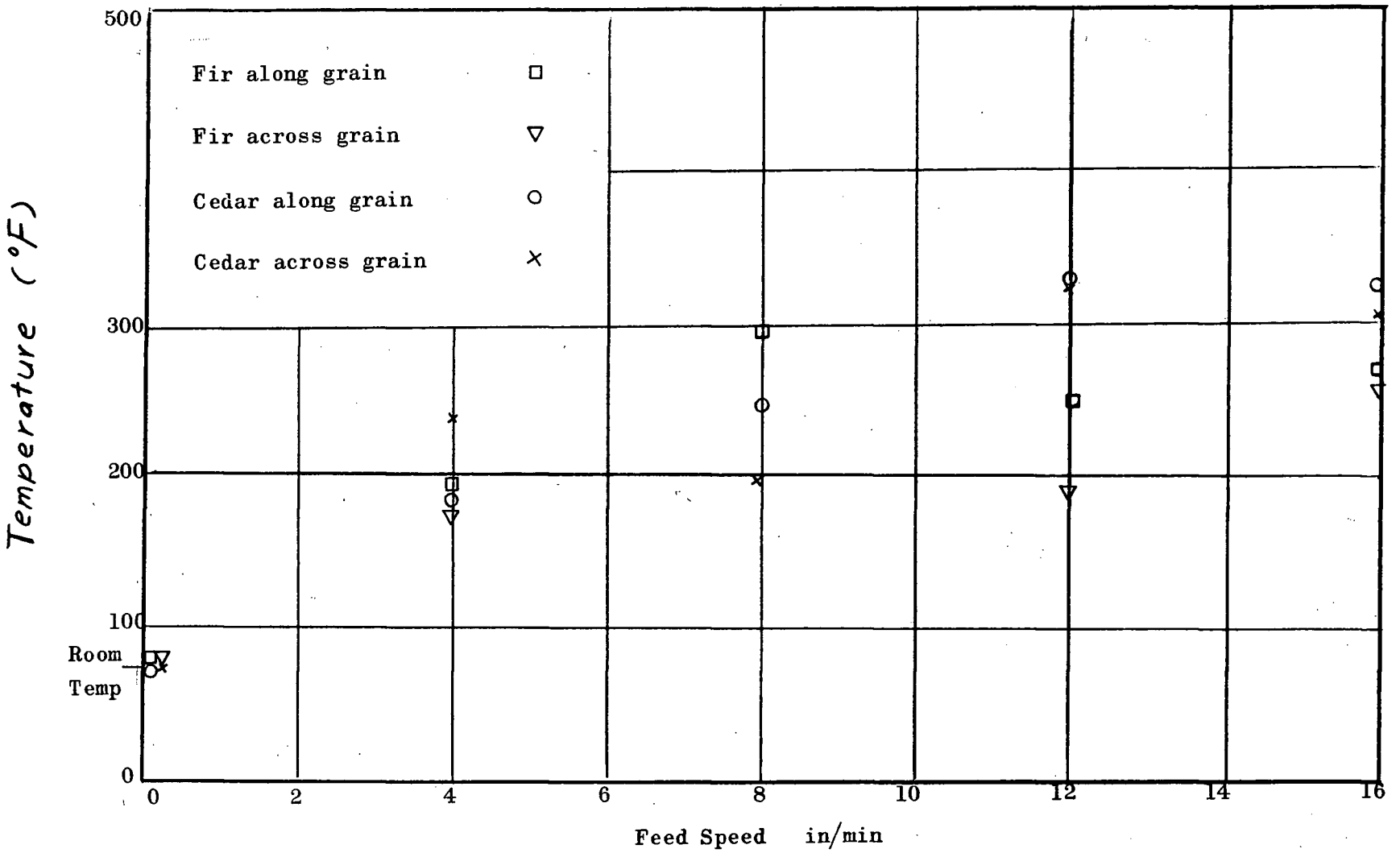

Fig. 41 Graph of Cutting Temperature versus Feed Speed.

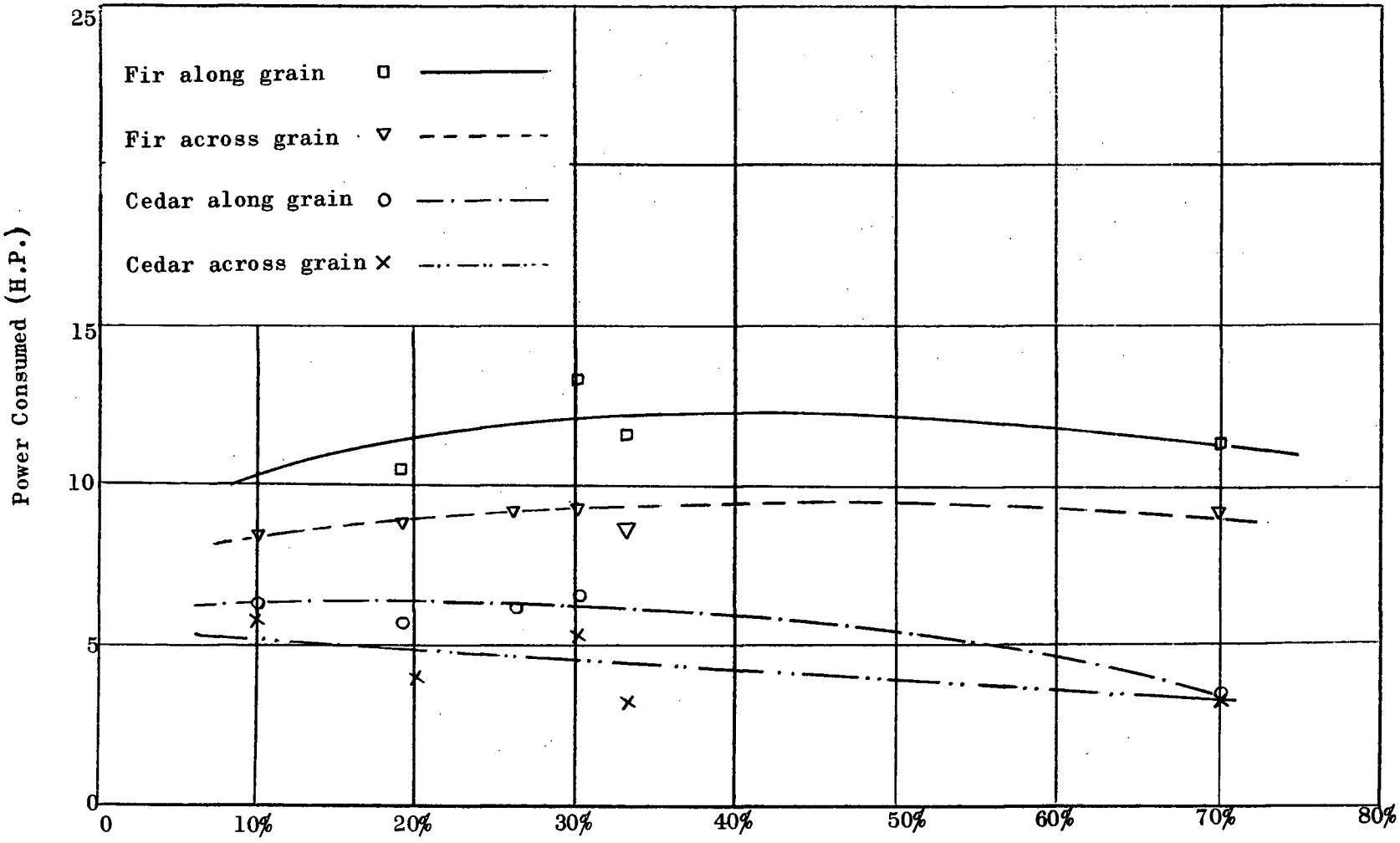

Fig. 42 Graph of Power Consumed versus Moisture Content(Feed Speed = 8 in/min)

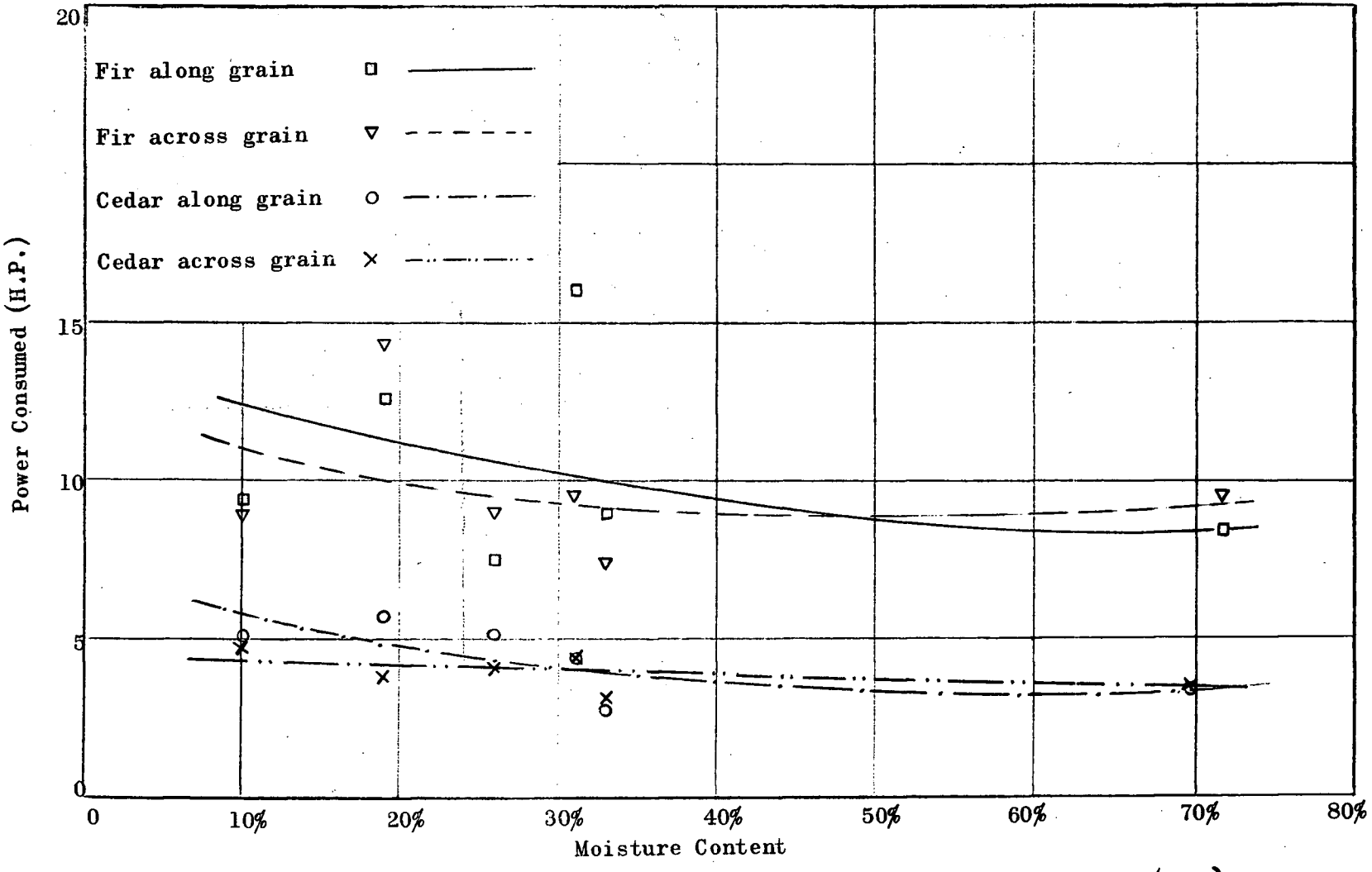

Fig. 43 Graph of Power Consumed versus Moisture Content(Feed Speed 12 in/min.)

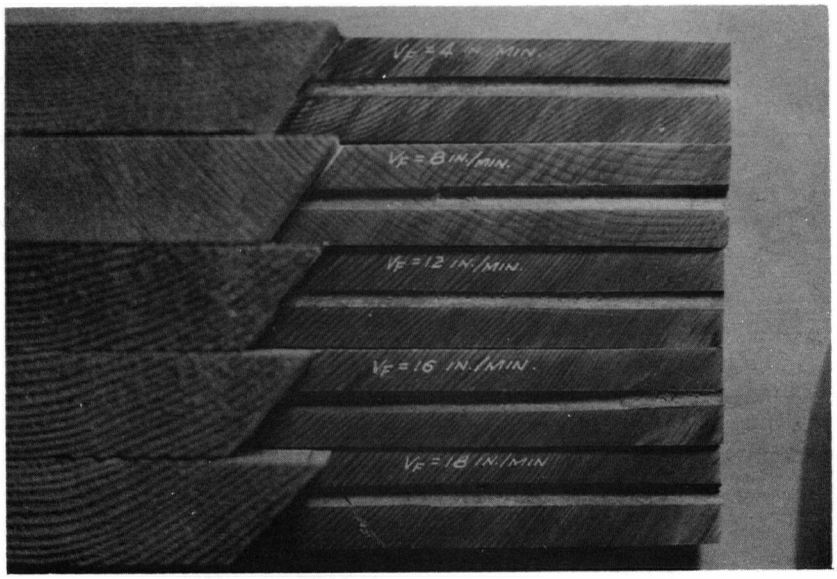

Fig. 44 Appearance of Cut Faces - Five Different Speeds.

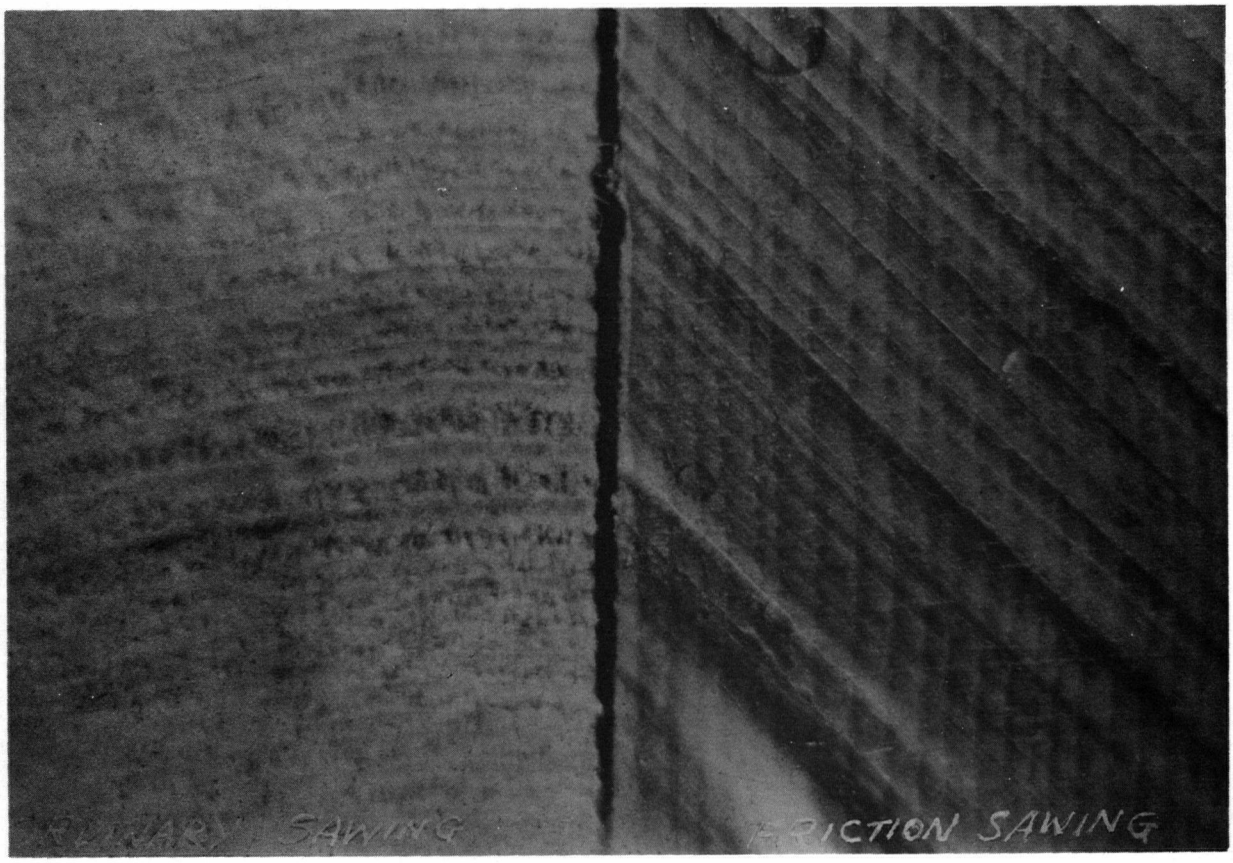

Fig.45 Comparison of Cut Faces Between Ordinary Sawing and Friction Sawing.

CHAPTER V.

V.1 DISCUSSION

Frictional heat raises the temperature at the cutting edge. Experimental results suggest that at low feed speed cutting the temperature may be less than the ignition temperature of wood. However, an elevated temperature, which is less than the ignition temperature, may substantially modify the structure of the wood, whereby it becomes fragile and may be removed by attrition.

Examination of Figs. 13 and 14 and Figs. 41 to 52 indicates that the frictional force (F_f), the normal force (F_N), and power consumed increase as the feed speed (V_f) increases. The explanation is related to the disposition of cut material. When the feed speed is low the cut material removed per unit time is small and the smooth edge of the sawing disk can dispose of the refuse with no accumulation on the kerf. But when the feed speed is high the disposal action of the smooth disk edge is not fast enough to meet the requirement with the result that cut material accumulated

on the kerf. The only way to dispose of the material is to burn it thoroughly. From Graf's "Ignition Temperature of Various Papers, Woods and Fabrics" [10], the ignition temperature of Douglas Fir is 489°F and that of Western red cedar is 468°F based on rates of temperature rise of 16°F per hour and 17°F per hour respectively. The rate of temperature rise influences the ignition temperature significantly; the higher the rate of temperature rise, the higher the ignition temperature. In the present work the rates of temperature rise were up to 3,000°F per hour or more, thus the ignition temperature in the cutting zone will be higher than the above mentioned values. Therefore far greater power is required when the wood in the kerf has to be removed by ignition.

It is interesting to note that at low feed speeds, the values of frictional force F_f are somewhat lower than the predictions of theory. Using the experimental results on power consumed and equation (2-14) from Chapter II, it was found that the temperatures near the cutting edge vary with the feed speed. Appendix F shows that at low feed speed (4 inches per minute) the cutting edge temperatures are lower than the ignition temperature of the wood while at high feed speeds, 8 inches per minute or higher, the cutting edge temperatures were extremely high. The low cutting edge temperatures at low feed speeds suggests that the wood becomes brittle and is removed by attrition before the ignition temperature is reached. At high feed speeds the calculated cutting edge temperature exceeds the ignition point of the wood. In some cases the calculated temperatures exceed the melting point of steel. Since no trace of molten metal was found on the rim of the disk it appeared that the actual cutting temperature was below the melting point of steel ($\simeq$ 1,400°C [11].) The results suggest that a part of the energy is used to raise the cutting temperature and some energy goes to fragmenting

and removal of material.

There are two general types of curve for coefficient of friction versus feed speed (Fig. 25 to 30). One general form is concave upward and other form is flatter and concave downward. The concave upward curves are due to pinching action which occurs when the wood bends inward after being cut, thus gripping the two side faces of the sawing disk and creating side frictional forces. The additional frictional forces add to the value of the cutting edge frictional forces and influence the shape of the μ- V_f curves. This side frictional force is a function of the spring constant of wood but independent of feed speed. Therefore it may be considered to be constant through all changes of feed speed. Since the values of F_f and F_N at low feed speeds are far less than that at high feed speeds then the influence of side frictional force adding to F_f at low feed speed to increase the value of μ is far greater than its influence on high feed speed. This behaviour is revealed by the high values of coefficient of friction at low feed speeds.

At high feed speeds another factor enters and causes the coefficient of friction to rise again. As previously mentioned the cutting temperature increases rapidly when the cut material in the kerf is burnt at high feed speed. The high cutting temperature melts the resin in the wood and causes it to cover the contact surfaces between the specimen and the sawing disk, especially on the side faces. Consequently the value of the coefficient of friction increases. Examination of the cutting edge of the disk and the side faces of the specimen through a microscope clearly shows layers of resin (Fig. 44 and 45). At higher speeds the resin layers are thicker and darker.

Wood is a natural product and its constituents are not homogeneous hence consistent results are hard to obtain. The flatter concave downward curves are produced by the wood bending outwards after being cut. At low

feed speed, when the cutting temperature is low, no melted resin is present to increase the frictional force. When the feed speed increases the cutting edge temperature also increases and the wood resin starts to melt. Further increase of feed speed causes higher cutting edge temperatures which melt the resin with the result that the frictional force is reduced.

Figs. 31 to 38 reveal that moisture content has little effect on friction cutting. Generally the moisture is only a small portion of the total weight of the wood specimen. In friction cutting the energy required for cutting wood of different moisture content is related to the heat required for evaporating the different amount of moisture in the wood. This difference of heat required for evaporating moisture is insignificant when compared with the total energy required for cutting.

It was interesting to note that the cut faces of the specimen were extremely smooth and polished. This finding suggests that friction cut wood may not require a secondary planing operation. This smooth and polished cutting edge is specially noticeable in plywood and veneer cutting. Plastic can be softened at a certain temperature hence it may be possible to cut successfully by this method.

CHAPTER VI.

VI.1 CONCLUSION

The research reveals that frictional heat can be utilized to saw wood. At low feed speed frictional heat appears to raise the temperature to a level lower than the ignition temperature of wood. This finding suggests that heat modifies the structure of the wood whereby it becomes fragile and is removed by attrition. The sawing performance was repeatable in the low feed speed cutting experiments. At high feed speed when waste was required to be burnt and removed, very high power consumption was required and the calculated cutting temperature was then higher than the ignition temperature of wood.

The cutting of plywood was attempted with successful results. The faces after being friction cut were clean, unchipped and were of a far better finish than produced by planing.

In all the experiments the cut edge was smooth, straight and the

kerf was narrow. The narrow kerf indicates that wood waste is reduced by friction cutting. Unfortunately the saving of wood cannot cover the disadvantages of high power consumption and low feed speed. These two disadvantages arise from poor removal of cut material. A smooth disk edge requires excessive feed pressure and cannot dispose of the cut material effectively. If some means to reduce the cutting edge contact area and to dispose of the cut material effectively can be found then the feeding pressure and consequently the power consumed will be reduced and the feed speed may also be increased. In so doing the drawbacks of this method of sawing may be eliminated.

Another factor giving excessive power consumption is related to the pinching action of the wood on the side faces of the disk. The two legs of the specimen after being cut bend inward and grip on the disk. If the outer rim is made slightly thicker than the inner part of the disk the undesirable pinching action may be eliminated.

VI.2 Recommendations

The main disadvantages of friction cutting of wood are high power consumption and low feed speed. These are probably caused by the smooth cutting edge of the sawing disk. Two types of cutting edge designed to reduce contact area and to give more effective disposal of cut material are recommended: (1) If several notches are introduced in the rim of the disk then the wood detritus can easily be carried away from the kerf by the notches and disposed of by centrifugal force. At the same time the notches would reduce the contact area of the cutting edge. (2) A second suggested type of sawing disk is shown in Fig. 46. Teeth are provided in the middle part of the rim having a diameter a little smaller than that of the two side face edges. This arrangement will greatly reduce the contact area of the

cutting

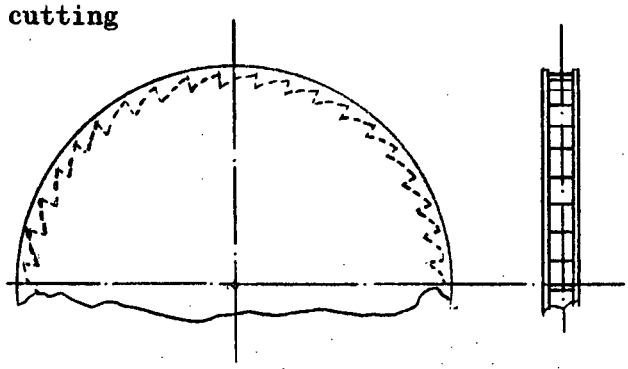

Fig. 46 Recommended Saw Blade to Reduce Contact Area and with Inner Teeth to Dispose Wood Waste.

edge while disposal of wood waste is carried out by the inner teeth.

In order to eliminate the undesirable pinch action the outer rim of the disk should be made a little thicker. (Fig. 47)

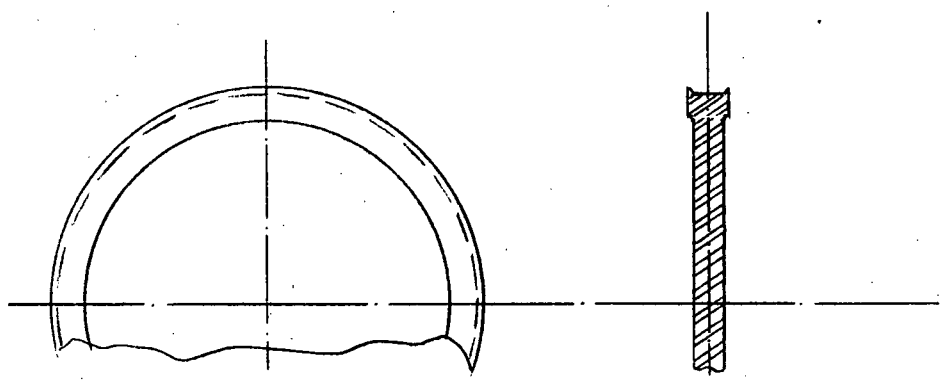

Fig. 47 Recommend Saw Blade to Eliminate Pinch Action.

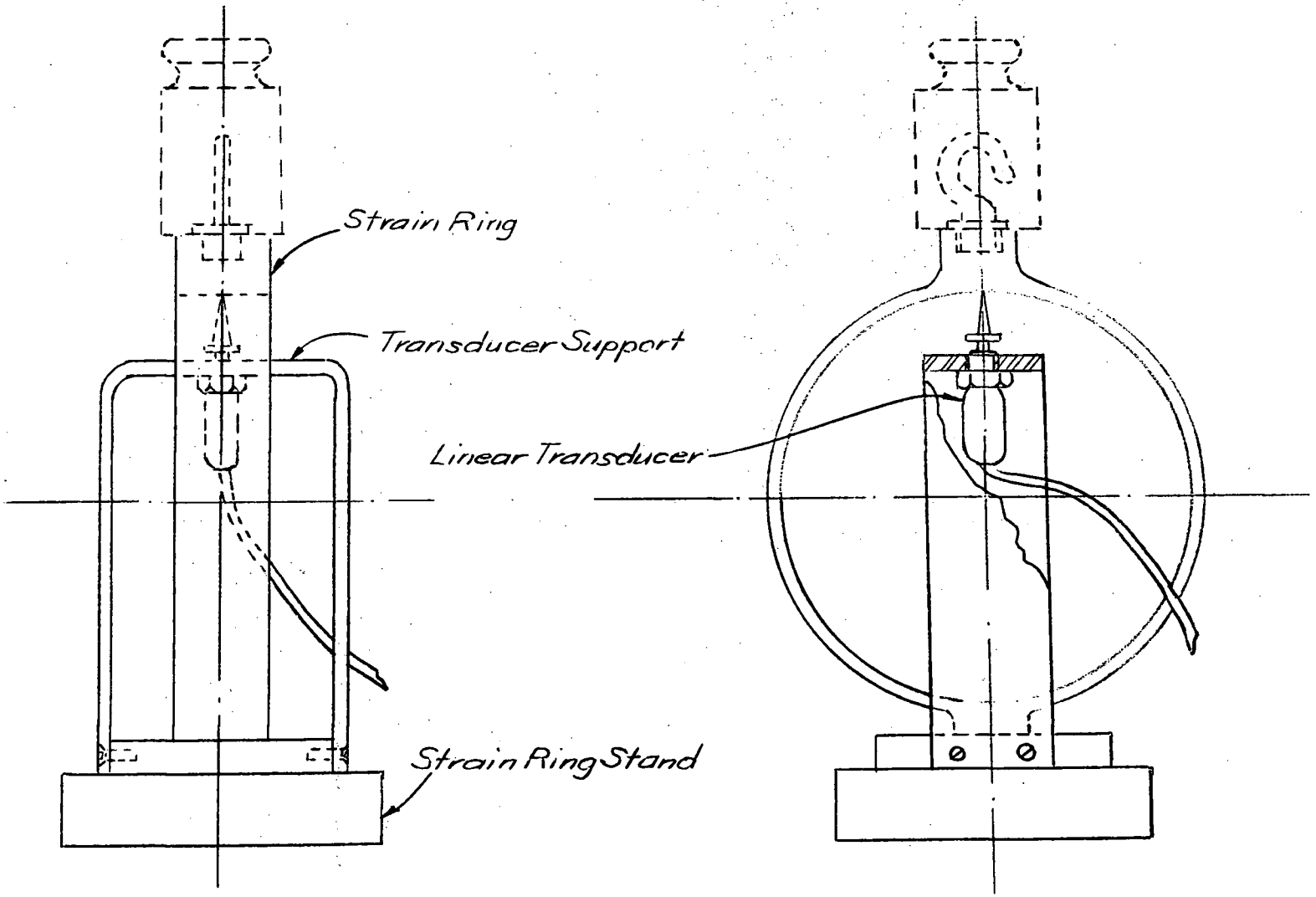

Fig. 48 Fixture of Daytronic 103A-80 Linear Transducer.

APPENDIX A.

CALIBRATION OF TABLE SUPPORT STRAIN RING

(a) Compression. Fig. 48 shows the strain ring in an upright position with a "Daytronic" 103A80 linear displacement transducer being fixed on the transducer support. The instrument connection has already been described in Chapter III, Section 2. Load was placed on the top of the strain ring and increased gradually (in 4 oz. increments for the low range and in 2 lbs. increments for the high range) until the maximum reading on the instrument was obtained. The load then was reduced in the same increments as the loading sequence until all the load was removed.

(b) Tension. The strain ring was calibrated for tension by the use of the pulley, string and weight system shown in Fig. 49.

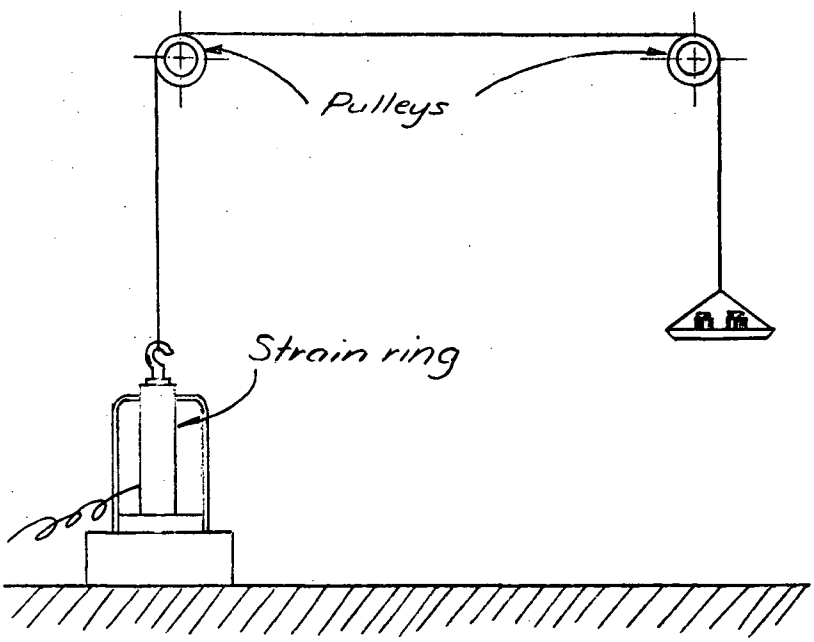

Fig. 49 Calibration of Table Support Strain Ring (Tension)

APPENDIX B.

CALIBRATION OF FEED THRUST MEASURING STRAIN RING

After the table support strain ring was calibrated, it was solidly clamped on one end of the carriage track (Fig. 50). With the push rod and strain ring fixed in position the carriage was engaged with the power screw which was then turned slowly until the push rod just contacted the table support strain ring. A gradual increase of the turning force on the power screw produced deflection of both rings. For each deflection reading on one strain ring there would be a corresponding reading on the other. As the table support strain ring was already calibrated the calibration curves for the thrust measuring strain ring could then be plotted.

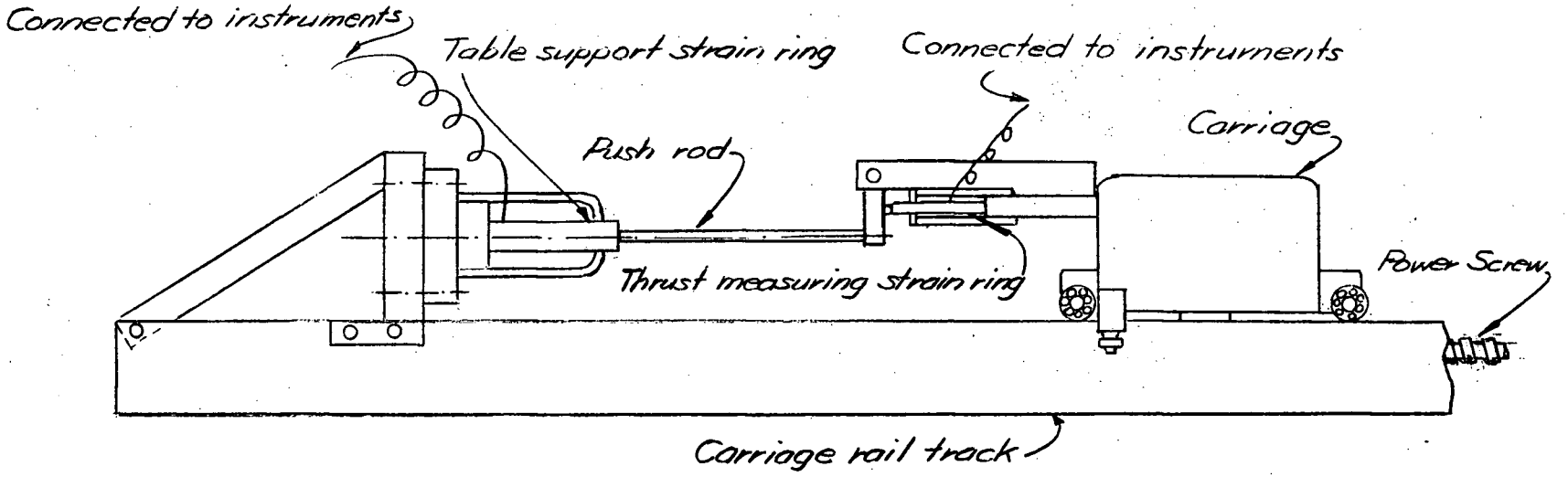

Fig. 50 Calibration of Thrust Measuring Strain Ring.

APPENDIX C

CALBRATION OF CHROMEL - CONSTANTAN THERMOCOUPLE FOR MEASURING CUTTING TEMPERATURE

The thermocouple was connected as described in Chapter III, Section 2. The cold junction (the tip of the probe) was placed in a beaker containing water. The water was then heated until it was boiling and then cooled down to room temperature. The temperature of the water was measured by a mercury thermometer and the chart record was read at 10°F intervals. (for increasing and decreasing temperatures) Fig. 50a shows the calibration curve and the extrapolation employed. Data from [12] reveals that the e.m.f. versus temperature curves for chromel and constantan are linear over an extended range (0° - 800°C) (Fig. 50b)

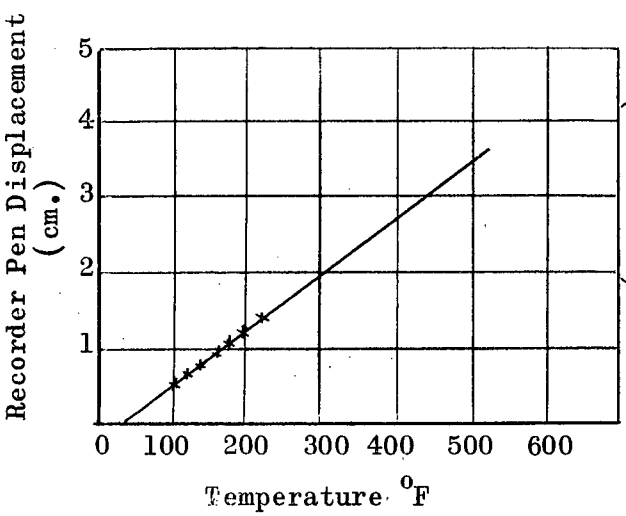

Fig. 50a.
Chromel-Constantan Thermocouple
Calibration Curve

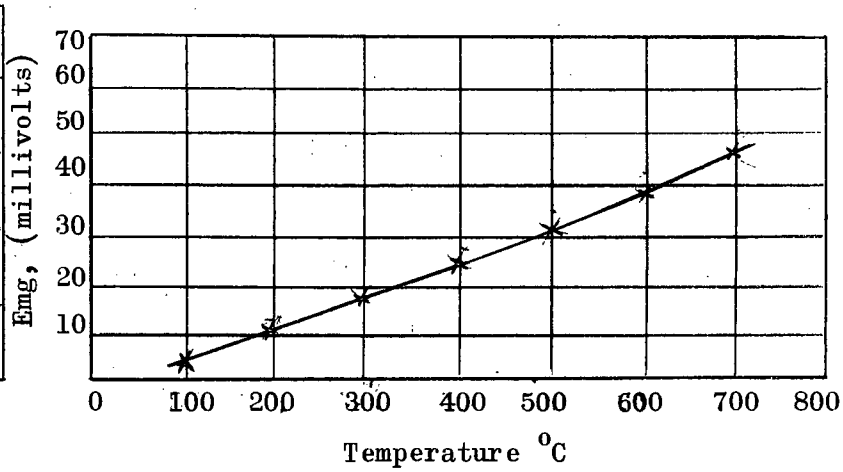

Fig. 50b.
Thermal emf of Chromel-Constantan Thermocouple.
(Data from W.D. Kingery: "Property Measurement at High Temperatures.")

APPENDIX D.

SEASONING OF WOOD SPECIMEN

The seasoning of the wood specimens was carried out in the Vancouver Laboratory of the Forest Products Laboratory. The specimens were placed in the kilns for one month. There were four kilns each with a different moisture content. They were:

Room No.1

Dry bulb temperature	30°F
Relative humidity	90%
Specimen average moisture content after seasoning	32%

Room No.2

Dry bulb temperature	75°F
Relative humidity	83%
Specimen average moisture content after seasoning	25%

Room No.3

Dry bulb temperature	70°F
Relative humidity	65%
Specimen average moisture content after seasoning	19%

Room No.4

Dry bulb temperature	70°F
Relative humidity	30%
Specimen average moisture content after seasoning	11%

APPENDIX E.

FORCE ANALYSIS DURING CUTTING

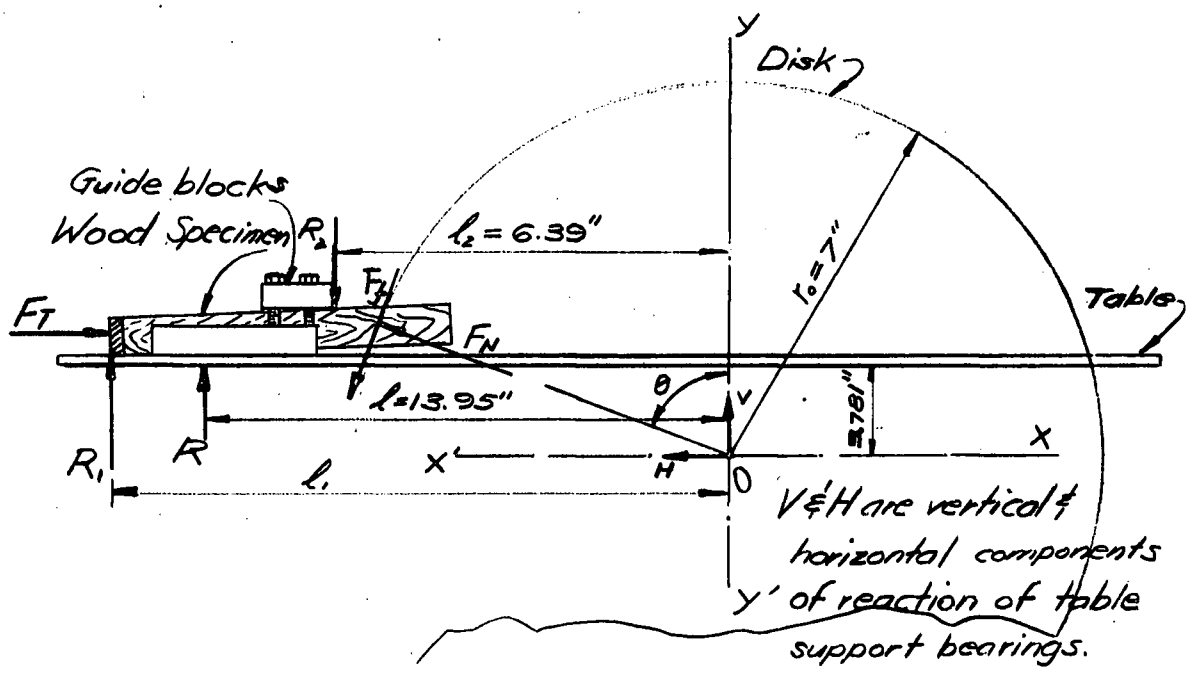

Fig. 51 Forces on specimen and Table

From Fig. 51:

l = Distance between R and Y-Y' = 13.95 inches

R_1 = Reaction exerted by tail edge of the wood specimen on the table;

R_2 = Reaction exerted on the wood specimen by the roller on the upper guide block;

l_2 = Distance between R_2 & Y-Y' = 6.39 inches.

As the friction between wood specimen and table and guide was reduced to a minimum by using Teflon, Arborite and rollers, this part of friction force may be neglected (Chapter III, Section iic)

$\Sigma M_o = 0$

$$R_1 \times l_1 - R \times l - R_2 \times l_2 = 0 \quad \ldots\ldots\ldots\ldots\ldots\ldots\ldots\ldots \quad (1)$$

Taking the wood specimen as a free body (Fig. 52):

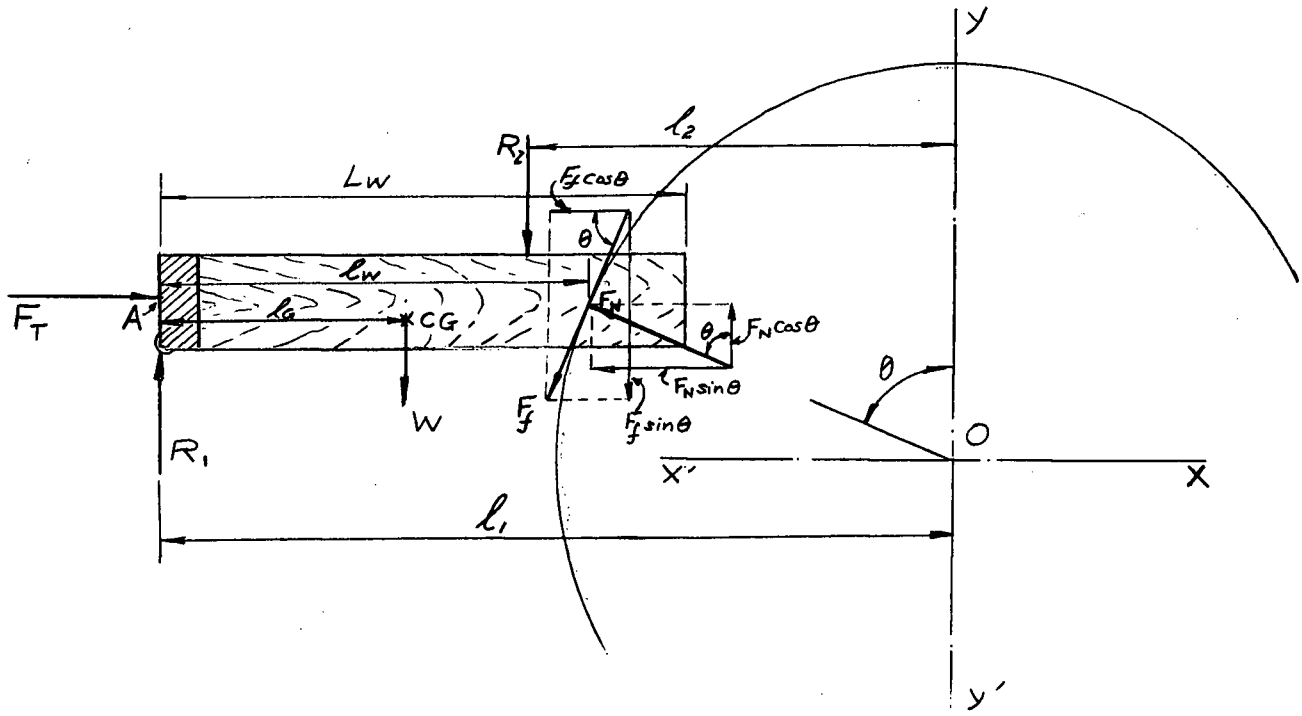

Fig. 52 Free Body of Wood Specimen

L_w = Length of the wood specimen

l_w = Distance between cutting edge and tail edge of the wood specimen

l_g = Distance between centre of gravity and tail edge of the wood specimen

$\Sigma F_x = 0$

$$F_N \text{ Sin } \theta + F_f \text{ Cos } \theta - F_T = 0 \quad \ldots\ldots\ldots\ldots\ldots\ldots\ldots\ldots \quad (2)$$

$\Sigma F_y = 0$

$$F_N \text{ Cos } \theta - F_f \text{ Sin } \theta + R_1 - R_2 - W = 0 \quad \ldots\ldots\ldots\ldots\ldots \quad (3)$$

$\Sigma M_A = 0$

$$F_N l_w \text{ Cos } \theta - F_f l_w \text{Sin } \theta - R_2(l_1 - l_2) - W l_g = 0 \quad \ldots\ldots \quad (4)$$

$$(4)/l_w \quad F_N \cos\theta - F_f \sin\theta - \left(\frac{l_1 - l_2}{l_w}\right) R_2 - \frac{l_g}{l_w} W = 0 \quad \ldots(5)$$

$$(3) - (5);\ R_1 - R_2 - W + \frac{(l_1 - l_2)}{l_w} R_2 + \frac{l_g}{l_w} W = 0 \quad \ldots\ldots\ (6)$$

$$R_1 = \frac{(l_w - l_1 + l_2)R_2 + (l_w - l_g)W}{l_w} \quad \ldots\ldots\ (7)$$

Substituting (7) in (1), we have

$$\frac{(l_w - l_1 + l_2)R_2 l_1 + (l_w - l_g)W l_1}{l_w} - Rl - R_2 l_2 = 0$$

Arranging terms;

$$R_2 = \frac{l l_w R - (l_w - l_g) l_1 W}{(l_1 - l_2)(l_w - l_1)} \quad \ldots\ldots\ (8)$$

Substituting (8) in (6) and arranging terms;

$$R_1 - R_2 - W = \frac{lR - (l_1 - l_g)W}{(l_1 - l_w)} \quad \ldots\ldots\ (9)$$

$$(2) \times \cos\theta;\ F_N \sin\theta \cos\theta + F_f \cos^2\theta - F_T \cos\theta = 0 \quad \ldots\ (10)$$

$$(3) \times \sin\theta;\ F_N \sin\theta \cos\theta - F_f \sin^2\theta + (R_1 - R_2 - W)\sin\theta = 0 \ldots\ (11)$$

(10) - (11)

$$F_f = F_T \cos\theta + (R_1 - R_2 - W) \sin\theta \quad \ldots\ldots\ (12)$$

(2) x Sin θ

$$F_N \sin^2\theta + F_f \sin\theta \cos\theta - F_T \sin\theta = 0 \quad \ldots\ldots\ (13)$$

(3) x Cosθ

$$F_N Cos^2\theta - F_f Sin\theta Cos\theta + (R_1 - R_2 - W)\, Cos\theta = 0 \quad .... \quad (14)$$

(13) + (14)

$$F_N = F_T Sin\theta - (R_1 - R_2 - W)\, Cos\theta \quad ..... \quad (15)$$

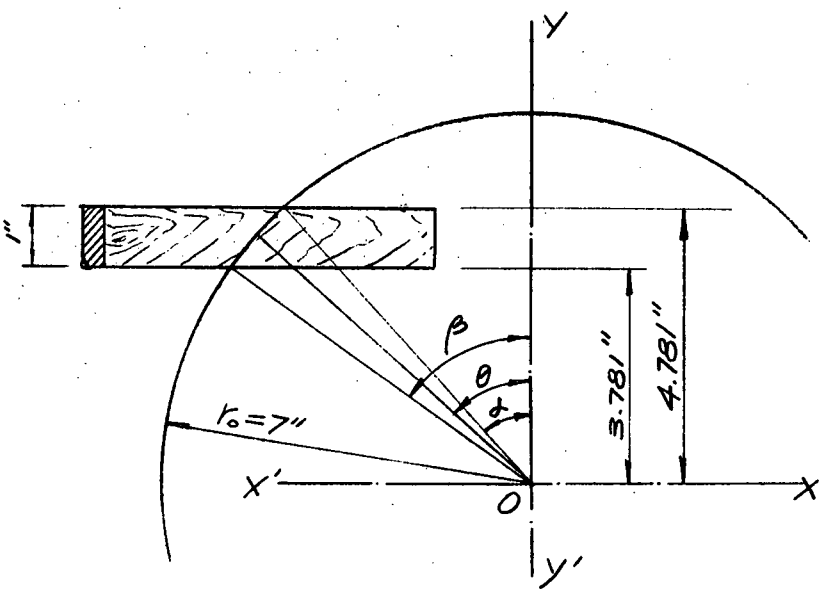

Fig. 53 Direction of Normal Force Acting on the Specimen

From Fig. 53 we see that

$$\beta = Cos^{-1}\frac{3.781}{7} = Cos^{-1}\ 0.5401$$

$$\therefore\ \beta = 57^0 18'$$

$$\alpha = Cos^{-1}\frac{4.781}{7} = Cos^{-1}\ 0.6830$$

$$\therefore\ \alpha = 46^0\ 55'$$

$$\theta = \alpha + \tfrac{1}{2}(\beta - \alpha) = \frac{\alpha + \beta}{2}$$

$$\theta = 52^{\circ}\ 6\tfrac{1}{2}'$$

$$\text{Sin}\theta = 0.789$$

$$\text{Cos}\theta = 0.614$$

$$l_1 - l_w = 7\text{Sin}\theta = 5.53 \text{ inches}$$

Let $$K = R_1 - R_2 - W = \frac{(l_g - l_1)W + 1R}{l_1 - l_w}$$

$$\therefore K = \frac{(l_g - l_1)W + 13.95R}{5.53}$$

Substituting the above in (12) and (15), we have

$$F_f = 0.614\ F_T + 0.789\ K \quad \ldots\ldots\ldots\ldots\ldots\ldots \quad (16)$$

and $$F_N = 0.789\ F_T - 0.614\ K \quad \ldots\ldots\ldots\ldots\ldots\ldots \quad (17)$$

also $$\mu = \frac{F_f}{F_N} = \frac{0.614\ F_T + 0.789\ K}{0.789\ F_T - 0.614\ K} \quad \ldots\ldots\ldots\ldots\ldots\ldots \quad (18)$$

APPENDIX F.

NUMERICAL RESULTS OBTAINED FROM THEORETICAL EQUATIONS

The following calculation is based on equations (2-11), (2-12), (2-13) and (2-14) from Chapter II:

$$\mu F_N = \left(\frac{2\pi J K_s b}{\omega}\right) \frac{I_1(\lambda r_o)}{I_o(\lambda r_o)} \lambda \Delta T_{max} \quad \ldots\ldots\ldots\ldots\ldots\ldots \quad (2\text{-}11)$$

$$\lambda = 41.83 \sqrt{\frac{K_a}{K_s b r_o}} \quad \ldots\ldots\ldots\ldots\ldots\ldots\ldots\ldots \quad (2\text{-}12)$$

$$\text{Power} = 2\pi K_s b r_o \frac{I_1(\lambda r_o)}{I_o(\lambda r_o)} \lambda \Delta T_{max} \quad \ldots\ldots\ldots\ldots\ldots \quad (2\text{-}13)$$

$$\Delta T_{max} = \frac{I_o(\lambda r_o)}{I_1(\lambda r_o)} \cdot \frac{\text{Power}}{2\pi J K_s b r_o \lambda} \quad \ldots\ldots\ldots\ldots\ldots\ldots \quad (2\text{-}14)$$

Now J = 778 ft. lb./Btu

r_o = 7/12 = 0.584 ft. (Actual disk radius)

$b = \frac{0.0766}{12}$ = 0.00638 ft. (Actual disk thickness, 14 gage)

ω = 4,620 x 60 x 2π = 1,741,700 rad/hr. (Actual disk speed)

K_s = 26 Btu/hr. ft. ^oF (Thermal conductivity of steel) [8]

Physical properties of air at 100^{o}F (Prantdl number P_r = 0.72) [8]:

Thermal conductivity K_a = 0.0154 Btu/hr. ft. ^oF

Kinematic viscosity ν_a = 0.00018ft.^{2}/sec.

= 0.648 ft^2/hr.

Thus

$$\lambda = 41.83\sqrt{\frac{0.0154}{26x0.00638x0.584}}$$

$$\therefore \lambda = 16.68 \quad ft^{-1}$$

$$\lambda r_o = 9.74$$

$$I_o(9.74) = 2,200$$

$$I_1(9.74) = 2,084$$

When r = 3 inches

$$\lambda r(r=3") = 4.17$$

$$I_o(4.17) = 13.09$$

$$I_1(4.17) = 11.39$$

Hence substituting the numerical values into (2-11) we have

$$\mu F_N = \left(\frac{2\pi x778x26x0.00638}{1,741,700}\right)\left(\frac{2,084}{2,200}\right) \times 16.68\Delta\tau_{max}$$

$$\mu F_N = 0.00736\Delta\tau_{max}$$

Graf's data [10] shows that the ignition temperature of Western red cedar is 468°F and that of Douglas fir is 489°F with moisture content 7% and a rate of temperature rise of 15° ~ 17°F/hr. The rates of temperature rise in the present system are much greater. Graf also found that the ignition temperature was higher when the rate of temperature rise was greater. The cutting temperature is difficult to assess but evidently it should be below the melting point of steel ($\simeq$ 1,400°C [11]). For illustrative purpose we assume the cutting temperature to be 900°F, then we have

$$\Delta\tau_{max} = 900 - 70 = 830^oF \quad (\tau_{am} = 70^oF)$$

$$\mu F_N = 0.00736 \times 830 = 6.11 \text{ lbs.}$$

From (2-13)

$$HP = \frac{2\pi JK_s br_o}{60x33,000} \frac{I_o(\lambda r_o)}{I_1(\lambda r_o)} \lambda \Delta T_{max}$$

$$= \frac{2\pi x778x26x0.00638x0.584}{60x33,000} x \frac{2,084}{2,200} x 16.68x830$$

$$\therefore HP = 3.15 \text{ h.p.}$$

It is interesting to note that at low feed speeds, the values of frictional force F_f are somewhat lower than the predictions of theory. Using the experimental results on power consumed and equation (2-14) we found that the cutting edge temperatures are as shown in the following tables:

From (2-14)

$$\Delta T_{max} = \frac{60x33,000}{2\pi x778x26x0.00638x0.584x16.68} \left(\frac{2,200}{2,084}\right) HP$$

$$\therefore \Delta T_{max} = 264.6 HP$$

32% moisture content

1. Douglas Fir, along grain cutting

Feed Speed (V_f) (in. / min.)	4	8	12	16
Power Consumed (Horse power)	1.235	2.93	5.4	10.12
ΔT_{max} (^oF)	327	774	1,423	2,675
$T = \Delta T_{max} + T_{am.}$ (^oF)	397	844	1,493	2,745

2. Douglas Fir, across grain cutting

Feed Speed (V_f) (in. / min.)	4	8	12	16
Power Consumed (Horse power)	1.028	3.5	7.57	12.85
ΔT_{max} (^oF)	272	926	1,998	3,385
$T = \Delta T_{max} + T_{am.}$ (^oF)	342	996	2,068	3,455

3. Western red cedar, along grain cutting:

Feed Speed (V_f) (in. / min.)	4	8	12	16
Power Consumed (Horse power)	0.925	2.06	3.5	5.66
ΔT_{max} (^oF)	244	543	922	1,492
$T = \Delta T_{max} + T_{am}$ (^oF)	314	613	992	1,562

4. Western red cedar, across grain cutting:

Feed Speed (V_f) (in./min)	4	8	12	16
Power Consumed (Horse power)	1.028	2.105	3.6	5.56
ΔT_{max} (^oF)	327	555	948	1,466
$T = \Delta T_{max} + T_{am}$ (^oF)	342	625	1,018	1,536

APPENDIX G. Comparison of Heat Transfer by Radiation with those by Convective and Conductive Processes

Heat transfer by radiation per unit area [8].

$$\frac{\dot{Q}_{Rad}}{S} = \epsilon\sigma \left(T_{ab}^{4} - T_{am}^{4}\right)$$

where ϵ = emissivity of saw disk

= 0.066 (the surface of the disk is polished) [4]

σ = Stefan - Boltzmann constant

= 0.1714×10^{-8} Btu./hr. ft^2 $(^{o}R)^4$

T_{ab} = absolute disk temperature (^{o}R)

T_{am} = absolute ambient temperature (^{o}R)

An upper bound upon the radiation flux will be obtained by taking the temperature of the disk adjacent to the rim to be 500°F and the ambient temperature to be 70°F. Then the heat loss per unit area is

$$\frac{\dot{Q}_{Rad}}{S} = 0.066 \times 0.1714 \left[\left(\frac{960}{100}\right)^{4} - \left(\frac{530}{100}\right)^{4}\right]$$

$$\therefore \frac{\dot{Q}_{Rad}}{S} = 87.12 \text{ Btu/hr. ft.}^2$$

From Chapter II and Appendix F, we have heat loss per unit area due to convection

$$\frac{\dot{Q}_{Conv.}}{S} = h_a \left(T - T_{am}\right)$$

where $h_a = 875 \frac{K_a}{r_o}$

$$= 875 \times \frac{0.0154}{0.584}$$

= 23.1 Btu./hr. ft^2 °F

$$\frac{\dot{Q}_{Conv.}}{S} = 23.1 \times (500 - 70)$$

$$\frac{\dot{Q}_{Conv.}}{S} = 9{,}990 \text{ Btu./ hr. ft.}^2$$

Also from Chapter II and Appendix F, we have the heat loss by conduction

$$\frac{\dot{Q}_{Cond.}}{A} = +K_s \frac{I_1(\lambda r_o)}{I_o(\lambda r_o)}$$

$$= +26 \times \frac{2{,}084}{2{,}200} \times 16.73 \times 430$$

$$\frac{\dot{Q}_{Cond.}}{A} = +177{,}000 \text{ Btu./hr. ft.}^2$$

hence we have

$$\frac{\dot{Q}_{Rad.}}{\dot{Q}_{Conv.}} = \frac{87.12}{9980.3} = 0.00875 < 1\%$$

$$\frac{\dot{Q}_{Rad.}}{\dot{Q}_{Cond.}} = \frac{87.12}{177{,}000} = 0.000492 < 0.1\%.$$

BIBLIOGRAPHY

1. "Friction Sawing"
Band Machining Handbook
DoAll Co.

2. Koch, P.
"Wood Machining Processes"
The Ronald Press Company, 1964

3. "Computed Thermal Conductivity of Common Woods"
United States Dept. of Agriculture, Forest Products Lab.
Technical Note No. 248, Dec. 1952

4. McAdams, W.H.
"Heat Transmission"
McGraw - Hill, 1954 3rd Ed.

5. Ingersoll, L.R., Zobel, O.J. and Ingersoll, A.C.
"Heat Conduction with Engineering and Geological Applications"
McGraw - Hill, 1954

6. Carslaw, H.S. and Jaeger, J.C.
"Conduction of Heat in Solids"
Oxford Clarendon Press, 1960

7. Bowden, F.P. and Tabor, D.
"The Friction and Lubrication of Solids" Volume 1.
Oxford Clarendon Press, 1960

8. Kreith, F.
"Principles of Heat Transfer"
International Textbook Co., 1962

9. Cobb, E.C. and Saunders, O.A.

"Heat Transfer from a Rotating Disk"

Proceedings of the Royal Society, A,

236, P. 343, 1956

10. Graf, S.H.

"Ignition Temperature of Various Papers, Wood and Fabrics"

Engineering Experimental Station, Oregon State College

Bulletin No. 26, March 1949

11. Hodgman, C.D.

"Handbook of Chemistry and Physics"

Cleveland, Chemical Rubber Pub. Co.

46th Ed. 1966 p. 1269 - 1270

12. Kingery

"Property Measurements at High Temperatures"

John Wiley & Sons, Inc., 1959